Remote sensing for estimating genetic parameters of biomass accumulation and modeling stability of growth curves in alfalfa.

Authors: Ranjita Thapa, Karl H. Kunze, Julie Hansen, Christopher Pierce, Virginia Moore, Ian Ray, Liam Wickes-Do, Nicolas Morales, Felipe Sabadin, Nicholas Santantonio, Michael A Gore, Kelly Robbins

Affiliations: Ranjita Thapa, Karl H. Kunze, Julie Hansen, Virginia Moore, Liam Wickes-Do, Nicolas Morales, Michael A Gore, Kelly Robbins, Plant Breeding and Genetics Section, School of Integrate Plant Science, Cornell University, Ithaca, NY 14853, USA; Christopher Pierce, Ian Ray, Plant and Environmental Sciences, New Mexico State University; Felipe Sabadin, Nicholas Santantonio, School of Plant and Environmental Sciences, Virginia Polytechnic Institute and State University, Blacksburg, Virgina

Corresponding Author Address: Kelly Robbins krr75@cornell.edu , 240 Emerson Hall, Ithaca NY 14853

Abbreviations:

ATC: average tester co-ordination; RCBD: randomized complete block design; BLUE: best linear unbiased estimators; FY: Forage yield; GDD: growing degree days; GGE: genotype main effects and genotype by environment; GNDVI: green normalized difference vegetation index; G×E: genotype by environment; HTP: high-throughput phenotyping; MSI: multispectral imaging; NDRE: normalized difference red edge index; NDVI: normalized difference vegetation index; OSAVI: optimized soil adjusted vegetation index; NIR: near infrared; NMSU: New Mexico State University; RR: random regression; RRLP: random regression Legendre polynomial; SCCCI: simplified canopy chlorophyll content index; ST-GBLUP: single trait genomic linear unbiased prediction; VARI: visible atmospherically resistant index; VI: vegetative index; cVI: cumulative vegetative index;
UAV: unmanned aerial vehicle

Abstract

Multi-spectral imaging (MSI) collection by unoccupied aerial vehicles (UAV) is an important tool to measure growth of forage crops. Information from estimated growth curves can be used to infer harvest biomass and to gain insights in the relationship of growth dynamics and

harvest biomass stability across cuttings and years. In this study, we used MSI to evaluate Alfalfa (*Medicago sativa* L. subsp. *sativa*) to understand the longitudinal relationship between vegetative indices (VIs) and forage/biomass, as well as evaluation of irrigation treatments and genotype by environment interactions (GEI) of different alfalfa cultivars. Alfalfa is a widely cultivated perennial forage crop grown for high yield, nutritious forage quality for feed rations, tolerance to abiotic stress, and nitrogen fixation properties in crop rotations. The direct relationship between biomass and VIs such as Normalized difference vegetation index (NDVI), green normalized difference vegetation index (GNDVI), red edge normalized difference vegetation index (NDRE), and Near infrared (NIR) provide a non-destructive and high throughput approach to measure biomass accumulation over subsequent alfalfa harvests. In this study, we aimed to estimate the genetic parameters of alfalfa VIs and utilize longitudinal modeling of VIs over growing seasons to identify potential relationships between stability in growth parameters and cultivar stability for alfalfa biomass yield across cuttings and years. We found VIs of GNDVI, NDRE, NDVI, NIR and simple ratios to be moderately heritable with median values for the field trial in Ithaca, NY to be 0.64, 0.56, 0.45, 0.45 and 0.40 respectively, Normal Irrigation (NI) trial in Leyendecker, NM to be 0.3967, 0.3813, 0.3751, 0.3239 and 0.3019 respectively, and Summer Irrigation Termination (SIT) trial in Leyendecker, NM to be of 0.11225, 0.1389, 0.1375, 0.2539 and 0.1343, respectively. Genetic correlations between NDVI and harvest biomass ranged from 0.52 - .99 in 2020 and 0.08 - .99 in 2021 in the NY trial. Genetic correlations for NI trial in NM for NDVI ranged from 0.72 - .98 in 2021 and SIT ranged from 0.34- 1.0 in 2021. Genotype by genotype by interaction (GGE) biplots were used to differentiate between stable and unstable cultivars for locations NY and NM, and Random regression modeling approaches were used to estimate growth parameters for each cutting. Results showed high correspondence between stability in growth parameters and stability, or persistency, in harvest biomass across cuttings and years. In NM, the SIT trial showed more variation in growth curves due to stress conditions. The temporal growth curves derived from NDVI, NIR and Simple ratio were found to be the best phenotypic indices on studying the stability of growth parameters across different harvests. The strong correlation between VIs and biomass present opportunities for more efficient screening of cultivars, and the correlation between estimated growth parameters and harvest biomass suggest longitudinal modeling of VIs can provide insights into temporal factors influencing cultivar stability.

Introduction

Alfalfa (*Medicago sativa* L. subsp. *sativa*) is one of the most widely cultivated perennial forage crops in the world with many desirable attributes such as high-yield capacity, good forage quality, tolerance to abiotic stresses, and ability to fix nitrogen and nutrient cycling (Annicchiarico et al. 2015; Hill et al. 1988). In the U.S. alfalfa is the fourth most widely grown crop with an estimated annual value of 11.7 billion dollars (USDA/ARS 2020). Alfalfa is allogamous and autotetraploid (2n = 4x = 32) and its cultivars are synthetic populations consisting of heterozygous plants (Annicchiarico and Pecetti 2021). The genetic gain in alfalfa has approached stagnation in the past few decades due to several factors including the perennial nature of the crop (long breeding cycles), multiple harvests per year, inability to make gain in harvest index due to harvesting of the entire crop, the high cost of phenotyping, tetrasomic inheritance, high genotype by environment interaction (G×E), and high levels of non-additive variance (Annicchiarico et al. 2015; Acharya et al. 2020). The narrow-sense heritability (h^2) of biomass yield of alfalfa is as low as 0.20 – 0.30 (Annicchiarico 2015; Acharya et al. 2020; Riday and Brummer 2005) demanding extensive replications for phenotypic evaluation which further limits the size of breeding materials to be evaluated, ultimately leading to low selection efficiency. However, the ability to screen more materials will lead to higher effective selection intensities leading to improved response to selection.

In recent years, the advancement in high-throughput phenotyping systems, including multi-spectral imaging (MSI) platforms, have enabled the collection of high dimensional phenotypic data from large experiments and breeding trials. MSI provides an effective and non-destructive approach to evaluate the crop growth parameters throughout the crop growing season. A number of reflectance vegetation indices can be derived from spectral reflectance which have been efficiently used for large scale phenotyping and dynamic estimation of biomass greenness, nitrogen content, pigment composition, photosynthesis status and water content (Claudio et al. 2006; Mistele and Schmidhalter 2008; Schlemmer et al. 2005). MSI consists of a set of images acquired at narrow wavelength bands including both visible and near infrared (NIR) regions of the electromagnetic spectrum (Blasco et al. 2007; Chen et al. 2002). The Normalized Difference Vegetation Index (NDVI), estimated by considering the difference NIR and red wavelengths, is widely used to quantify biomass production. The green Normalized

Difference Vegetation Index (GNDVI) is estimated by measuring the difference between NIR and green wavelengths and is used to measure photosynthetic activity. Other vegetation indices such as Normalized Difference Red-Edge (NDRE), Optimized Soil Adjusted Vegetation Index (OSAVI), Simplified Canopy Chlorophyll Content Index (SCCCI), and Visible Atmospherically Resistant Index ($VARI_{green}$), have been used to predict grain yield but their use has been limited on quantification of crop biomass. Santana et al. (2021) evaluated the relationship between vegetation indices (VI)s obtained from multispectral imagery and leaf N content and yield-related traits in maize cultivars grown in different N levels, and found a positive relationship between NDVI, NDRE and grain yield under adequate N levels. Da Silva et al. (2020) evaluated the relationship between different VIs and soybean grain yield and verified a direct positive effect of NDVI and SAVI on grain yield of soybean. However, there are limited studies conducted on the relationship between different VIs and biomass yield of alfalfa crops, so further studies assessing the relationship between VIs and crop forage/biomass yield are needed. Identifying the cause-and-effect relationship between spectral and biomass yield provides an efficient phenotyping process in breeding programs. Genotypes with better spectral variables can be selected to achieve an efficient selection for biomass yield.

The use of MSI data could also be leveraged for monitoring crop growth over the growing season. Extensions of crop growth models have been proposed to incorporate functional relationships between the environmental variables and the phenotypic traits influencing yield and agronomic performance of elite breeding lines (Chapman et al. 2002; Chapman et al. 2003; Messina et al. 2015; Hammer et al. 2002; Chenu et al. 2009), and recent advancements in MSI have increased the scalability of collecting non-destructive phenotypes on a large number of experimental plots throughout the crop growth cycle. Collection of phenotypic data from multiple time points allows the monitoring of crop growth and development and hence, can increase the understanding of dynamic interactions of crop and environment.

The study of genotype by environment (G×E) interaction is one of the most important areas in plant breeding whereby breeders try to understand the stability and plasticity of the genotypes across different environments. In a perennial crop like alfalfa, the concept of persistence, or consistent performance across seasons in the same location, is a key trait for elite cultivar performance. While it may be viewed as a distinct concept from GxE, many of the same

124 factors driving GxE are likely to play a role in persistence. For the purposes of this study we will
125 use the terms stability, and instability, to encompass the concepts of GxE and persistence in
126 harvest biomass yield. The traditional approach to study GxE and persistence relies on terminal
127 traits such as harvest biomass yield, which lack the temporal resolution to study the driving
128 factors leading to inconsistent performance across cuttings and growing seasons. In such
129 scenarios, images taken throughout the production years of a stand can enable the longitudinal
130 evaluation of a large number of breeding materials, providing insights into growth characteristics
131 leading to the stability or instability of cultivar performance under differing conditions.
132 Important growth parameters could be evaluated by studying the changes in (co)variance
133 between adjacent time points and end-of-season traits. Quantitative genetic models can be built
134 to accurately predict forage yields from MSI, especially given that the harvested product is
135 imaged directly. However, the challenge lies on fitting parsimonious models that can accurately
136 model the changes in covariance parameters across the growing season.

137 The phenotypic indices from high-throughput phenotyping (HTP) platforms are measured
138 at multiple time points throughout the crop growing season and hence, are considered as
139 longitudinal data. Repeatability models, multi-trait models, and random regression (RR) models
140 are used to fit such longitudinal data. Repeatability models assume constant variance and
141 correlation between measurements dates, which may not be true for longitudinal data collected at
142 different time points throughout the crop growth cycle (Meyer and Hill 1997). In the case of
143 multi-trait models, phenotypic traits measured at different time points are considered as distinct
144 response variables for each cultivar. The number of parameters required to be estimated is
145 directly related to number of time points. Hence, a strong correlation between consecutive
146 measurements, large (co)variance matrix structure between measurements at different time
147 points, and computational requirements restrict the application of a multi-trait model (MT)
148 model (Speidel 2011; Anche et al. 2020). However, the RR model requires fewer parameters
149 than MT models, can capture the change of a trait throughout the growth season, and does not
150 require the assumption of constant variances and correlations between measurement time points
151 (Meyer, 2020). RR models enable fitting of genetic and environmental effects over time
152 (Schaeffer 2004), and hence results in higher accuracy of breeding values (BVs) compared to
153 other statistical models. RR model also provide additional insights on temporal variation of

biological and physiological processes underlying the trait of interest (Strucken et al. 2015) and these models have been widely used in different area of research including G×E (Calus and Veerkamp 2003; Oliveira et al. 2018). RR models commonly uses splines or Legendre polynomials to model the (co)variance of measurements at or between each time points. The objectives of this study were to (1) identify predictive image features for modeling growth and development curves for alfalfa.; (2) determine the heritability and genetic variation for image features collected throughout the growing season and (3) estimate the relationship between observed stability for development/growth parameters and stability for alfalfa biomass yield.

Materials and Methods

Experimental materials and biomass phenotyping

In this study, we analyzed the data from two experimental locations, (1) Cornell University Agricultural Research Experiment Station in Ithaca, NY, and (2) the Leyendecker Plant Science Research Center of New Mexico State University (NMSU) located near Las Cruces, New Mexico. A total of 36 cultivars were evaluated in the NY trial, representing both publicly released cultivars and breeding populations including 'Guardsman II'(Viands et al., 2005), 'Regen' (Viands et al., 2007), 'Algonquin' (Baenziger, 1975),'Oneida VR' (Viands et al., 1990), 'Oneida Ultra' (Viands et al., 2004), and 'Ezra' (Viands et al., 2012). Entries were planted on June 12, 2019, in a replicated trial with five replications in a randomized complete block design (RCBD). Plots were 6 rows of alfalfa that were 1 m by 4 m and the space between adjacent plots was 0.3 m. Forage yield was measured using a plot flail harvester, and dry matter yield for each plot was calculated from fresh forage weight and dry matter content samples. Forage yield (FY) was collected on June 5, July 9, and August 26 of 2020 and June 16, July 26, and September 13 of 2021.

A total of 24 cultivars and breeding populations with one covariate cultivar were planted in the NMSU trial on September 27, 2019. The experiment was conducted under two irrigation treatment conditions including normal irrigation (NI) and summer irrigation termination (SIT). The NI treatment received flood irrigations approximately every 14 days from March through late October. The SIT treatment only received flood irrigations from March through June and again from late September through October. Both treatment fields were planted as RCBDs with each having four replications. All experimental plots were located adjacent to a covariate plot of

the cultivar, 'NuMex Bill Melton' (Ray et al., 2012). Each plot was comprised of three rows of alfalfa, 3.35 m in length, with 30 cm spacing between rows within a plot, and 60 cm spacings between neighboring plots and alfalfa borders. Forage biomass was harvested in 2020 with six and three harvests occurring in the NI and SIT treatments, respectively. In 2021, forage biomass was harvested seven times in the NI treatment and six times in the SIT treatment fields. All forage biomass was harvested using a Carter flail harvester to collect fresh plot weights. Subsamples of fresh chop forage were collected, weighed, and dried down to establish dry matter weights.

Aerial phenotyping

NY trial

Aerial phenotyping for the NY trial commenced on April 6, 2020 in Ithaca, NY. A total of 56 flights were conducted throughout the crop growth season. A total of 7, 6, and 7 flights were flown before the first harvest (2020cut1), second harvest (2020cut2) and third harvest in 2020 (2020cut3) and a total of 22, 8, and 6 flights were flown before the first harvest (2021cut1), second harvest (2021cut1) and third harvest of 2021 (2021cut1). Four ground control points positioned at the four corners of the trial were measured with a Trimble RTK-GPS, which was used to geo-locate plots. A DJI Matrice 600 Pro unmanned aerial vehicle (UAV) equipped with a Micasense Rededge-MX multi-spectral camera was used for all flights. A flight plan was designed to obtain an 80% overlap in images collected at a flight speed of 2 m/s and an altitude of 20 m. Flights were conducted within 2 hours of solar noon on clear days when possible.

NMSU trial

Due to UAV equipment unavailability in 2020 and early 2021, aerial phenotyping commenced on June 3, 2021, during the third harvest cycle's regrowth initiation for both the NI and SIT trials. A total of five harvests data from NI including NIcut3, NIcut4, NIcut5, NIcut6, NIcut7 and a total of four harvests from SIT trials including SITcut3, SITcut4, SITcut5, SITcut7 from 2021 were used for crop growth modelling and stability analysis. Ground control points were included near the four corners of each treatment field. The control points were placed on permanent stand mounts prior to each imagery flight. Upon installation, each stand was geo-located using an RTK-GPS. Multispectral imagery was captured using a DJI Matrice 600 Pro UAV and a MicaSense RedEdge-MX camera. All imagery was captured with 75% side overlap and 80% front overlap from a 20m altitude at 2.0 m/s. Imagery for both irrigation treatment

fields was captured within the same flight cycle. Flights were conducted in mornings (10:00am – 12:00pm), within 3 hours of solar noon, while temperatures were cool enough to not affect UAV performance. Imagery capture occurred once per week, averaging five flights per harvest cycle, with the last flight occurring no more than two days prior to each biomass harvest. In total, 25 imaging flights were conducted over the NMSU alfalfa studies in 2021.

Image processing and index calculations

Orthomosacis were constructed using Pix4D mapping software (https://www.pix4d.com), and were subsequently uploaded into Imagebreed (www.imagebreed.org), a plot image database (Morales et al. 2020), for image processing and storage and calculation of vegetative indices (VI) at the plot level. Using these summary statistics, multiple VIs were calculated for each plot. Normalized difference vegetation indices (NDVI) were calculated from mean pixel values of near infrared (NIR) and Red bands of plot level images as:

$$NDVI = \frac{(R_{NIR} - R_R)}{(R_{NIR} + R_{R)}} \quad (1)$$

where R_{NIR} is the near infrared reflectance and R_R is the red reflectance. Green normalized difference vegetation indices (GNDVI) and Normalized difference red edge indices (NDRE) were calculated using green and red edge reflectance instead of the red reflectance in Eq. 1, respectively.

A simple Ratio was calculated as:

$$Ratio = \frac{R_{NIR}}{R_R} \quad (2)$$

Additionally, the cumulative value of the above mentioned phenotypic indices at a specific time point, *t*, was calculated using using the rollmean function of zoo package in *R* statistical software that takes phenotypic indices values and growing degree day(s) (GDD)(s) at each time point. The equation is represented as:

$$AUC_t = NDVI_1 + \sum_{i=1}^{t} (\Delta D_i \times rollmean(NDVI_i, 2)) \quad (3)$$

where AUC_t represents the calculated AUC value at time point *t*, ΔD_i represents the time interval between consecutive time points ($\Delta D_i = 0$ for time point 1) , $rollmean(NDVI_i, 2)$ represents the rolling mean of NDVI values at time point *t*, and $NDVI_i$ represents the NDVI value at time point *t*.

GDDs were calculated as:

$$GDD = \frac{T_{max} + T_{min}}{2} - T_{base} \quad (4)$$

where T_{max} is the maximum temperature, T_{min} is the minimum temperature, and T_{base}= 4 °C as the base temperature. The GDDs calculated for each time point were used as time covariates in the RR models. For the first cuttings, GDDs were calculated starting on date of planting and up to and including the date of harvest. For subsequent harvests, GDDs were calculated starting from the day after the preceding harvest. The GDDs calculated for each time point were used as time covariates in the RR models.

Models

A single-trait best linear unbiased prediction (ST-BLUP) model was fit to estimate the genetic and residual variances. The ST-BLUP is defined as:

$$\boldsymbol{y} = \mathbf{1}\mu + \mathbf{X}\boldsymbol{b} + \mathbf{Z}\boldsymbol{g} + \boldsymbol{e} \quad (5)$$

where $\boldsymbol{y}$ is the vector of raw phenotype variables (phenotypic indices derived from MSI in this study), $\mathbf{1}$ is the vector with elements of 1; μ is the overall mean; $\boldsymbol{b}$ is the vector of fixed effect of replicate; $\mathbf{X}$ is the design matrix that associates the fixed effect of replicates with response variables; $\mathbf{Z}$ is the design matrix with $\boldsymbol{g}$ as a vector of random genetic effects $\boldsymbol{g} \sim N(\mathbf{0}, \mathbf{I}\sigma_g^2)$; $\boldsymbol{e}$ is the vector of random residuals modeled as $\boldsymbol{e} \sim N(\mathbf{0}, \mathbf{I}\sigma_e^2)$ with an identically and independently normal distribution of residuals and $\mathbf{I}$ is the identity matrix.

The ratio of estimated genetic variance to the sum of the genetic variance and residual variance was calculated to represent the broad sense heritability of biomass yield, and phenotypic indices derived from MSI.

A bi-variate multi-trait model was fit to estimate the genetic and residual correlations between biomass yield and mean values of VIs at each time point.

$$\begin{bmatrix}\boldsymbol{y_1}\\ \boldsymbol{y_2}\end{bmatrix} = \begin{bmatrix}1 & \mu_1\\ 1 & \mu_2\end{bmatrix} + \begin{bmatrix}\mathbf{X_1} & \mathbf{0}\\ \mathbf{0} & \mathbf{X_2}\end{bmatrix}\begin{bmatrix}\boldsymbol{b_1}\\ \boldsymbol{b_2}\end{bmatrix} + \begin{bmatrix}\mathbf{Z_1} & \mathbf{0}\\ \mathbf{0} & \mathbf{Z_2}\end{bmatrix}\begin{bmatrix}\boldsymbol{g_1}\\ \boldsymbol{g_2}\end{bmatrix} + \begin{bmatrix}\boldsymbol{e_1}\\ \boldsymbol{e_2}\end{bmatrix} \quad (6)$$

where $\boldsymbol{y_1}$ and $\boldsymbol{y_2}$ are the vector of response variables of traits 1 and 2; μ_1 and μ_2 are the overall means; $\boldsymbol{g_1}$ and $\boldsymbol{g_2}$ are the vectors of random genetic effects; $\boldsymbol{b_1}$ and $\boldsymbol{b_2}$ are the vectors of replication effects; $\mathbf{X_1}$ and $\mathbf{X_2}$ are the incidence matrices linking $\boldsymbol{b_1}$ to $\boldsymbol{y_1}$ and $\boldsymbol{b_2}$ to $\boldsymbol{y_2}$; $\mathbf{Z_1}$ and $\mathbf{Z_2}$ are the incidence matrices linking $\boldsymbol{g_1}$ to $\boldsymbol{y_1}$ and $\boldsymbol{g_2}$ to $\boldsymbol{y_2}$; $\boldsymbol{e_1}$ and $\boldsymbol{e_2}$ are vectors of random residual effects for trait 1 and 2, respectively. It was also assumed that $[\boldsymbol{g_1} \quad \boldsymbol{g_2}] \sim N(\mathbf{0}, \mathbf{\Sigma} \otimes \mathbf{I})$, where $\mathbf{\Sigma} = \begin{bmatrix}\sigma^2_{g_1} & \sigma_{g_{12}}\\ \sigma_{g_{21}} & \sigma^2_{g_2}\end{bmatrix}$ is the unstructured genetic variance and covariance matrix of the traits and $[\boldsymbol{e_1} \quad \boldsymbol{e_2}] \sim N\left(\mathbf{0}, \begin{bmatrix}\sigma^2_{e_1} & \sigma_{e_{12}}\\ \sigma_{e_{21}} & \sigma^2_{e_2}\end{bmatrix} \otimes \mathbf{I}\right)$.

Random regression

Random regression models using third order of Legendre polynomials (RRLP) were used to fit a model for mean VI values and cumulative values of VI (cVI) from all time points. The biomass yield data was used as the final time point observations in the model. The variance of biomass yield was scaled to match the variance of preceding observation of VIs ensuring that yield data has similar variability pattern as VIs. The RR models were used to continuously model the (co)variance of VI and cVI measurements at different time points as a function of time.

The general random regression model for a single trait can be formulated as (Schaeffer 2004):

$$\mathrm{VI}_{tj} = \beta_{r(t)} + \sum_k^{K2} \phi(t)_{jk} u_{jk} + \sum_k^{K3} \phi(t)_{jk} p_{jk} + \boldsymbol{\epsilon}_{tj} \quad (7)$$

where, VI_{tj} is the plot level value of the j^{th} accession for VI at time point t; $\phi(t)_{jk}$ is a time covariate coefficient defined by a basis function evaluated at time point t; $\beta_{r(t)}$ is the fixed effect

or replicate *r* nested in time point *t*; u_{jk} is a k^{th} random regression coefficient associated with the genetic effects of the j^{th} accession; $K1$ is the number of random regression parameters for fixed effect time trajectories; $K2$ and $K3$ are the number of random regression parameters for random effects; p_{jk} is a k^{th} permanent environmental random regression coefficient for the accession *j*; ϵ_{tj} is the vector of residuals. The random effects at any time point were calculated as a function of the estimated RR coefficients and standardized measure of GDDs calculated from equation 3 on a per harvest basis during the growing season.

GGE biplot analysis

The genotype main effect plus genotype by environment (GGE) biplot analysis was performed using the statistical R package called "metan" (Olivoto and Lúcio 2020). Mean biomass yield and its stability for all genotypes were visualized using GGE biplot. The GGE biplots were constructed by plotting the first principal component (PC1) against the second principal component (PC2) of the genotypes and environment calculated from a genotype-focused singular value decomposition. The following GGE biplot model was used (Yan and Kang 2002):

$$Y_{ij} - Y_j = l_1 x_{i1} h_{j1} + l_2 x_{i2} h_{j2} + e_{ij} \quad (8)$$

where Y_{ij} is the mean biomass yield of genotype *i* in environment *j*; Y_j is the mean yield across all genotypes in environment *j*; l_1 and l_2 are the singular values for PC1 and PC2, respectively; x_{i1} and x_{i2} are the PC1 and PC2 scores, respectively, for genotype *i*; h_{j1} and h_{j2} are the PC1 and PC2 scores, respectively, for environment *j*; and e_{ij} is the residual of the model associated with genotype *i* in environment *j*.

Correlation between variance in biomass yield across environments and variance in VIs across environments

In order to have both the yield data and VIs in the same scale, z-score normalization was done by subtracting the mean (μ) from the distribution and by dividing with the standard deviation of the distribution (σ). The z-score normalization was done for each environment. Each environment was defined as a specific planting location and growth period. The correlation between the

variance in yield and the variance in VIs of each genotype across locations was calculated using Pearson's correlation method for both NY and NM trials.

Results

Heritability of phenotypic indices and biomass yield

For the Helfer trial, the minimum heritability of GNDVI, NDVI, NDRE, NIR and Ratio was 0, whereas the maximum heritability of GNDVI, NDVI, NDRE, NIR and Ratio was 0.92, 0.84, 0.92, 0.88 and 0.85, respectively (Fig. 1). The maximum heritability value of GNDVI and NDRE was highest among all indices followed by NIR. The median value of heritability was highest for GNDVI, followed by NDRE, NDVI, NIR and Ratio, 0.64, 0.56, 0.45, 0.45 and 0.40, respectively (Fig. 1). For 2020, the heritability of biomass yield was highest for the first harvest (0.56) followed by the third harvest (0.32) and second harvest (0.31). For 2021, the heritability was highest for the third harvest (0.62) followed by the second harvest (0.57) and the first harvest (0.31).

For the NMSU trial in 2021, the minimum and median heritability values of the phenotypic indices under NI were higher than those under SIT whereas the maximum heritability of the phenotypic indices were higher under SIT. Under the NI, GNDVI, NDVI, NDRE, NIR and Ratio had minimum heritability values of 0.1827, 0.1076, 0.1867, 0 and 0.1112, respectively. Maximum heritability values for NMSU, GNDVI, NDVI, NDRE, NIR and Ratio were 0.7122, 0.7015, 0.6987, 0.662 and 0.6972, respectively; and median heritability values were 0.3967, 0.3813, 0.3751, 0.3239 and 0.3019, respectively (Fig. 2(a)).

Under SIT, GNDVI, NDVI, NDRE, NIR and Ratio had minimum heritability values of 0.0357, 0.027, 0.0209, 0.028 and 0.0189 respectively. Maximum heritability values for GNDVI, NDVI, NDRE, NIR and Ratio were 0.7824, 0.7764, 0.7377, 0.6905 and 0.7047 respectively; and median heritability values were 0.11225, 0.1389, 0.1375, 0.2539 and 0.1343 respectively (Fig. 2(b)). Under NI, the heritability of biomass yield was highest for seventh (0.40) followed by third (0.31) and fourth (0.29). Under SIT, the heritability of biomass yield was highest for sixth (0.79) followed by the third (0.196) harvest (Fig. 2(b)).

Phenotypic correlation of phenotypic indices and biomass yield

For the Ithaca, NY trial, the last imaging of the crop growing season was taken 9, 3 and 4 days before the first, second and third harvest of 2020, respectively, and 6, 3, and 3 days before first, second and third harvest of 2021, respectively. For both years the genetic correlation of all phenotypic indices with biomass yield was strongest for the second harvest followed by the third harvest and first harvest (Fig. 3(a), Fig. 3(b)).

Among all phenotypic indices in 2020, the phenotypic correlation with biomass yield was strongest for NIR (0.57) followed by Ratio (0.56) and NDVI (0.56) for the first harvest; Ratio (0.81) followed by NDVI (0.78) and GNDVI (0.76) for the second harvest; and GNDVI (0.68) followed by NIR (0.65) and NDRE (0.64) for the third harvest (Fig. 3(a)). In 2021, the phenotypic correlation with biomass yield was strongest for Ratio (0.19), followed by GNDVI (0.18) and NDVI (0.15) for the first harvest; the phenotypic correlation with biomass yield was strongest for GNDVI (0.78) followed by NDRE (0.74) and NDVI (0.64) for the second harvest; the phenotypic correlation with biomass yield was highest strongest for NDRE (0.73) followed by GNDVI (0.61) and NDVI (0.58) for the third harvest (Fig. 3(b)).

Genetic correlation between biomass yield and phenotypic indices at different imaging time points

NY trial

For the first harvest of 2020, biomass yield demonstrated the highest genetic correlations with NDVI (range: 0.90 – 0.99) and NIR (range: 0.93 – 0.99) whereas biomass yield had lowest correlation with Ratio (range: 0.69 - 0.96) (Fig. 4). For the second and third harvests of 2020, Ratio showed the highest genetic correlations with ranges of 0.94 - 0.99 and 0.69 - 0.99, respectively, while NDRE had the lowest genetic correlations ranging from 0.18 to 0.94 and 0.70 to 0.98, respectively (Fig. 4).

For the first harvest of 2021, the genetic correlation of Ratio and NIR with the biomass yield was strongest ranging from 0.68 – 0.99 and 0.1 – 0.99 respectively. The genetic correlation of NIR with biomass yield was lower than other phenotypic indices in early crop growth stage for the same harvest (Fig. 4). This pattern was only seen for one harvest out of six harvests. For the second and third harvest of 2021, the genetic correlation of NIR was strongest for second

harvest and third harvest ranging from 0.84 – 0.99 and 0.91 to 1 respectively whereas genetic correlation of NDVI and GNDVI had lowest genetic correlations for second and third harvest. The genetic correlation of second and third harvest of NDVI ranged from 0.08 to 0.94 and 0.72 to 0.99 respectively for second and third harvest and the genetic correlation of second and third harvest of GNDVI ranged from 0.53 – 0.98 and 0.23 to 0.97 respectively (Fig. 4).

NMSU trial

Under NI, the genetic correlation of NDVI and Ratio at all imaging time points were highest for all harvests except for June 25 to Jul 22 regrowth cycle of 2021 (Fig. 5). The genetic correlation of NDVI ranged from 0.8 to 0.97 for May 28 to June 24 regrowth cycle , 0.72 to 0.97 for June 25 to Jul 22 regrowth cycle, 0.78 to 0.96 for July 23 to August 27 regrowth cycle , 0.77 to 0.97 for August 28 to September 29 regrowth cycle, 0.88 to 0.98 for September 30 to November 12 regrowth cycle and the genetic correlation of Ratio ranged from 0.69 to 0.95 for May 28 to June 24 regrowth cycle, 0.69 to 0.97 for June 25 to Jul 22 regrowth cycle, 0.69 to 0.94 for July 23 to August 27 regrowth cycle, 0.69 to 0.96 for August 28 to September 29 regrowth cycle, and 0.69 to 0.97 for September 30 to November 12 regrowth cycle (Fig. 5).

Under SIT, NDVI and Ratio had highest genetic correlation with biomass yield compared to other phenotypic indices. Genetic correlations ranged from 0.84 to 0.97 for May 28 to June 25 regrowth cycle, 0.91 to 0.97 for June 26 to Jul 22 regrowth cycle, 0.99 to 1 for July 23 to August 26 regrowth cycle and 0.69 to 0.99 for August 27 to November 11 regrowth cycle for NDVI and genetic correlation ranged from 0.69 to 0.95 for May 28 to June 25 regrowth cycle, 0.69 to 0.91 for June 26 to Jul 22 regrowth cycle, 0.69 to 1 for July 23 to August 26 regrowth cycle and 0.69 to 0.99 for August 27 to November 11 regrowth cycle for Ratio (Fig. 6).

Genetic correlation among phenotypic indices at different imaging time points

Ithaca, NY trial

The genetic correlation of phenotypic indices at different time points were evaluated running multi-trait models Supplemental Figure 1 (a) to (e)). The genetic correlation among NIR and Ratio at different time points were strongest compared to other indices (Supplemental Figure

1 (d), Supplemental Figure 1 (e)). The genetic correlation of Ratio at different time points were greater than 0.71 for all harvests of 2020 and 2021 except for the first harvest of 2021, where genetic correlations between the first time point and the last 14 time points ranged from 0.49 to 0.67. The genetic correlations among NIR at different time points were greater than 0.65 for all harvests of 2020 and 2021 except for third harvest of 2020 and first harvest of 2021, where the genetic correlations ranged from -0.17 to 0.04 between first and last five imaging time points and 0.04 to 0.05 between first and last 14 imaging time points. The genetic correlations of NDVI, GNDVI, and NDRE at different time points were in the range of 0.52 – 1, 0.2 -1, and 0.18 – 0.1, respectively, for all three harvests of 2020 and the third harvest of 2021. Genetic correlations were lower for first and second harvest of 2021 across all harvests (Supplemental Figure 1 (a) to (e)). The genetic correlation of cumulative value of all the indices from second time point to other time points were 1 whereas the genetic correlation of cumulative value of all the indices of first time point with other time points were in the range of 0.9 – 0.99 (Supplemental Figure 2 (a) to (e)).

NMSU trial

Under NI, among all phenotypic indices, the genetic correlation of NDVI and Ratio at different time points were strongest (Supplemental Figure 3 (c), Supplemental Figure 3 (e)). The genetic correlation of Ratio at different time points ranged from 0.69-0.98, 0.69-0.97, 0.69-0.98, 0.69-0.99, 0.69-0.98 for the May 28 to June 24 regrowth cycle, June 25 to Jul 22 regrowth cycle, July 23 to August 27 regrowth cycle, August 28 to September 29 regrowth cycle and September 30 to November 12 regrowth cycle, respectively (Supplemental Figure 3 (e)). Similarly, the genetic correlation of NDVI at different time points ranged from 0.72 - 0.99, 0.74 – 0.97, 0.76 – 0.98, 0.76 – 0.99 and 0.81 – 0.99 for the May 28 to June 24 regrowth cycle, June 25 to Jul 22 regrowth cycle, July 23 to August 27 regrowth cycle, August 28 to September 29 regrowth cycle and September 30 to November 12 regrowth cycle, respectively (Supplemental Figure 3 (c)). The genetic correlations of NIR, GNDVI, and NDRE at different time points were lowest compared to other indices (Supplemental Figure 3 (d), Supplemental Figure 3 (a), Supplemental Figure 3 (b)). The genetic correlation of the cumulative value of all the phenotypic indices of first time points with other time points were 0.99 and 1.0 for all other time points (Supplemental Figure 4 (a) to (e)).

Similarly, under SIT, the genetic correlation of Ratio and NDVI at different time points were strongest (Supplemental Figure 5 (a) to (e)). The genetic correlation of Ratio at different time points ranged from 0.69 – 0.98, 0.69 – 0.98, 0.69 – 1 and 0.69 – 0.99 for the May 28 to June 25 regrowth cycle, June 26 to Jul 22 regrowth cycle, July 23 to August 26 regrowth cycle and August 27 to November 11 regrowth cycle, respectively (Supplemental Figure 5 (e)). Similarly, the genetic correlation of NDVI ranged from 0.54 – 0.97, 0.56 – 0.97, 0.79 – 1, 0.34 – 0.98 for the May 28 to June 25 regrowth cycle, June 26 to Jul 22 regrowth cycle, July 23 to August 26 regrowth cycle and August 27 to November 11 regrowth cycle, respectively (Supplemental Figure 5 (a)). Among the other indices at different time points, the genetic correlation among GNDVI ranged from 0.59 – 0.97, 0.49 – 0.96, 0.58 – 1, 0.06 – 0.98 for the third, fourth, fifth and seventh harvest, respectively (Supplemental Figure 5 (a)), NDRE ranged from 0.71 – 0.98, 0.56 – 0.97, 0.48 – 1, -0.09 – 0.97 for the May 28 to June 25 regrowth cycle, June 26 to Jul 22 regrowth cycle, July 23 to August 26 regrowth cycle and August 27 to November 11 regrowth cycle harvest, respectively (Supplemental Figure 5 (b)), and NIR ranged from 0.2 – 0.95, 0.65 – 0.98, 0.12 – 1, and -0.05 – 0.98 respectively for May 28 to June 25 regrowth cycle, June 26 to Jul 22 regrowth cycle, July 23 to August 26 regrowth cycle and August 27 to November 11 regrowth cycle, respectively (Supplemental Figure 5 (d)). The genetic correlation of the cumulative value of all the phenotypic indices of first time points and other time points were 0.99 whereas for other time points were 1 (Supplemental Figure 6 (a) to (e)).

Growth curve analysis using genetic merit calculated from Random Regression Model

The temporal growth curves of all alfalfa genotypes were constructed using breeding values calculated using RRLP and different phenotypic indices as longitudinal phenotypic traits (Supplemental Figures 7, 8, 9). The high-resolution temporal growth curves of different alfalfa genotypes showed clear differences between high yielding and low yielding genotypes. Both raw values of phenotypic indices and their respective cumulative values were used to run RR model. Compared to the raw value, cumulative value of phenotypic indices gave better model fit and higher resolution of temporal growth curves (Supplemental Figure 7(f) to 7(j), Supplemental Figure 9(f) to 9(j)). Using the raw value of phenotypic indices as the phenotypic trait, a larger spread in breeding values of the genotypes were observed in the early stages of growth,

indicating greater genetic variance captured by the proximal sensing phenotypes in early growth stages.

GGE biplot analysis

The GGE Biplots in Figs. 7 and 8, provide a "mean versus stability" graph of cultivar performance in NY and NMSU trials, respectively (Yan et al. 2007). The green single arrowed line, referred to as the "average environment axis", provides an indication of the mean performance of cultivars, with the arrow pointing to a greater value according to their mean performance across all environments. The green line that is perpendicular to the average environment axis, provides an indication of stability in cultivar performance across environments. As such, cultivars with projections closer to the average environment axis exhibited more stable performance for harvested biomass across cuttings and years. An ideal cultivar would have a high mean performance, further along in the average environment axis in the direction indicated by the arrow, and would show stable performance with a projection near the average environment axis. For the cultivars tested in NY (Fig. 7), the cultivars g1, g2, g10, g29, and g32 were relatively stable and high yielding, and g8 was relatively stable and low yielding. Cultivars g3, g13, g18, g22, g31 were relatively unstable and low yielding, and g4, g15, g20, g23 were relatively unstable and high yielding. A similar analysis was applied to the NMSU trial data (Fig. 8), identifying G13, G14 and G15 as stable and low yielding cultivars, and G25, G7 and G9 as relatively stable and high yielding cultivars. Results indicate that G24, G23 and G21 were relatively unstable and high yielding, and G2, G8, G15, G17 were relatively unstable and low yielding.

Stability and plasticity analysis using a growth curve modeling approach.

Among the most unstable and stable genotypes identified from GGE biplot analysis, five stable and five unstable cultivars were selected (Fig.7, Fig.8). To determine whether stability in biomass yield across cuttings was reflected in the plasticity of the plant growth, the growth curves of these most stable and unstable cultivars across different environments were plotted (Fig.9 - Fig.25). Results showed high variance in the growth curves of unstable cultivars across all cuttings when compared to the stable cultivars in the Ithaca, NY trial (Fig.9 - Fig.13). Similar, although less pronounced, results were observed for NMSU trial (Fig.14 - Fig.17). Among all phenotypic indices, the growth curves estimated using NDVI and Ratio at Ithaca, NY were found

to give clear separation in the stability and plasticity (Fig.10, Fig.13). Both the stable and unstable cultivars were found to be more stable in NI than SIT of NMSU (Fig.18 – Fig. 25), with differing growth patterns between the two irrigation treatments.

Using GNDVI, NDVI and Ratio as the phenotypic trait, the variance of stable cultivars g1, g2, g6, g8, and g14 across all environments were less than the variance of unstable cultivars g3, g13, g21, g22, g35 (Fig. 9, 10, 13) in Ithaca, NY trial. There was more separation during early growth among the cultivars than at later timepoints. Similar results were observed for NMSU trial. The temporal growth curves derived from NDVI, NIR and Ratio were found to be the best discriminating the variance of genetic merit for stable and unstable cultivars across different harvests (Fig. 15, Fig. 16, Fig. 17).

Stability and plasticity analysis across different irrigation conditions

The growth trajectories of stable and unstable cultivars were compared separately across all cuttings of NI and SIT conditions (Fig. 18 to Fig. 25). The variance in growth curves of both stable cultivars derived from GNDVI, NDVI and Ratio were found to be higher in summer irrigation termination condition than in normal irrigation condition (Fig. 18, Fig. 20, Fig. 24). Similar results were observed for unstable cultivars (Fig. 19, Fig. 21, Fig. 25).

Correlation of variance in yield and variance in genetic merit of phenotypic indices across different environments

The variance in yield of all genotypes across different harvests was calculated for both NY and NMSU trials. Similarly, the variance in genetic merit of all genotypes for VIs at different time points across cuttings was calculated to determine if there was a relationship between variation in growth curves and variation in harvest biomass. The estimated correlation between the variance in yield and variance in genetic merit estimated from VIs at different time points showed a significant correlation in NY, with values ranging from 0.61 to 0.67, 0.63 to 0.66, 0.60 to 0.71, 0.66 to 0.68, and 0.37 to 0.43 for NDVI, GNDVI, NDRE, NIR and Ratio respectively (Table 1). For trials in NM, the correlation between the variance in harvest biomass and the variance in genetic merit

estimated from growth curves of all genotypes at different time points across different harvests showed correlations that ranged from 0.19 to 0.35, 0.27 to 0.44, 0.16 to 0.36, 0.68 to 0.79 and 0.91 to 0.93 for GNDVI, NDVI, NDRE, NIR and Ratio, respectively (Table 2).

Discussion

One of the objectives of this study was to evaluate the heritability of VIs derived from MSIs and their genetic correlation with the terminal trait biomass yield. Results of this study showed that the VIs have a moderate heritability (Fig 3, Fig 4) comparable to the heritability of harvest biomass. Lower heritability was attributed to poor days of imaging such as the days with cloudy and windy weather. Babar et al. (2007) reported moderate to high heritability of spectral reflectance indices (SRIs) and higher heritability than for grain yield in wheat. Petsoulas et al. (2022) reported moderate to high level of broad sense heritability where the heritability of NDRE ranged from 0.292 to 0.879 and heritability of NDVI ranged from 0.446 to 0.928 in sesame. In the same study, heritability of VIs were reported to be increased with growth stages and started to reduce entering the ripening stage of sesame whereas Anche et al. (2020) reported lower heritability of VIs in early reproductive stage and higher heritability estimates at mid-reproductive stage and late reproductive stage of maize. Another study from (Galán et al. 2020), showed moderate to high heritability estimates ($H2 > 0.50$) of 23 VIs in winter rye hybrids estimated from hyperspectral reflectance data. Sun et al. (2017) reported that the heritability of NDVI and NDRE ranged from moderate to high across different locations of wheat trial. Sharma et al. (2022) reported consistently higher heritability of VARI and NDVI across growth phases and locations where NDVI and VARI had higher heritability than dry biomass yield. In our study, among all five VIs, GNDVI had highest value of maximum and median heritability. GNDVI measures reflection in near infra-red region and green region of the electromagnetic spectrum (Gitelson et al. 1996). GNDVI provides information about chlorophyll A concentration in plants. The higher heritability of GNDVI might be due to the high biomass of the crop. Sandhu et al. (2021) reported GNDVI as the best predictor of grain protein content of wheat. Previous studies (Hassan et al. 2019; Yang et al. 2020) also reported GNDVI and NDRE as the best predictor of grain yield and nutrient uptake efficiencies across the growth stages.

572 Multi-trait models were fit to evaluate the correlation between VIs at different time points
573 and harvest biomass yield. The genetic correlations of all five VIs and the biomass yield was
574 found to be strong and statistically significant for all harvests and years. Among five VIs, NIR,
575 NDVI and Ratio had the strongest genetic correlations with biomass. Natarajan et al. (2019)
576 reported a strong correlation between NDVI and sugarcane stalk population and sugarcane yield
577 suggesting that canopy reflectance measurements at an early stage could be used as a screening
578 tool to estimate yield potential. Another study by Prabhakara et al. (2015) used NDVI for
579 prediction of biomass percentage of ground cover in winter forage crops. Other studies have also
580 reported significant association between NDVI and both biomass and GY in irrigated or high-
581 rainfall conditions (Reynolds et al. 1999; Aparicio et al. 2000; Freeman et al. 2003; Gutiérrez-
582 Rodríguez et al. 2004; Babar et al. 2006a; Prasad et al. 2007b; Erdle et al. 2013; Christopher et
583 al. 2014) drought stress (Gutiérrez-Rodríguez et al. 2004; Babar et al. 2006b; Reynolds et al.)
584 and heat stress environments (Reynolds et al. ; Gutierrez et al. 2010; Hazratkulova et al. 2012;
585 Lopes and Reynolds 2012). NDVI was also reported to predict grain yield in soybean (Ma et al.
586 2001), winter wheat (Raun et al. 2001), and durum wheat (Aparicio et al. 2000). The VIs NDVI,
587 GNDVI, SAVI, G-R were reported to be accurate for estimating biomass at an early stage
588 (Prabhakara et al. 2015) and they were saturated at later stages (Mutanga and Skidmore 2004;
589 Thenkabail et al. 2000). Chen et al. (2009) reported TVI (Triangular Vegetative Index) as useful
590 index for predicting canopy biomass at later stage. NDVI and SR are based on the red (visible)
591 and NIR wavelengths and give higher values at early growth stages, but their values decrease
592 with the advancement in growth cycle because plants are losing photosynthetically active plant
593 parts. Serrano et al. (2000) reported that simple ratio (SR) can reliably predict winter wheat grain
594 yield under nitrogen stresses. Among the three spectral indices, simple ratio (SR), normalized
595 difference vegetation index (NDVI), and photochemical reflectance index (PRI), SR was
596 identified as the best index for assessment of crop growth and yield in durum wheat (Aparicio et
597 al., 2000). Another study by Gutierrez et al. (2004) found the strongest correlation of SR and
598 NIR with cotton lint yield showing 60% and 58% of variations in cotton lint yield respectively.
599 In the same study, SR and NIR had higher coefficients of determination in cotton biomass and
600 leaf area index (LAI) compared to NDVI as these indices were not saturated at late growth stage
601 whereas (Aparicio et al. 2000; Aparicio et al. 2002) reported that NDVI and SR were not able to
602 predict variations in biomass successfully when estimated at later growth stages of durum wheat.

603 Hence, the use of multiple indices is recommended to get better predictions of biomass yield as
604 different types of VIs are sensitive to different stages of crop growth and amount of biomass.
605 The high heritability and strong genetic correlation between VIs and biomass yield of alfalfa in
606 our study suggest that VIs can be used as a selection tool and help plant breeders to reliably
607 evaluate cultivars in a fast and nondestructive (Lobos et al. 2019; El-Hendawy et al. 2019;
608 Prasad et al. 2007a; Babar et al. 2007; Gutierrez et al. 2010).
609
610 RR models with third order Legendre polynomials provided the best fit and were used to
611 model the growth curve trajectories using VIs as phenotypes. Estimate RR coefficients were used
612 to obtain breeding values (BVs) for all time points between the first day of imaging and harvest.
613 Sun et al (2017) used RR model with cubic splines in wheat (*Triticum aestivum*) to obtain best
614 linear unbiased predictions of secondary traits derived from high-throughput hyperspectral and
615 thermal imaging. RR model with a linear spline was also reported as a potential alternative
616 approach to mixed model to fit the VIs from multiple time points (Anche et al. 2020), but
617 Legendre polynomials were found to provide a better fit to maize data in subsequent analyses
618 (Anche et al. 2023). When cumulative indices were used as phenotypes, the correlation was
619 found to increase through time (Fig 3-6). This could be because cumulative indices accounts for
620 earlier season VI data, and therefore becomes more informative than raw data on predicting
621 biomass yield of the growing season. Similar results were reported in maize (Anche et al. 2023),
622 concluding that cumulative VIs were better phenotype to model the covariance structures as they
623 provided more stable and consistent results compared to using raw VIs as a phenotype.
624
625 In our study, we observed a decreasing trend in the variance components over time for
626 each harvest. Higher genetic variation was observed in the breeding values of VIs in early
627 growth stages compared to later stages as cultivars reached full canopy cover. In alfalfa stands,
628 allowing the crop to reach maximum vegetation saturation before flowering is the ideal balance
629 to develop maximum biomass while also maintaining nutritional quality. A declining ability of
630 spectral indices to discriminate different genotypes was reported in other crops as the canopy
631 closes and its spectral reflectance saturated (Marti et al. 2007). In this study, all VIs showed
632 strong correlations with biomass yield across all time points, and the growth trajectories could

633 separate high yielding and low yielding genotypes rapidly and efficiently starting in the early
634 stage of growth season.
635
636 The moderate heritability and moderate to strong genetic correlations with harvest
637 biomass observed in NY and NM trials, indicate that VIs collected via UAV can be used to
638 model temporal genetic variation associated with harvest biomass yield. RR models provided a
639 parsimonious approach to estimate temporal covariance functions and assess cultivar persistence
640 and stability, which can be affected by biotic and abiotic effects of the environment. The RR
641 model depicted dynamic aspects of phenotypes, which can enable better analysis cultivar
642 plasticity, adaptability, stability and yield performance (Alves et al. 2020) across a range of
643 dynamic environmental conditions through growth periods. As such, information on growth
644 curves can provide additional information for selecting lines that are best adapted to the target
645 environments.
646
647 The growth trajectories of stable genotypes and unstable genotypes in NI and SIT
648 termination of NMSU trial showed more instability in growth curves in SIT than NI (Figs 18 to
649 25). This is likely due to higher genetic variance among different cultivars in stressed
650 environment compared to normal condition and indicates that growth parameters may provide
651 additional information on stress tolerance. The observed correspondence in plasticity of growth
652 curves and stability in biomass harvest demonstrate the potential to model GxE temporally
653 throughout the growth period as a function of dynamic environmental variables. Esten et al.
654 (2018) reported stronger correlation of NDVI and GY ($r = 0.25 – 0.54$) and NDVI and biomass (r
655 $= 0.17 – 0.46$) in lowest yielding sites-years. In the same study, NDVI was reported to have
656 greater ability to detect biomass differences between lines in low-yielding environments, where
657 canopy closure was not present. Similar results were previously presented where stronger
658 correlations of NDVI and grain yield was observed under abiotic stress compared with high-
659 yielding environments (Gutiérrez-Rodríguez et al. 2004; Gutierrez et al. 2010; Lopes and
660 Reynolds 2012).
661

Conclusion

The use of multi-spectral imaging for alfalfa over the growing seasons in NY and NMSU demonstrated that VIs are heritable and that genetic correlations were significant for most time points and years. The measurement of cumulative NDVI showed that correlations of NDVI to biomass increased over time closer to harvest/cutting date. Strong correlations of NDVI to biomass harvest increase the possibility of using MSI to reduce the amount of biomass harvest phenotyping needed, potentially reducing phenotyping costs. The use of random regressions and Legendre polynomials demonstrated that longitudinal modeling of VIs can capture genetic variation, and stability in growth curves across cuttings was associated with stability in harvest biomass over harvests, years, locations and irrigation treatments. These results indicate that random regressions of VIs captures throughout a growth period can provide a greater dynamic understanding of aspects of phenotypic plasticity, stability and yield performance for crop improvement.

Data availability

R Code and data are available in the github:
https://github.com/rthapa1/FFAR_RandomRegressionModel_growthcurve_modelling_stabilityanalysis_alfalfa

Authors contributions

Ranjita Thapa: Processed MSI data; Developed statistical model; Conducted statistical analysis; Investigation; Methodology; Software; Validation; Visualization; Writing – original draft, review & editing. Karl H. Kunze: Review & editing. Julie Hansen: Review & editing. Christopher Pierce: Data collection; Review & editing. Virginia Moore: Review & editing. Ian Ray: Funding acquisition; Validation; Visualization; review & editing. Liam Wickes-Do: Data collection. Nicolas Morales: Data collection. Felipe Sabadin: Review & editing. Nicholas Santantonio: Conceptualization; Funding acquisition; Writing – review & editing. Michael A Gore: Funding acquisition; Writing – review & editing. Kelly Robbins: Conceptualization; Funding acquisition; Methodology; Project administration; Resources; Supervision; Validation; Visualization; review & editing

Acknowledgments

We would like to thank Jesse Chavez, Ryan Crawford and Jamie Crawford for their assistance with harvesting and data collection of the NY alfalfa trials.

Funding

This study was funded by Foundation for Food & Agriculture Research (CA20-SS-0000000103); National Alfalfa and Forage Alliance (90423); National Institute of Food and Agriculture, US Department of Agriculture, Hatch grant (3110006036).

Conflicts of Interest

The authors declare no conflict of interest.

References

Acharya, J.P., Y. Lopez, B.T. Gouveia, I. de Bem Oliveira, M.F. Resende Jr *et al.*, 2020 Breeding alfalfa (Medicago sativa L.) adapted to subtropical agroecosystems. *Agronomy* 10 (5):742.

Alves, R.S., M.D.V. de Resende, C.F. Azevedo, F.F.e. Silva, J.R.d.A.S.d.C. Rocha *et al.*, 2020 Optimization of Eucalyptus breeding through random regression models allowing for reaction norms in response to environmental gradients. *Tree Genetics & Genomes* 16:1-8.

Anche, M.T., N.S. Kaczmar, N. Morales, J.W. Clohessy, D.C. Ilut *et al.*, 2020 Temporal covariance structure of multi-spectral phenotypes and their predictive ability for end-of-season traits in maize. *Theoretical and Applied Genetics* 133:2853-2868.

Anche, M.T., N. Morales, N.S. Kaczmar, N. Santantonio, M.A. Gore *et al.*, 2023 Scalable growth models for time-series multispectral images. *The Plant Phenome Journal* 6 (1):e20064.

Annicchiarico, P., 2015 Alfalfa forage yield and leaf/stem ratio: narrow-sense heritability, genetic correlation, and parent selection procedures. *Euphytica* 205:409-420.

Annicchiarico, P., B. Barrett, E.C. Brummer, B. Julier, and A.H. Marshall, 2015 Achievements and challenges in improving temperate perennial forage legumes. *Critical Reviews in Plant Sciences* 34 (1-3):327-380.

Annicchiarico, P., and L. Pecetti, 2021 Comparison among nine alfalfa breeding schemes based on actual biomass yield gains. *Crop Science* 61 (4):2355-2371.

Aparicio, N., D. Villegas, J. Araus, J. Casadesus, and C. Royo, 2002 Relationship between growth traits and spectral vegetation indices in durum wheat. *Crop Science* 42 (5):1547-1555.

Aparicio, N., D. Villegas, J. Casadesus, J.L. Araus, and C. Royo, 2000 Spectral vegetation indices as nondestructive tools for determining durum wheat yield. *Agronomy Journal* 92 (1):83-91.

Babar, M., M. Reynolds, M. Van Ginkel, A. Klatt, W. Raun *et al.*, 2006a Spectral reflectance to estimate genetic variation for in-season biomass, leaf chlorophyll, and canopy temperature in wheat. *Crop Science* 46 (3):1046-1057.

Babar, M., M. Van Ginkel, A. Klatt, B. Prasad, and M. Reynolds, 2006b The potential of using spectral reflectance indices to estimate yield in wheat grown under reduced irrigation. *Euphytica* 150:155-172.

Babar, M., M. Van Ginkel, M. Reynolds, B. Prasad, and A. Klatt, 2007 Heritability, correlated response, and indirect selection involving spectral reflectance indices and grain yield in wheat. *Australian Journal of Agricultural Research* 58 (5):432-442.

Blasco, J., N. Aleixos, J. Gómez, and E. Moltó, 2007 Citrus sorting by identification of the most common defects using multispectral computer vision. *Journal of Food Engineering* 83 (3):384-393.

Calus, M.á., and R. Veerkamp, 2003 Estimation of environmental sensitivity of genetic merit for milk production traits using a random regression model. *Journal of dairy science* 86 (11):3756-3764.

Chapman, S., M. Cooper, D. Podlich, and G. Hammer, 2003 Evaluating plant breeding strategies by simulating gene action and dryland environment effects. *Agronomy Journal* 95 (1):99-113.

Chapman, S.C., M. Cooper, and G.L. Hammer, 2002 Using crop simulation to generate genotype by environment interaction effects for sorghum in water-limited environments. *Australian Journal of Agricultural Research* 53 (4):379-389.

Chen, J., S. Gu, M. Shen, Y. Tang, and B. Matsushita, 2009 Estimating aboveground biomass of grassland having a high canopy cover: an exploratory analysis of in situ hyperspectral data. *International journal of remote sensing* 30 (24):6497-6517.

Chen, Y.-R., K. Chao, and M.S. Kim, 2002 Machine vision technology for agricultural applications. *Computers and Electronics in Agriculture* 36 (2-3):173-191.

Chenu, K., S.C. Chapman, F.o. Tardieu, G. McLean, C. Welcker *et al.*, 2009 Simulating the yield impacts of organ-level quantitative trait loci associated with drought response in maize: a "gene-to-phenotype" modeling approach. *Genetics* 183 (4):1507-1523.

Christopher, J.T., M. Veyradier, A.K. Borrell, G. Harvey, S. Fletcher *et al.*, 2014 Phenotyping novel stay-green traits to capture genetic variation in senescence dynamics. *Functional plant biology* 41 (11):1035-1048.

Claudio, H.C., Y. Cheng, D.A. Fuentes, J.A. Gamon, H. Luo *et al.*, 2006 Monitoring drought effects on vegetation water content and fluxes in chaparral with the 970 nm water band index. *Remote sensing of Environment* 103 (3):304-311.

da Silva, E.E., F.H.R. Baio, L.P.R. Teodoro, C.A. da Silva Junior, R.S. Borges *et al.*, 2020 UAV-multispectral and vegetation indices in soybean grain yield prediction based on in situ observation. *Remote Sensing Applications: Society and Environment* 18:100318.

El-Hendawy, S.E., M. Alotaibi, N. Al-Suhaibani, K. Al-Gaadi, W. Hassan *et al.*, 2019 Comparative performance of spectral reflectance indices and multivariate modeling for assessing agronomic parameters in advanced spring wheat lines under two contrasting irrigation regimes. *Frontiers in plant science* 10:1537.

Erdle, K., B. Mistele, and U. Schmidhalter, 2013 Spectral high-throughput assessments of phenotypic differences in biomass and nitrogen partitioning during grain filling of wheat under high yielding Western European conditions. *Field Crops Research* 141:16-26.

Freeman, K., W. Raun, G. Johnson, R. Mullen, M. Stone *et al.*, 2003 Late-season prediction of wheat grain yield and grain protein. *Communications in Soil Science and Plant Analysis* 34 (13-14):1837-1852.

Galán, R.J., A.-M. Bernal-Vasquez, C. Jebsen, H.-P. Piepho, P. Thorwarth *et al.*, 2020 Hyperspectral reflectance data and agronomic traits can predict biomass yield in winter rye hybrids. *BioEnergy research* 13:168-182.

Gitelson, A.A., Y.J. Kaufman, and M.N. Merzlyak, 1996 Use of a green channel in remote sensing of global vegetation from EOS-MODIS. *Remote sensing of Environment* 58 (3):289-298.

Gutierrez, M., M.P. Reynolds, W.R. Raun, M.L. Stone, and A.R. Klatt, 2010 Spectral water indices for assessing yield in elite bread wheat genotypes under well-irrigated, water-stressed, and high-temperature conditions. *Crop Science* 50 (1):197-214.

Gutiérrez-Rodríguez, M., M.P. Reynolds, J.A. Escalante-Estrada, and M.T. Rodríguez-González, 2004 Association between canopy reflectance indices and yield and physiological traits in bread wheat under drought and well-irrigated conditions. *Australian Journal of Agricultural Research* 55 (11):1139-1147.

Hammer, G., M. Kropff, T. Sinclair, and J. Porter, 2002 Future contributions of crop modelling—from heuristics and supporting decision making to understanding genetic regulation and aiding crop improvement. *European Journal of Agronomy* 18 (1-2):15-31.

Hassan, M.A., M. Yang, A. Rasheed, G. Yang, M. Reynolds *et al.*, 2019 A rapid monitoring of NDVI across the wheat growth cycle for grain yield prediction using a multi-spectral UAV platform. *Plant Science* 282:95-103.

Hazratkulova, S., R.C. Sharma, S. Alikulov, S. Islomov, T. Yuldashev *et al.*, 2012 Analysis of genotypic variation for normalized difference vegetation index and its relationship with grain yield in winter wheat under terminal heat stress. *Plant Breeding* 131 (6):716-721.

Hill, R., J. Shenk, and R. Barnes, 1988 Breeding for yield and quality. p. 809–825. AA Hanson et al.(ed) Alfalfa and alfalfa improvement. Agron. Monogr. 29. ASA, CSSA, and SSSA, Madison, WI. *Breeding for yield and quality. p. 809–825. In AA Hanson et al.(ed) Alfalfa and alfalfa improvement. Agron. Monogr. 29. ASA, CSSA, and SSSA, Madison, WI.*:-.

Lobos, G.A., A. Escobar-Opazo, F. Estrada, S. Romero-Bravo, M. Garriga *et al.*, 2019 Spectral reflectance modeling by wavelength selection: Studying the scope for blueberry physiological breeding under contrasting water supply and heat conditions. *Remote Sensing* 11 (3):329.

Lopes, M.S., and M.P. Reynolds, 2012 Stay-green in spring wheat can be determined by spectral reflectance measurements (normalized difference vegetation index) independently from phenology. *Journal of experimental botany* 63 (10):3789-3798.

Ma, B., L.M. Dwyer, C. Costa, E.R. Cober, and M.J. Morrison, 2001 Early prediction of soybean yield from canopy reflectance measurements. *Agronomy Journal* 93 (6):1227-1234.

Marti, J., J. Bort, G. Slafer, and J. Araus, 2007 Can wheat yield be assessed by early measurements of normalized difference vegetation index? *Annals of applied biology* 150 (2):253-257.

Messina, C.D., T.R. Sinclair, G.L. Hammer, D. Curan, J. Thompson *et al.*, 2015 Limited-transpiration trait may increase maize drought tolerance in the US Corn Belt. *Agronomy Journal* 107 (6):1978-1986.

Meyer, K., and W.G. Hill, 1997 Estimation of genetic and phenotypic covariance functions for longitudinal or 'repeated'records by restricted maximum likelihood. *Livestock Production Science* 47 (3):185-200.

Mistele, B., and U. Schmidhalter, 2008 Spectral measurements of the total aerial N and biomass dry weight in maize using a quadrilateral-view optic. *Field Crops Research* 106 (1):94-103.

Morales, N., N.S. Kaczmar, N. Santantonio, M.A. Gore, L.A. Mueller *et al.*, 2020 ImageBreed: open-access plant breeding web–database for image-based phenotyping. *The Plant Phenome Journal* 3 (1):e20004.

Mutanga, O., and A.K. Skidmore, 2004 Narrow band vegetation indices overcome the saturation problem in biomass estimation. *International journal of remote sensing* 25 (19):3999-4014.

Natarajan, S., J. Basnayake, X. Wei, and P. Lakshmanan, 2019 High-throughput phenotyping of indirect traits for early-stage selection in sugarcane breeding. *Remote Sensing* 11 (24):2952.

Oliveira, D., D. Lourenco, S. Tsuruta, I. Misztal, D. Santos *et al.*, 2018 Reaction norm for yearling weight in beef cattle using single-step genomic evaluation. *Journal of animal science* 96 (1):27-34.

Olivoto, T., and A.D.C. Lúcio, 2020 metan: An R package for multi-environment trial analysis. *Methods in Ecology and Evolution* 11 (6):783-789.

Petsoulas, C., E. Evangelou, A. Tsitouras, V. Aschonitis, A. Kargiotidou *et al.*, 2022 Spectral Reflectance Indices as a High Throughput Selection Tool in a Sesame Breeding Scheme. *Remote Sensing* 14 (11):2629.

Prabhakara, K., W.D. Hively, and G.W. McCarty, 2015 Evaluating the relationship between biomass, percent groundcover and remote sensing indices across six winter cover crop fields in Maryland, United States. *International journal of applied earth observation and geoinformation* 39:88-102.

Prasad, B., B.F. Carver, M.L. Stone, M. Babar, W.R. Raun *et al.*, 2007a Genetic analysis of indirect selection for winter wheat grain yield using spectral reflectance indices. *Crop Science* 47 (4):1416-1425.

Prasad, B., B.F. Carver, M.L. Stone, M. Babar, W.R. Raun *et al.*, 2007b Potential use of spectral reflectance indices as a selection tool for grain yield in winter wheat under great plains conditions. *Crop Science* 47 (4):1426-1440.

Raun, W.R., J.B. Solie, G.V. Johnson, M.L. Stone, E.V. Lukina *et al.*, 2001 In-season prediction of potential grain yield in winter wheat using canopy reflectance. *Agronomy Journal* 93 (1):131-138.

Ray, I. M., Pierce, C. A., & Currier, C. G. (2012). Registration of 'NuMex Bill Melton' Alfalfa for Variable-Soil-Moisture Environments. *Journal of Plant Registrations, 6*(2), 137–140. https://doi.org/10.3198/jpr2011.10.0561crc

Reynolds, M., P. CS, and S. ASI, M. Vargas, and AG Condon, 2007. Evaluating potential genetic grains in wheat associated with stress-adaptive trait expression in elite genetic resources under drought and heat stress. *Crop Science* 47:172-189.

Reynolds, M., S. Rajaram, and K. Sayre, 1999 Physiological and genetic changes of irrigated wheat in the post–green revolution period and approaches for meeting projected global demand. *Crop Science* 39 (6):1611-1621.

Riday, H., and E.C. Brummer, 2005 Heterosis in a broad range of alfalfa germplasm. *Crop Science* 45 (1):8-17.

Sandhu, K.S., P.D. Mihalyov, M.J. Lewien, M.O. Pumphrey, and A.H. Carter, 2021 Combining genomic and phenomic information for predicting grain protein content and grain yield in spring wheat. *Frontiers in plant science* 12:613300.

Santana, D.C., M.F. Cotrim, M.S. Flores, F.H.R. Baio, L.S. Shiratsuchi *et al.*, 2021 UAV-based multispectral sensor to measure variations in corn as a function of nitrogen topdressing. *Remote Sensing Applications: Society and Environment* 23:100534.

Schaeffer, L.R., 2004 Application of random regression models in animal breeding. *Livestock Production Science* 86 (1-3):35-45.

Schlemmer, M.R., D.D. Francis, J. Shanahan, and J.S. Schepers, 2005 Remotely measuring chlorophyll content in corn leaves with differing nitrogen levels and relative water content. *Agronomy Journal* 97 (1):106-112.

Serrano, L., I. Filella, and J. Penuelas, 2000 Remote sensing of biomass and yield of winter wheat under different nitrogen supplies. *Crop Science* 40 (3):723-731.

Speidel, S.E., 2011 Random regression models for the prediction of days to finish in beef cattle. Colorado State University.

Strucken, E.M., Y.C. Laurenson, and G.A. Brockmann, 2015 Go with the flow—biology and genetics of the lactation cycle. *Frontiers in Genetics* 6:118.

Sun, J., J.E. Rutkoski, J.A. Poland, J. Crossa, J.L. Jannink *et al.*, 2017 Multitrait, random regression, or simple repeatability model in high-throughput phenotyping data improve

genomic prediction for wheat grain yield. *The plant genome* 10 (2):plantgenome2016.2011.0111.

Thenkabail, P.S., R.B. Smith, and E. De Pauw, 2000 Hyperspectral vegetation indices and their relationships with agricultural crop characteristics. *Remote sensing of Environment* 71 (2):158-182.

VanRaden, P.M., 2008 Efficient methods to compute genomic predictions. *Journal of dairy science* 91 (11):4414-4423.

Yan, W., and M.S. Kang, 2002 *GGE biplot analysis: A graphical tool for breeders, geneticists, and agronomists*: CRC press.

Yan, W., M. S. Kang, B. Ma, S. Woods, and P. L. Cornelius, 2007 GGE biplot vs. AMMI analysis of genotype-by-environment data. *Crop science* 47(2), 643-653.

Yang, M., M.A. Hassan, K. Xu, C. Zheng, A. Rasheed *et al.*, 2020 Assessment of water and nitrogen use efficiencies through UAV-based multispectral phenotyping in winter wheat. *Frontiers in plant science* 11:927.

Fig 1. Heritability of Phenotypic indices in the Ithaca, NY trial.

Fig 2. Heritability of Phenotypic indices in (a) Normal Irrigation (NMSU trial), (b) Summer termination (NMSU trial)

Fig 3. Phenotypic correlation of different phenotypic indices with biomass yield (a) Harvest year 2020 and (b) Harvest year 2021

Fig 4. Genetic correlation of different phenotypic indices with harvest biomass yield for Ithaca, NY trial ("Helfer" field). X-axis represents Growing degree days (GDD) and Y-axis represents genetic correlation.

Fig 5. Genetic correlation of different phenotypic indices with final harvest biomass yield under normal irrigation condition of NMSU trial. X-axis represents Growing degree days (GDD) and Y-axis represents genetic correlation.

Fig 6. Genetic correlation of different phenotypic indices with final harvest biomass yield under summer irrigation termination condition of NMSU trial. X-axis represents Growing degree days (GDD) and Y-axis represents genetic correlation.

Fig. 7. The "mean vs. stability" view of the genotype main effects plus genotype environment interaction (GGE) biplot based on genotype environment yield data of 36 alfalfa genotypes evaluated in six environments (First, Second and Third Harvest of 2020, and First, Second and Third Harvest of 2021) of Helfer field in Ithaca, NY.

Fig. 8. The "mean vs. stability" view of the genotype main effects plus genotype environment interaction (GGE) biplot based on genotype environment yield data of 24 alfalfa genotypes and one covariate (G4) evaluated in nine environments - NIcut3, NIcut4, NIcut5, NIcut6, and NIcut7 of normal irrigation and SITcut3, SITcut4, SITcut5 and SITcut7 of summer irrigation termination of NMSU.

Fig. 9. Growth curves derived from GNDVI of five stable and five unstable alfalfa cultivars across five different harvest seasons (excluding first harvest) of the Ithaca, NY trial. X-axis indicates Growing degree days (GDD) and Y-axis indicates breeding values estimated using Random Regression model with third order of Legendre polynomials.

Fig. 10. Growth curves derived from NDVI of five stable and five unstable alfalfa cultivars across five different harvest seasons (excluding first harvest) of the Ithaca, NY trial. X-axis indicates Growing degree days (GDD) and Y-axis indicates breeding values estimated using Random Regression model with third order of Legendre polynomials.

Fig. 11. Growth curves derived from NDRE of five stable and five unstable alfalfa cultivars across five different harvest seasons (excluding first harvest) of the Ithaca, NY trial. X-axis indicates Growing degree days (GDD) and Y-axis indicates breeding values estimated using Random Regression model with third order of Legendre polynomials.

Fig. 12. Growth curves derived from NIR of five stable and five unstable alfalfa cultivars across five different harvest seasons (excluding first harvest) of the Ithaca, NY trial. X-axis indicates Growing degree days (GDD) and Y-axis indicates breeding values estimated using Random Regression model with third order of Legendre polynomials.

Fig. 13. Growth curves derived from Ratio of five stable and five unstable alfalfa cultivars across five different harvest seasons (excluding first harvest) of the Ithaca, NY trial. X-axis indicates Growing degree days (GDD) and Y-axis indicates breeding values estimated using Random Regression model with third order of Legendre polynomials.

Fig. 14. Growth curves derived from GNDVI of five stable and five unstable alfalfa cultivars across nine different harvest seasons of the NMSU trial. X-axis indicates Growing degree days (GDD) and Y-axis indicates breeding values estimated using Random Regression model with third order of Legendre polynomials.

Fig. 15. Growth curves derived from NDVI of five stable and five unstable alfalfa cultivars across nine different harvest seasons of the NMSU trial. X-axis indicates Growing degree days (GDD) and Y-axis indicates breeding values estimated using Random Regression model with third order of Legendre polynomials.

Fig. 16. Growth curves derived from NIR of five stable and five unstable alfalfa cultivars across nine different harvest seasons of the NMSU trial. X-axis indicates Growing degree days (GDD) and Y-axis indicates breeding values estimated using Random Regression model with third order of Legendre polynomials.

Fig. 17. Growth curves derived from Ratio during the growing season of five stable and five unstable alfalfa cultivars across nine different harvest seasons of the NMSU trial. X-axis indicates Growing degree days (GDD) and Y-axis indicates breeding values estimated using Random Regression model with third order of Legendre polynomials.

Fig. 18. Growth curves derived from GNDVI of five stable alfalfa cultivars across five different harvest seasons of normal irrigation and four different harvest seasons of early termination. The left-hand side figures and right-hand side figures represents growth curves of stable cultivars in normal irrigation condition (NI) and summer irrigation termination condition (SIT) respectively.

Fig. 19. Growth curves derived from GNDVI of five unstable alfalfa cultivars across five different harvest seasons of normal irrigation and four different harvest seasons of early termination. The left-hand side figures and right-hand side figures represents growth curves of stable cultivars in normal irrigation condition (NI) and summer irrigation termination condition (SIT) respectively.

Fig. 20. Growth curves derived from NDVI of five stable alfalfa cultivars across five different harvest seasons of normal irrigation and four different harvest seasons of early termination. The left-hand side figures and right-hand side figures represents growth curves of stable cultivars in normal irrigation condition (NI) and summer irrigation termination condition (SIT) respectively.

Fig. 21. Growth curves derived from NDVI of five unstable alfalfa cultivars across five different harvest seasons of normal irrigation and four different harvest seasons of early termination. The left-hand side figures and right-hand side figures represents growth curves of stable cultivars in normal irrigation condition (NI) and summer irrigation termination condition (SIT) respectively.

Fig. 22. Growth curves derived from NIR of five stable alfalfa cultivars across five different harvest seasons of normal irrigation and four different harvest seasons of early termination. The left-hand side figures and right-hand side figures represents growth curves of stable cultivars in normal irrigation condition (NI) and summer irrigation termination condition (SIT) respectively.

Fig. 23. Growth curves derived from NIR of five unstable alfalfa cultivars across five different harvest seasons of normal irrigation and four different harvest seasons of early termination. The left-hand side figures and right-hand side figures represents growth curves of stable cultivars in normal irrigation condition (NI) and summer irrigation termination condition (SIT) respectively.

Fig. 24. Growth curves derived from Ratio of five stable alfalfa cultivars across five different harvest seasons of normal irrigation and four different harvest seasons of early termination. The left-hand side figures and right-hand side figures represents growth curves of stable cultivars in normal irrigation condition (NI) and summer irrigation termination condition (SIT) respectively.

Fig. 25. Growth curves derived from Ratio of five unstable alfalfa cultivars across five different harvest seasons of normal irrigation and four different harvest seasons of early termination. The left-hand side figures and right-hand side figures represents growth curves of stable cultivars in normal irrigation condition (NI) and summer irrigation termination condition (SIT) respectively.

Table 1. Correlation of variance of yield and variance of genetic merit estimated from random regression legendre polynomial (RRLP) model with VIs (GNDVI, NDVI, NDRE, NIR, and Ratio) of all cultivars across different environments of the Ithaca, NY trial at different time points of growing season.

Growing Degree Days (GDD)	GNDVI	NDVI	NDRE	NIR	Ratio
178.55	0.65*	0.67*	0.6*	0.68*	0.43*
218.55	0.64*	0.67*	0.61*	0.68*	0.43*
258.55	0.64*	0.67*	0.62*	0.68*	0.42*
298.55	0.63*	0.67*	0.64*	0.67*	0.42*
338.55	0.64*	0.65*	0.63*	0.66*	0.37
358.55	0.64*	0.65*	0.66*	0.66*	0.42*
378.55	0.65*	0.65*	0.67*	0.66*	0.42*
418.55	0.66*	0.63*	0.69*	0.65*	0.42*
438.55	0.66*	0.62*	0.69*	0.65*	0.42*
478.55	0.65*	0.61*	0.71*	0.66*	0.42*

* indicates P-value < 0.05

Table 2. Correlation of variance of yield and variance of genetic merit estimated from random regression legendre polynomial (RRLP) model with VIs (GNDVI, NDVI, NDRE, NIR, and Ratio) of all cultivars across different environments of the NMSU trial at different time points of growing season

Growing Degree Days (GDD)	GNDVI	NDVI	NDRE	NIR	Ratio
342	0.19	0.27	0.16	0.68*	0.91*
402	0.2	0.28	0.18	0.69*	0.91*
462	0.22	0.3	0.2	0.7*	0.91*
522	0.24	0.33*	0.22	0.72*	0.92*
582	0.26	0.35*	0.25	0.73*	0.92*
642	0.29	0.38*	0.28	0.75*	0.92*
702	0.31*	0.4*	0.31	0.76*	0.92*
762	0.33*	0.42*	0.34*	0.77*	0.93*
822	0.35*	0.42*	0.35*	0.78*	0.93*
902	0.35*	0.44*	0.36*	0.79*	0.93*

* indicates P-value < 0.05

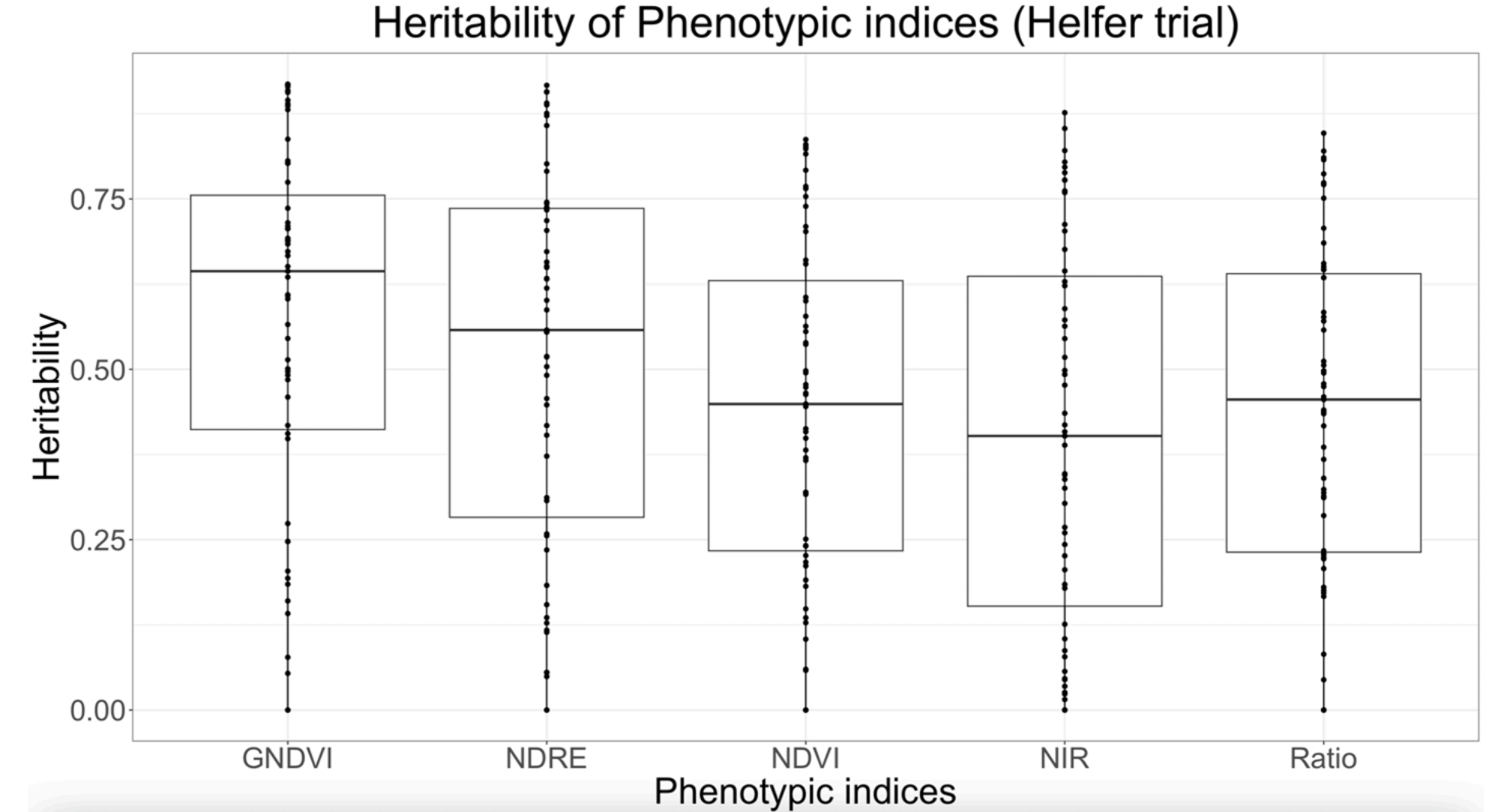
Heritability of Phenotypic indices (Helfer trial)
Heritability
0.00
0.25
0.50
0.75
GNDVI
NDRE
NDVI
NIR
Ratio
Phenotypic indices

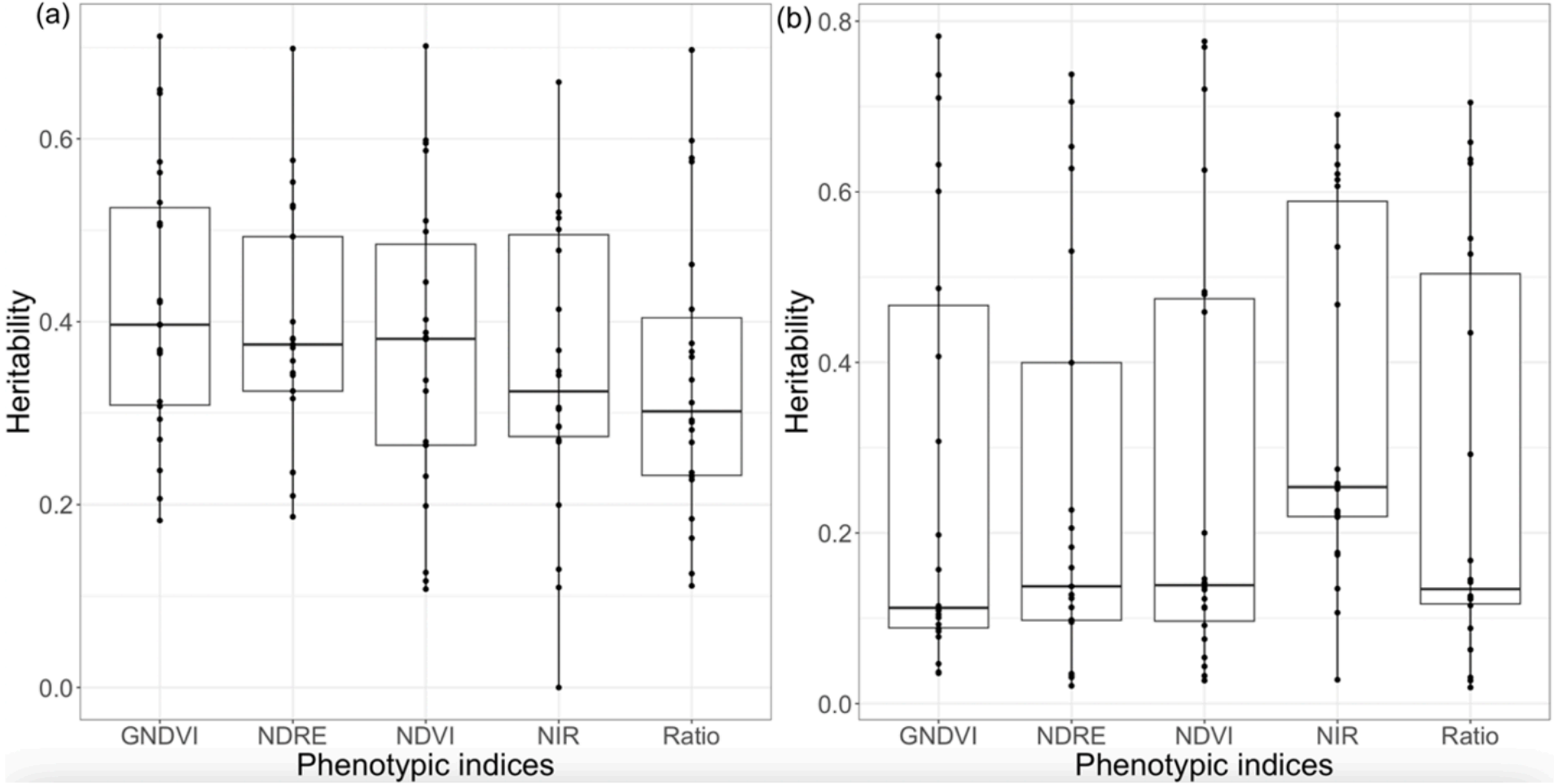
(a)
Heritability
0.0
0.2
0.4
0.6
GNDVI
NDRE
NDVI
NIR
Ratio
Phenotypic indices
(b)
Heritability
0.0
0.2
0.4
0.6
0.8
GNDVI
NDRE
NDVI
NIR
Ratio
Phenotypic indices

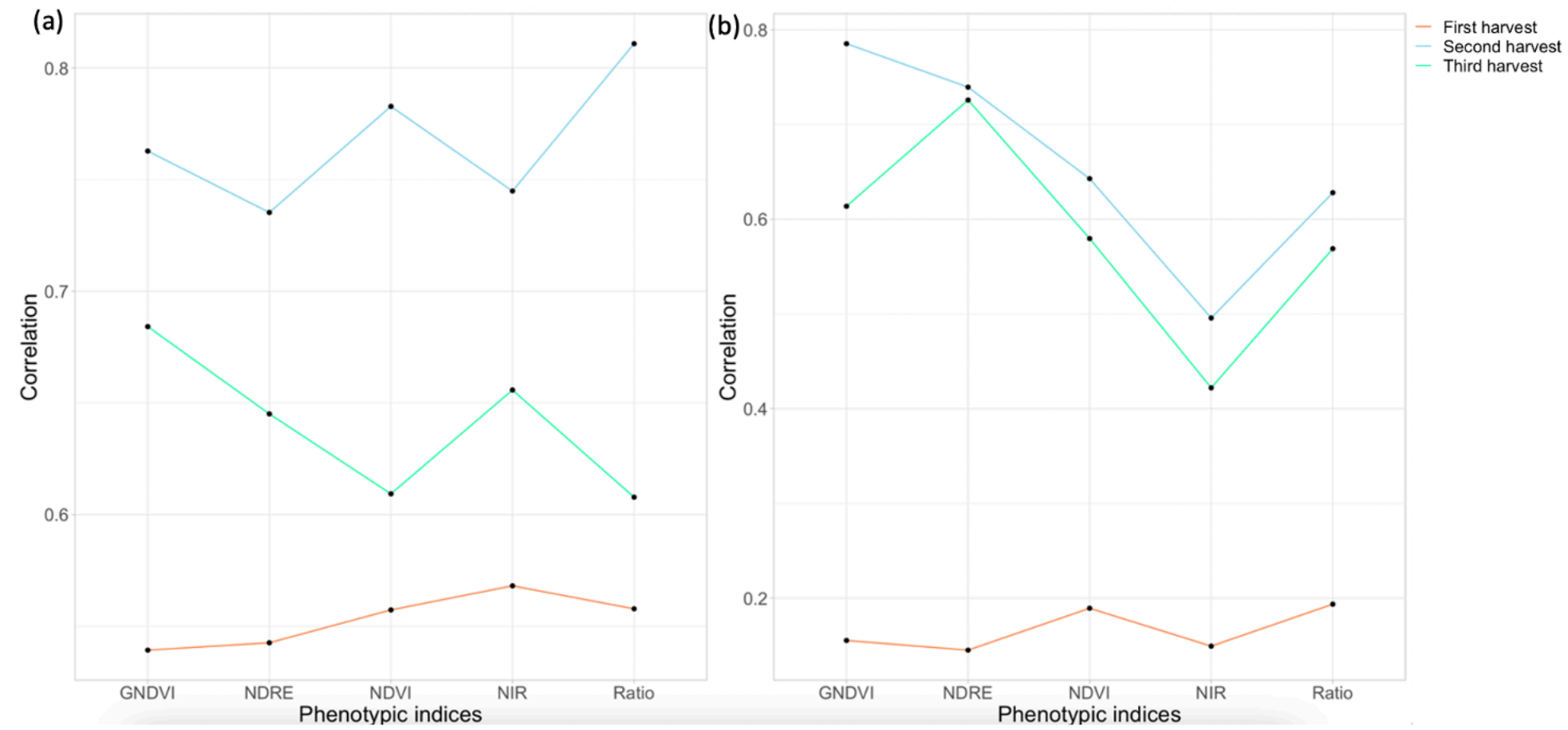
(a)
(b)
Correlation
0.8
0.7
0.6
0.4
0.2
GNDVI
NDRE
NDVI
NIR
Ratio
Phenotypic indices
First harvest
Second harvest
Third harvest

(a) First Harvest of 2020

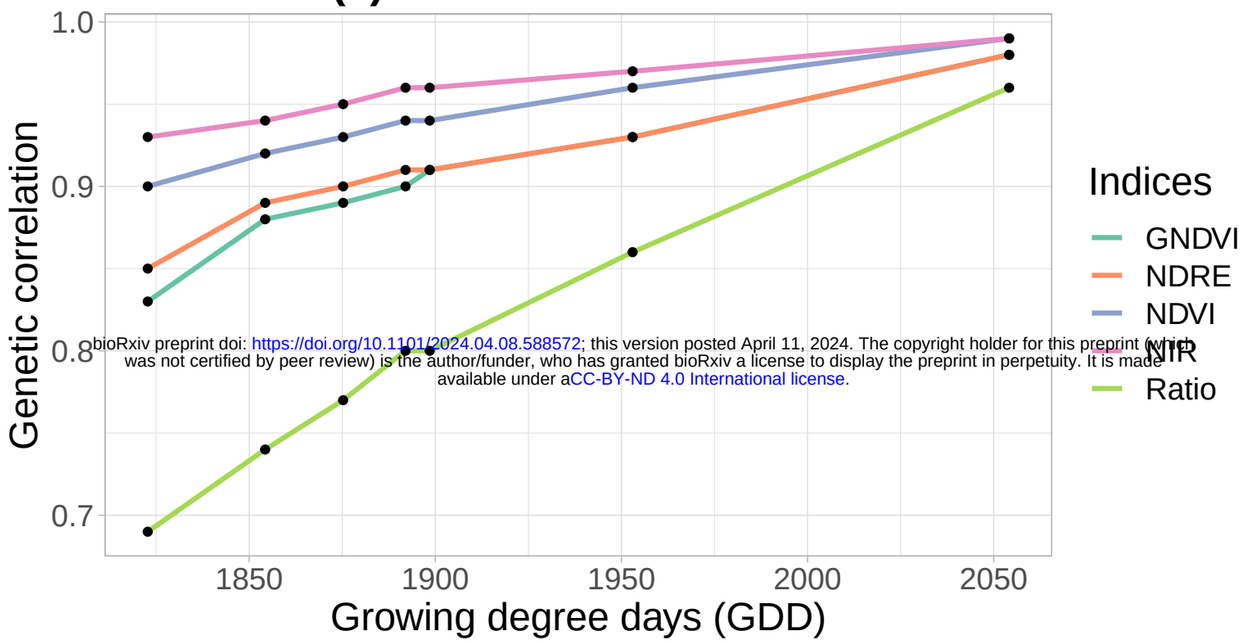

(b) Second Harvest of 2020

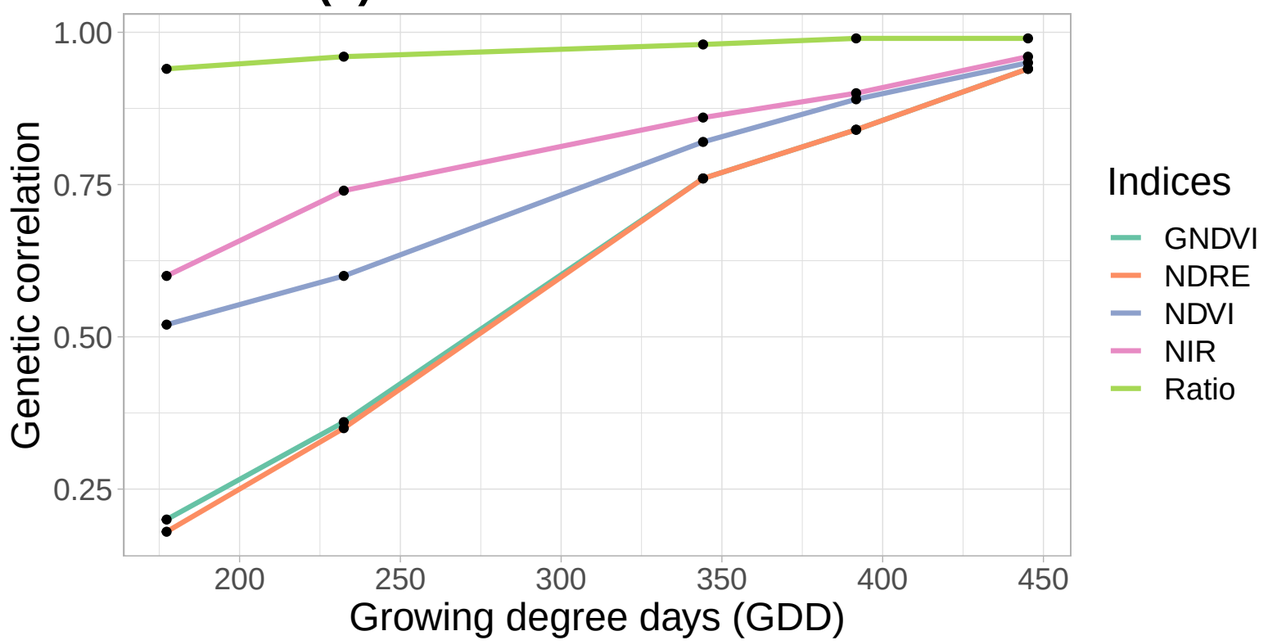

(c) Third Harvest of 2020

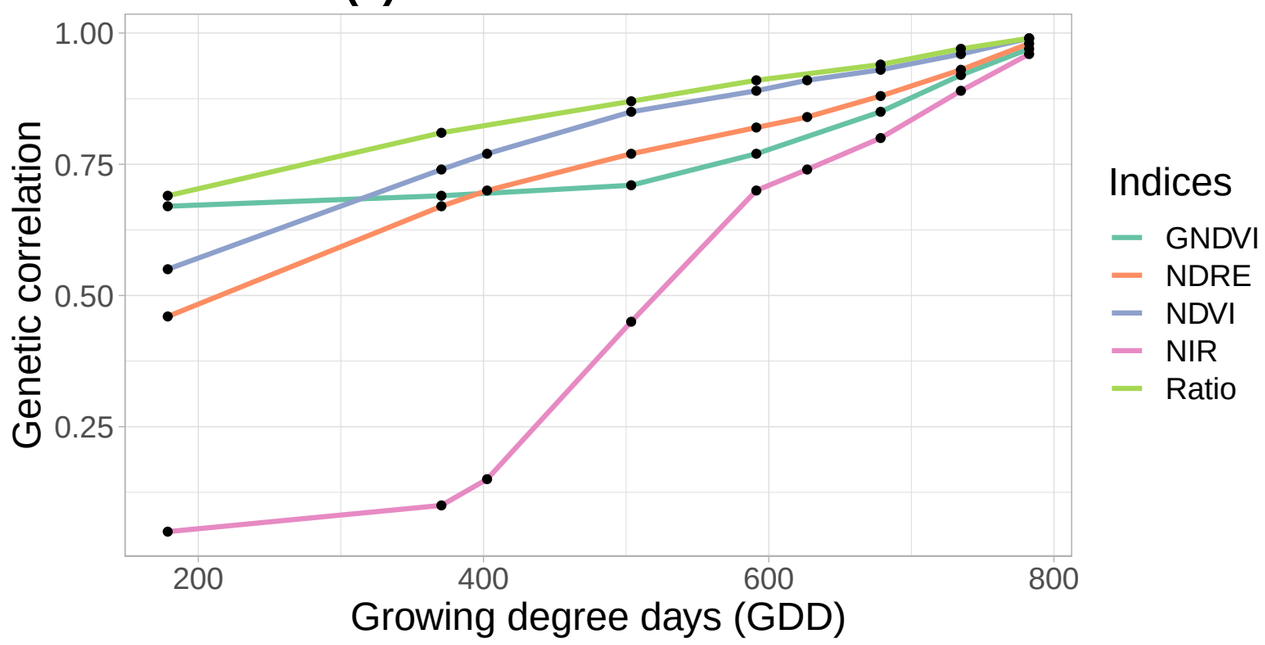

(d) First Harvest of 2021

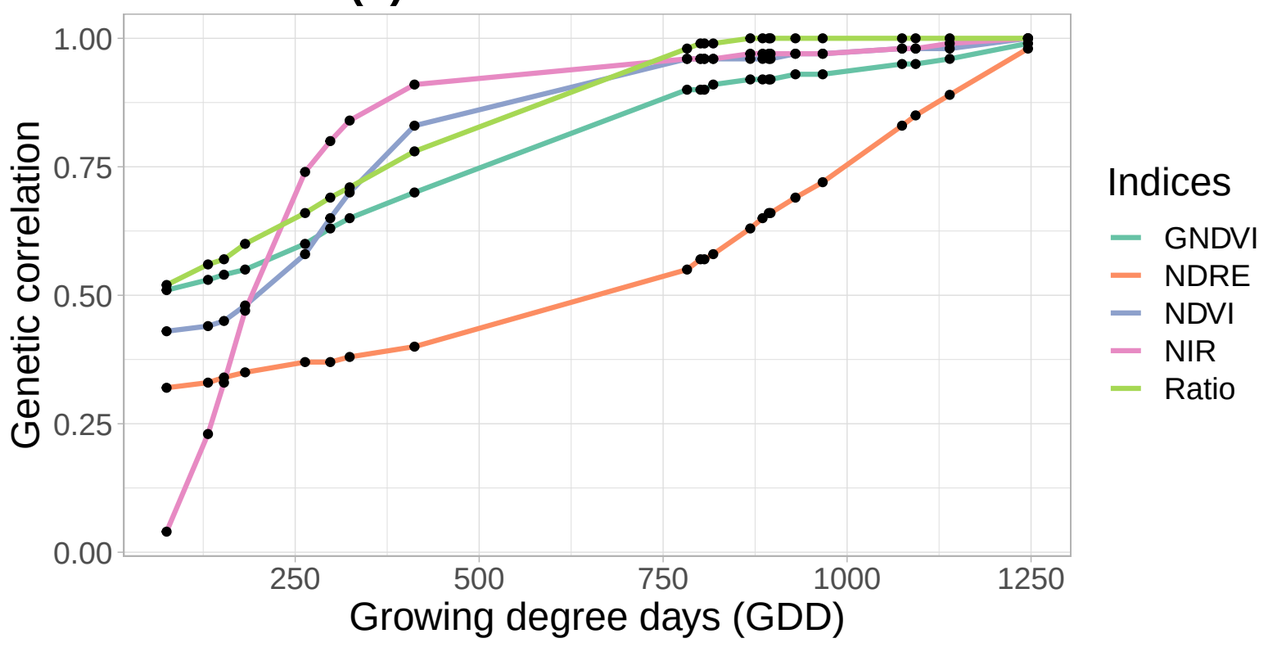

(e) Second Harvest of 2021

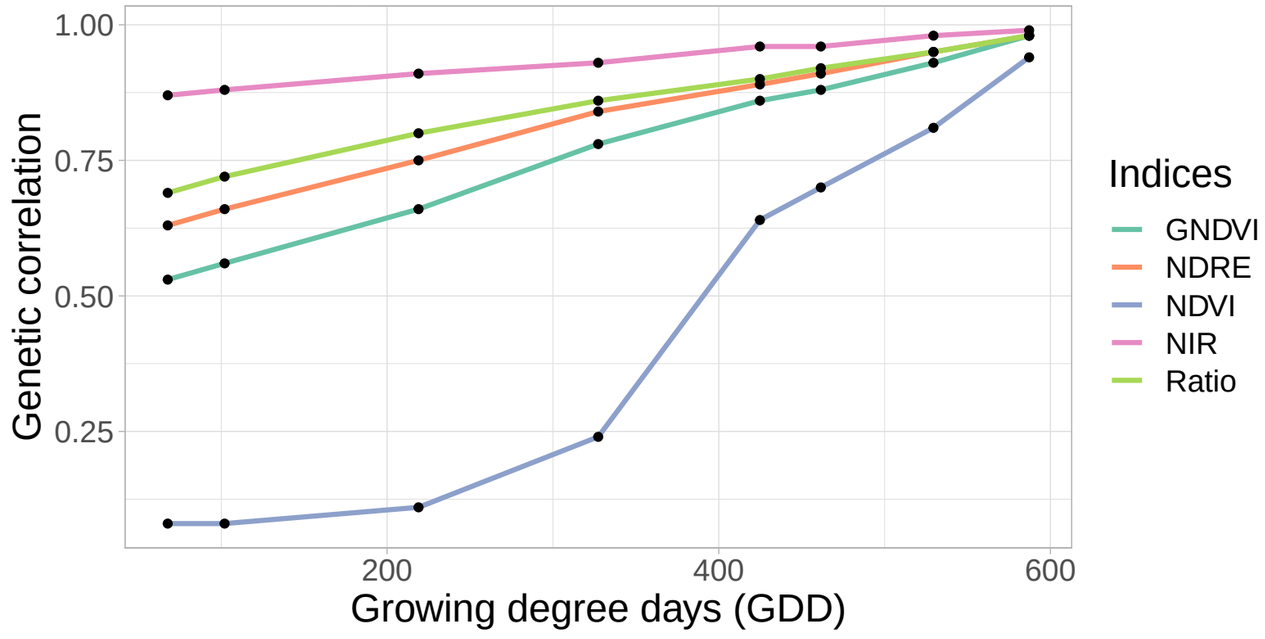

(f) Third Harvest of 2021

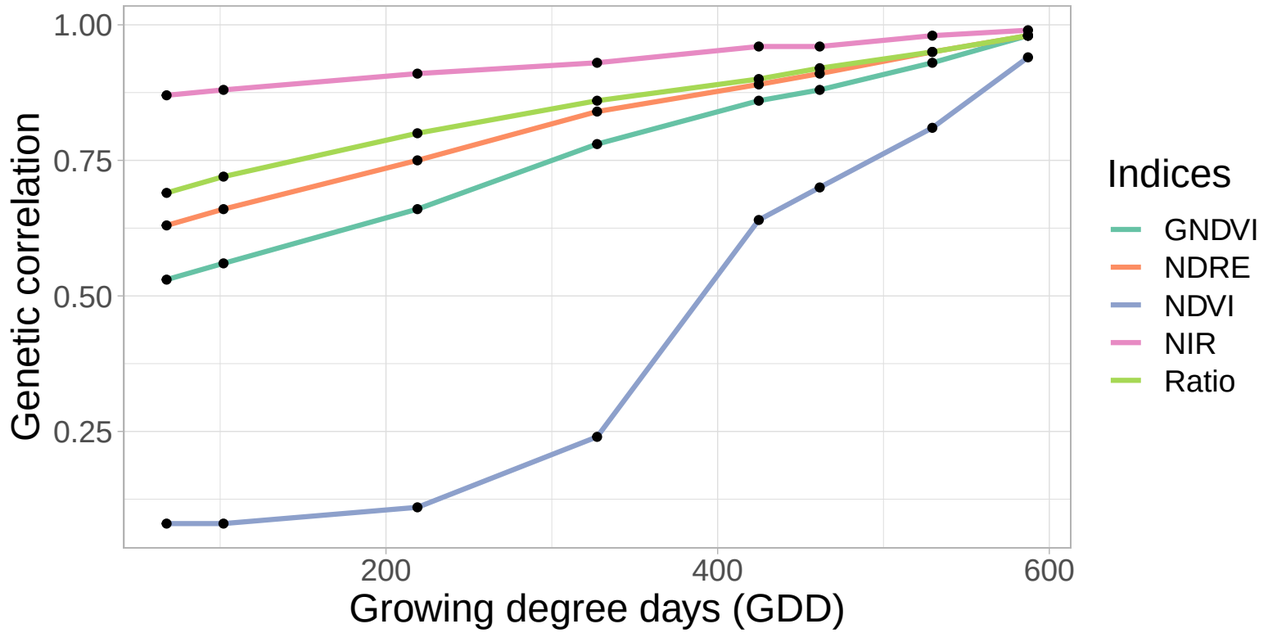

(a) May 28 to June 24 regrowth cycle of 2021 under normal irrigation

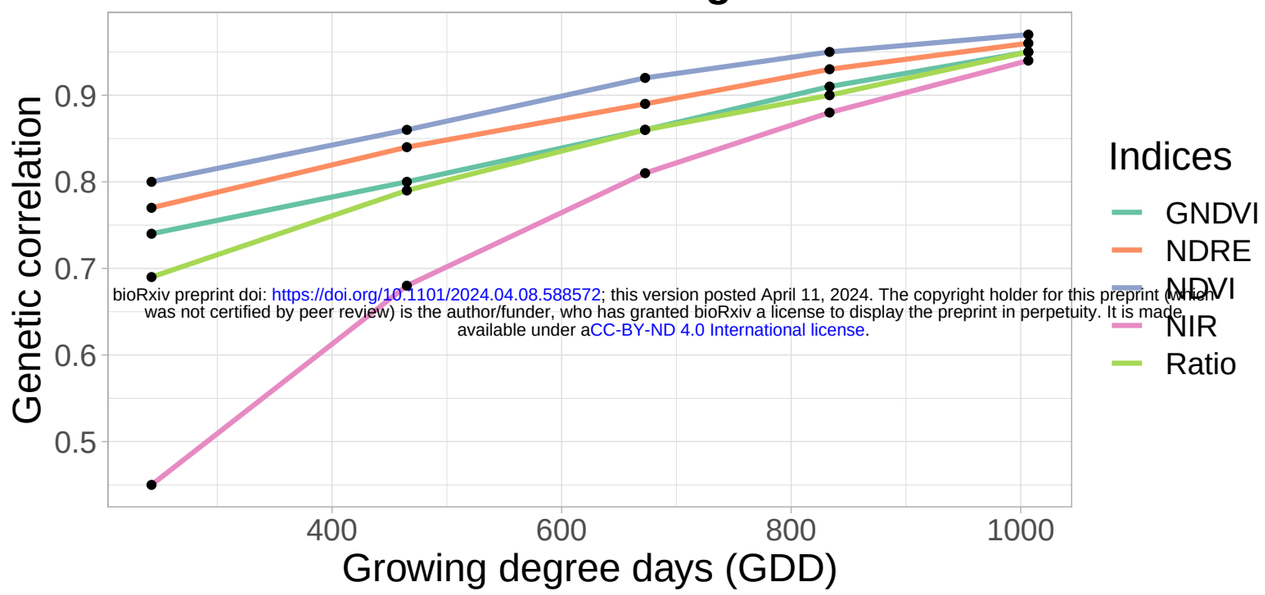

(b) June 25 to Jul 22 regrowth cycle of 2021 under normal irrigation

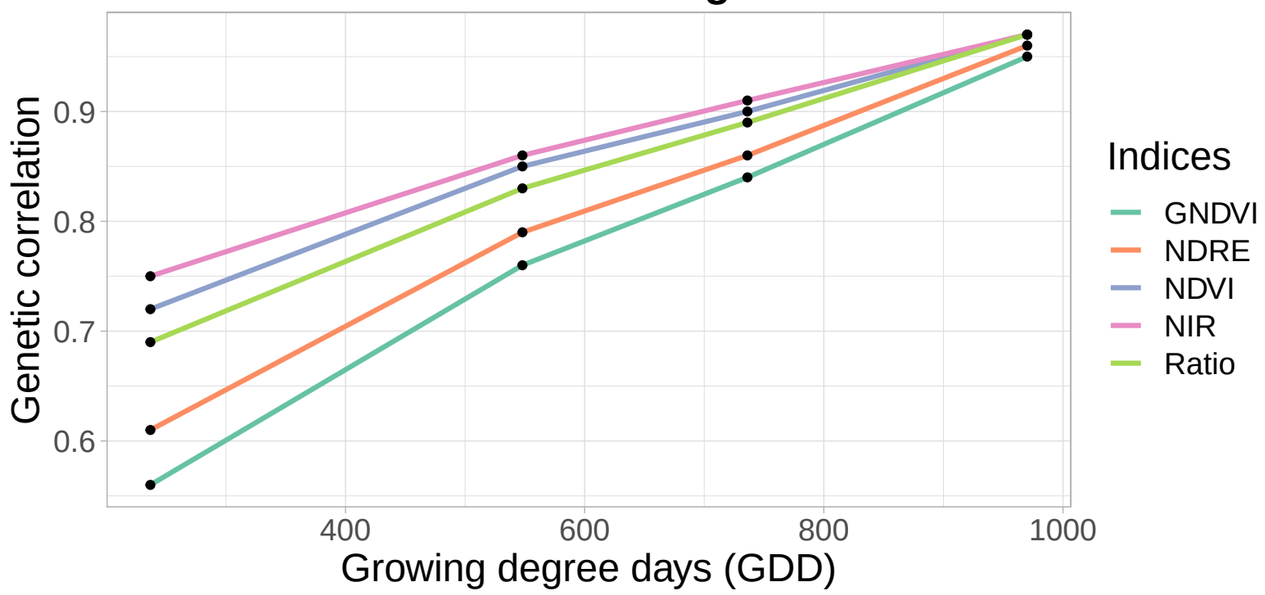

(c) July 23 to August 27 regrowth cycle of 2021 under normal irrigation

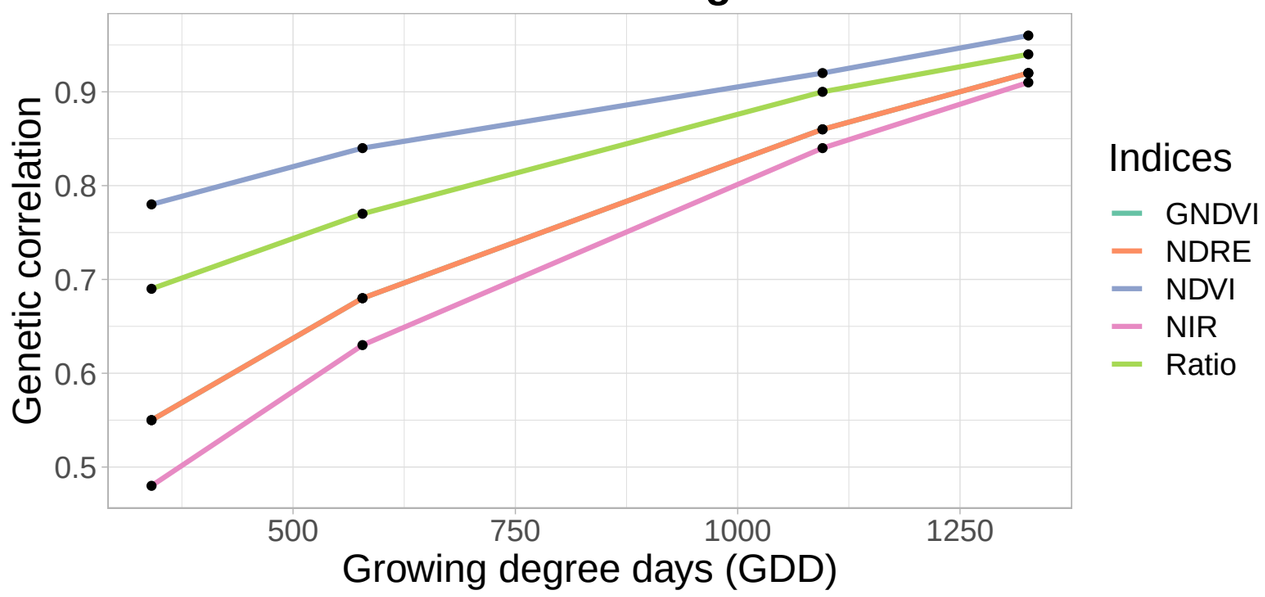

(d) August 28 to September 29 regrowth cycle of 2021 under normal irrigation

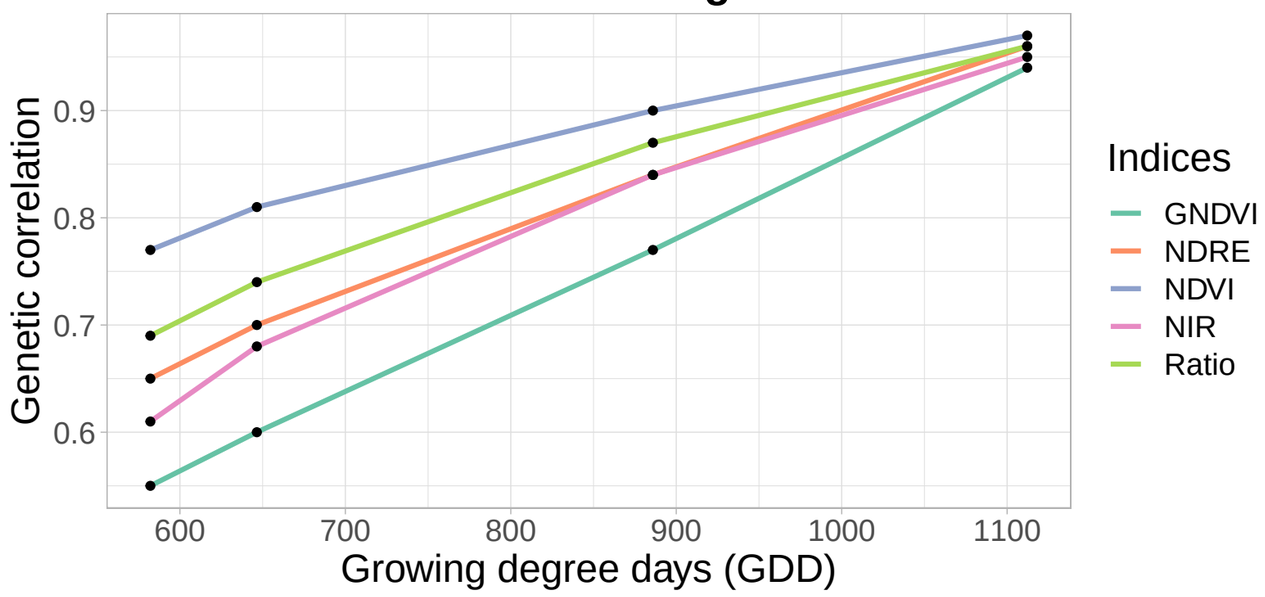

(e) September 30 to November 12 regrowth cycle of 2021 under normal irrigation

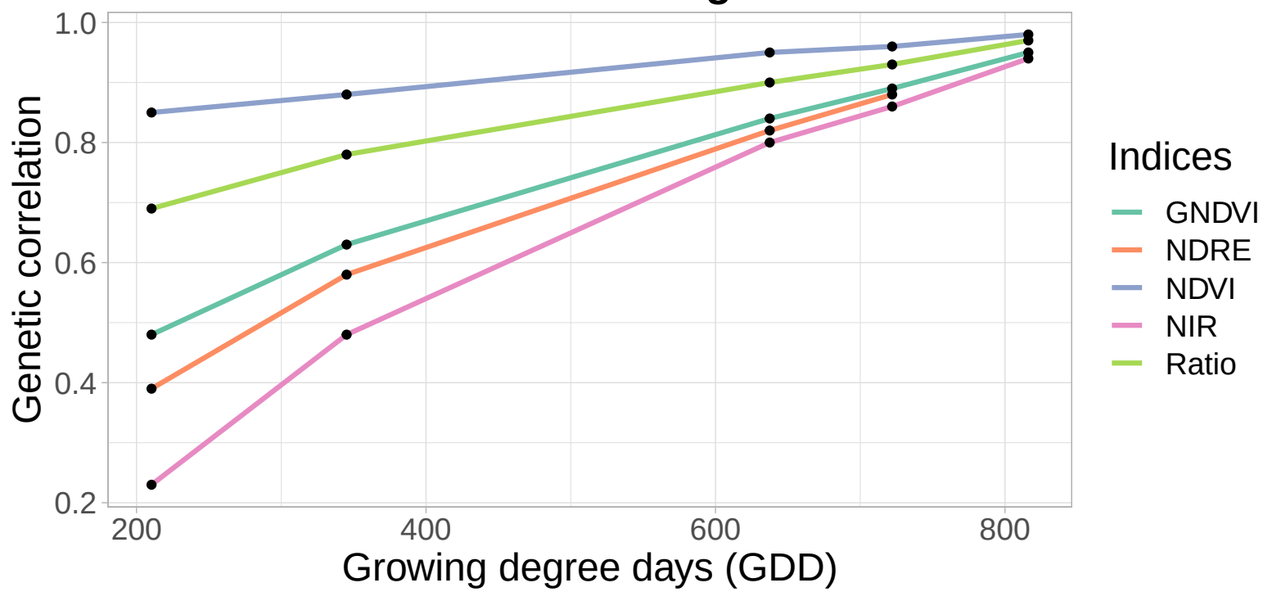

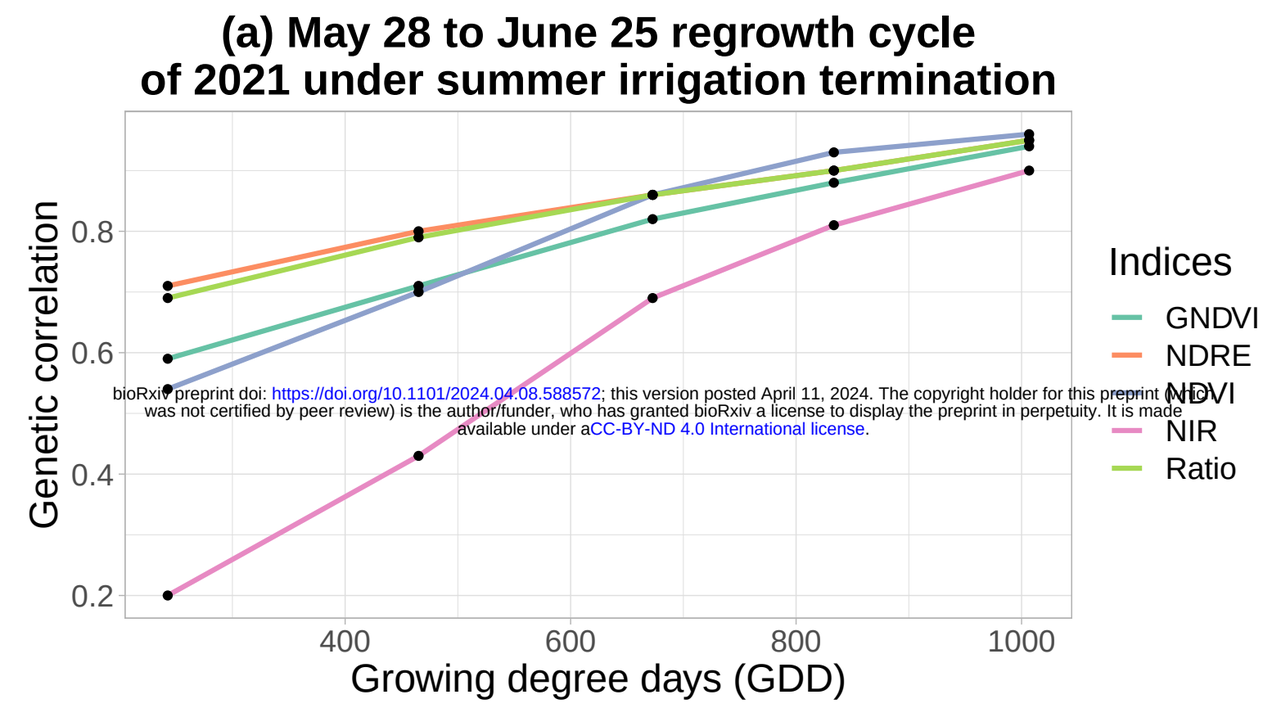

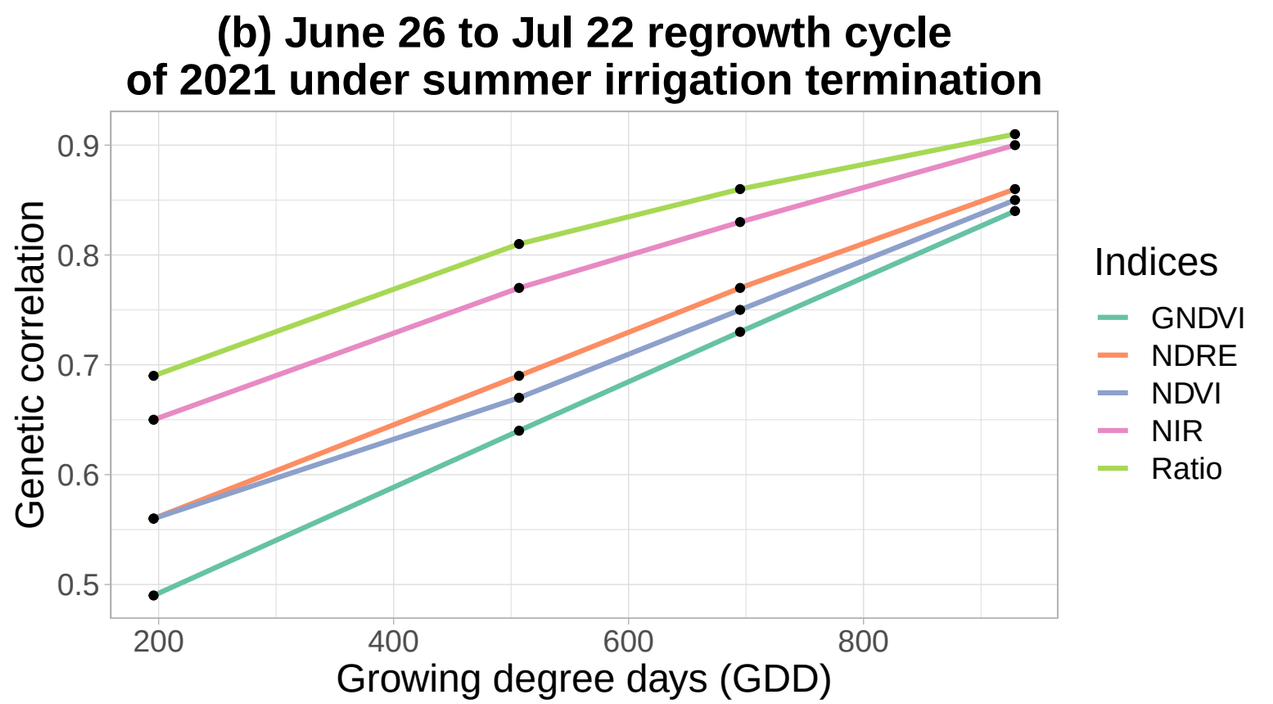

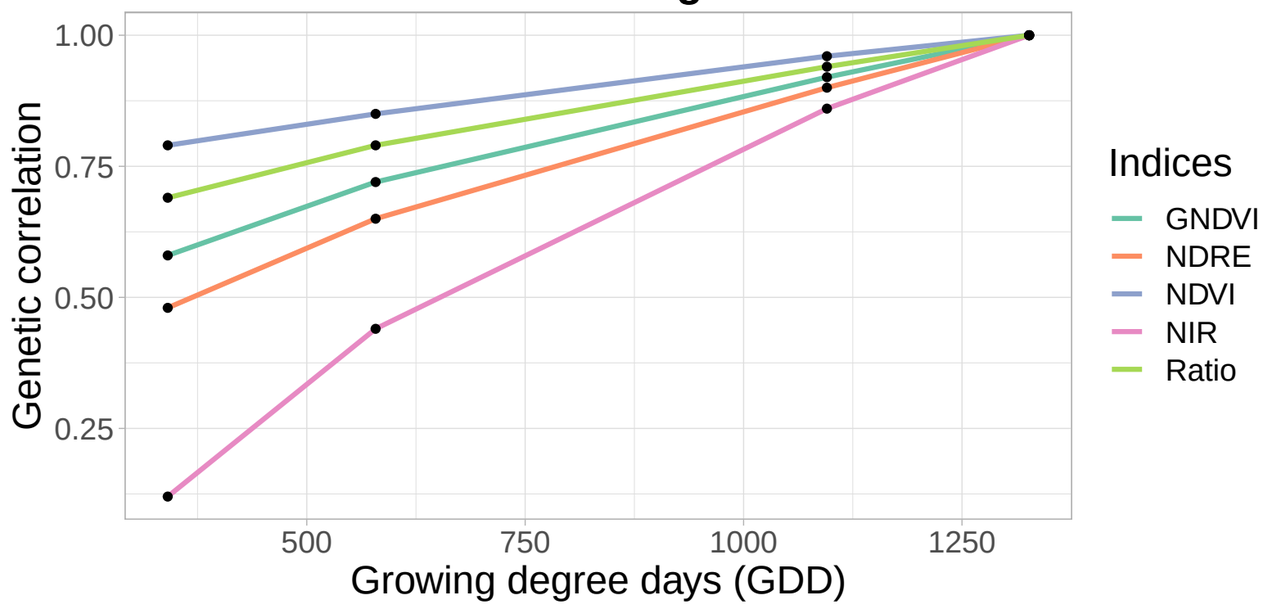

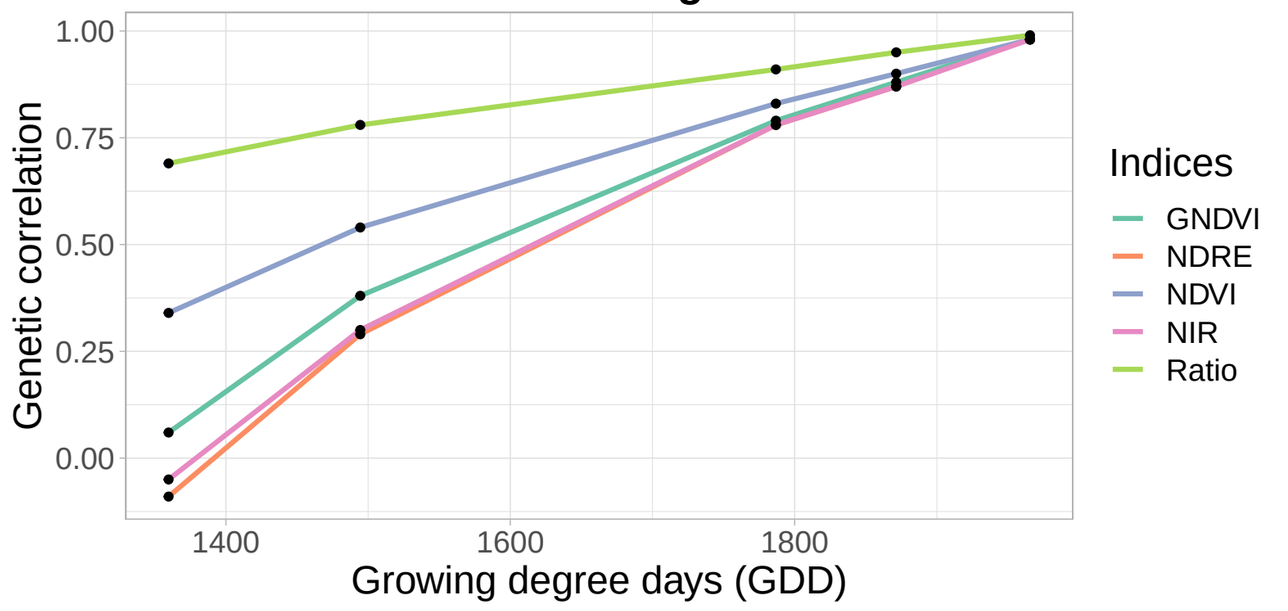

Mean vs. Stability

Scaling = 0, Centering = 2, SVP = 1

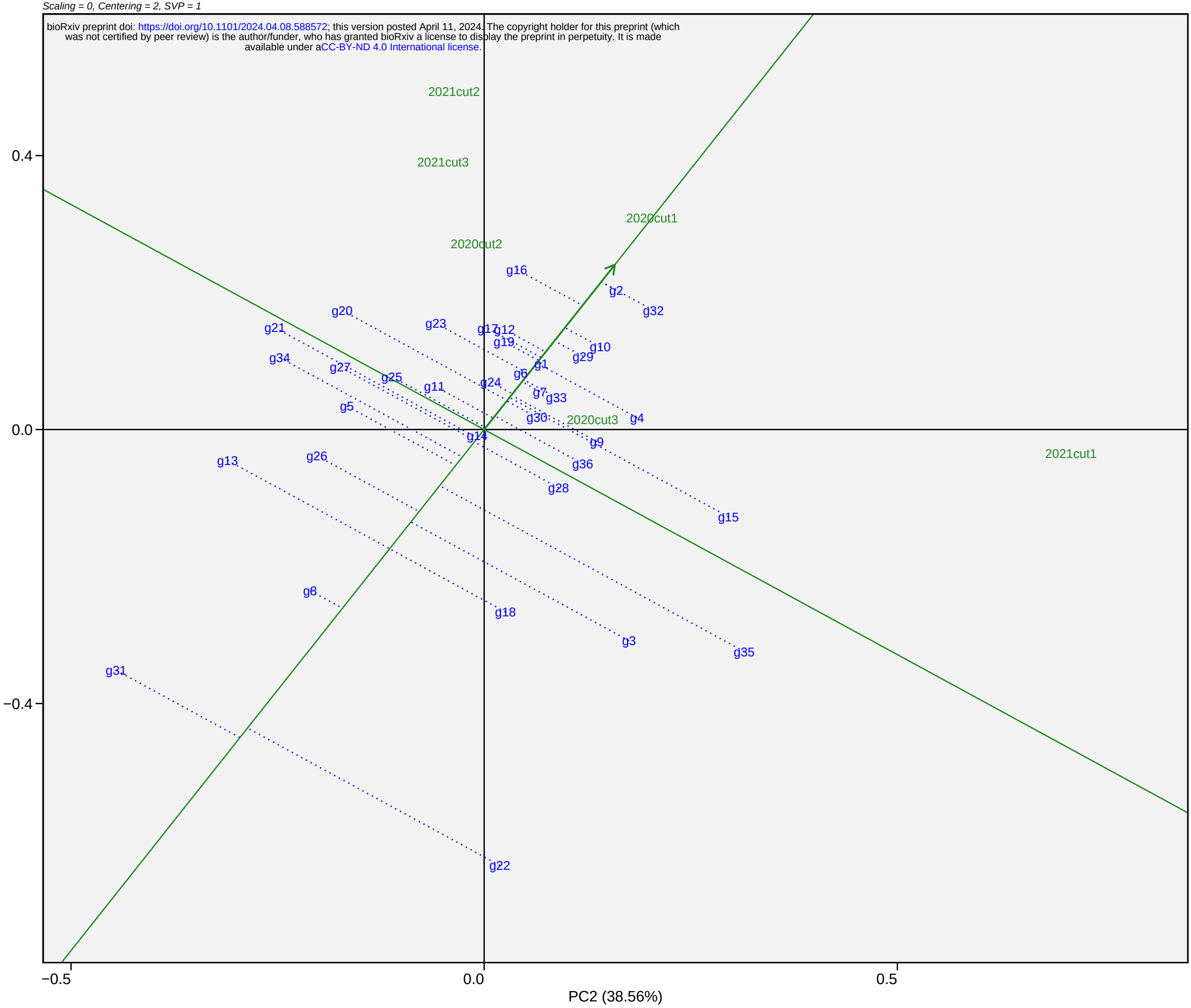

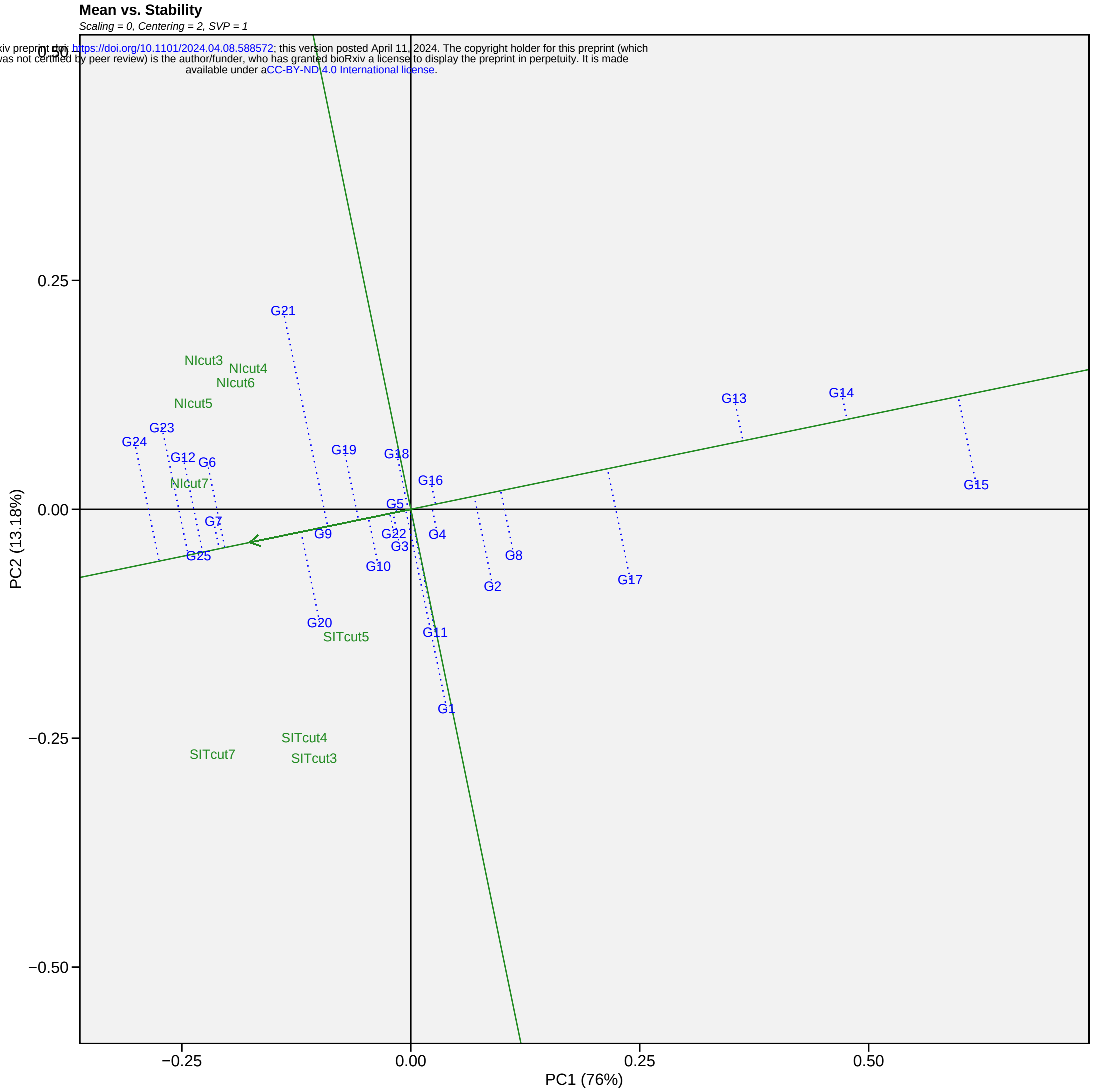

Stable line (g1)

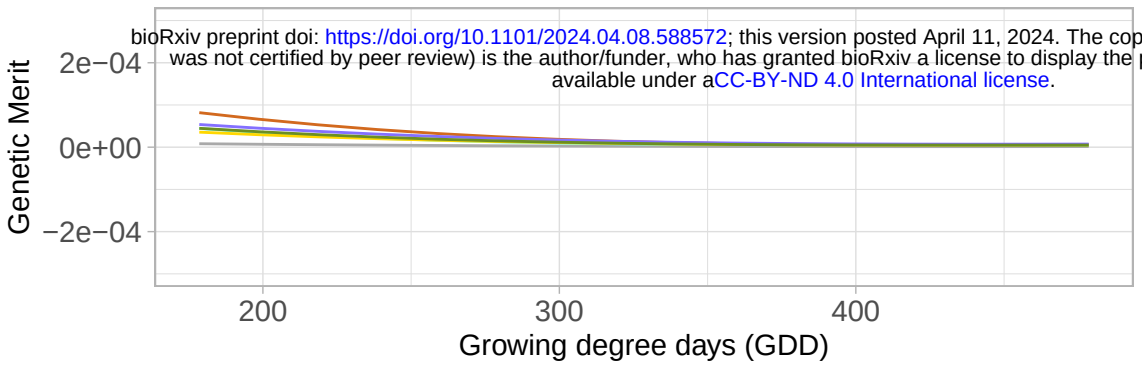

Unstable line (g3)

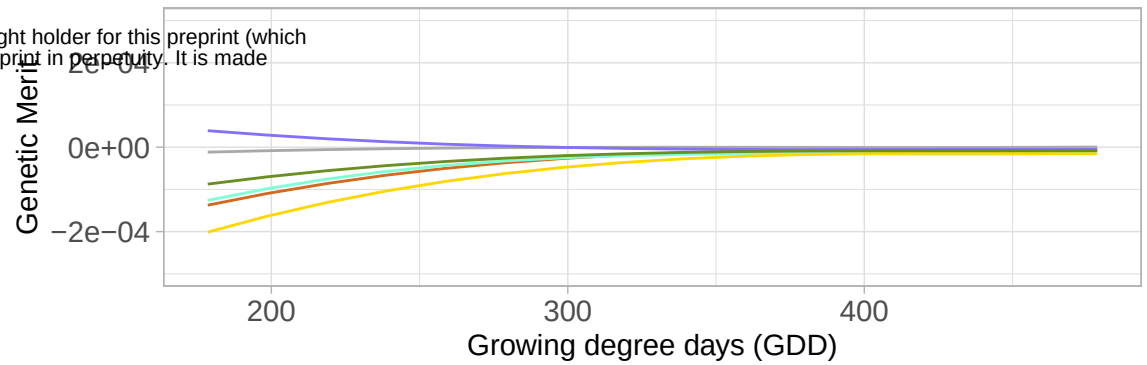

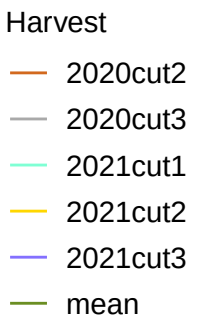

Stable line (g2)

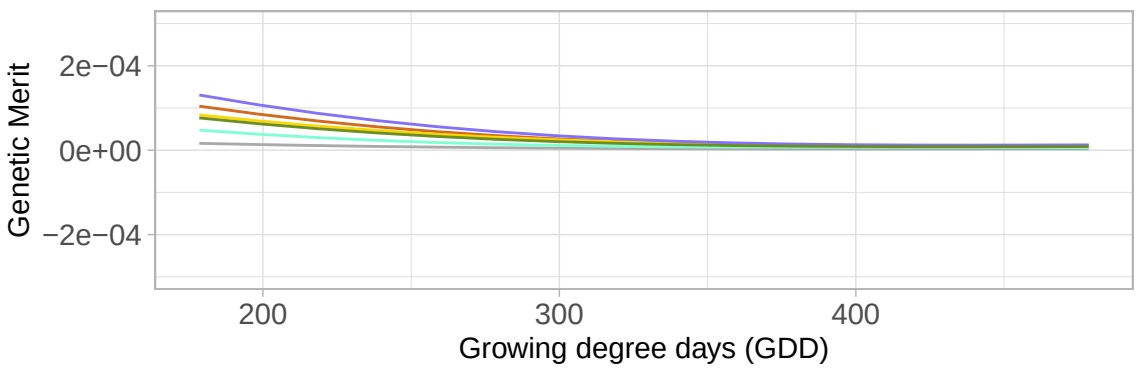

Unstable line (g13)

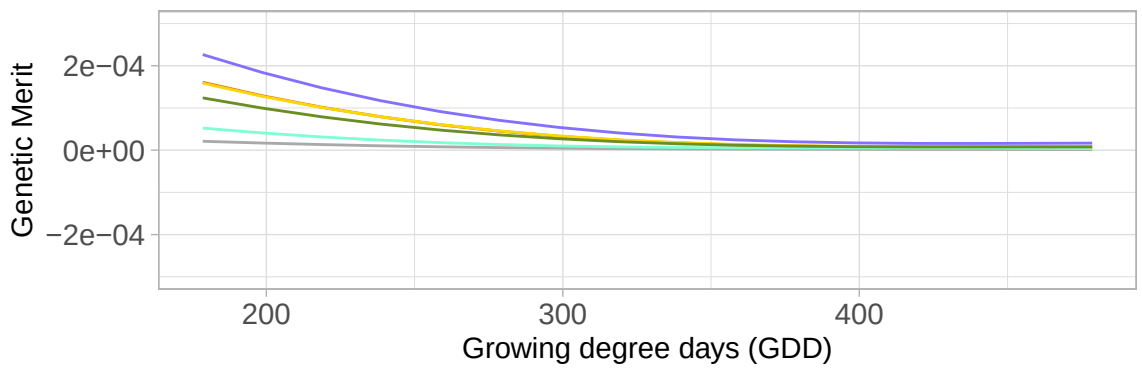

Stable line (g6)

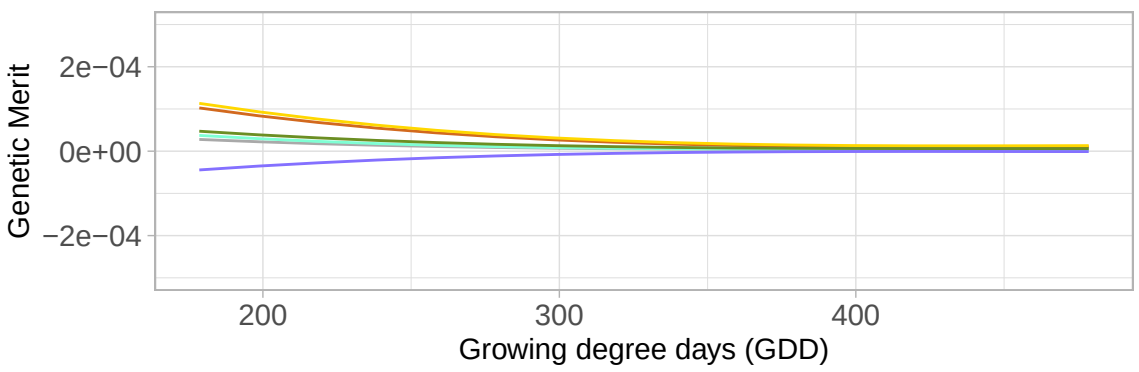

Unstable line (g21)

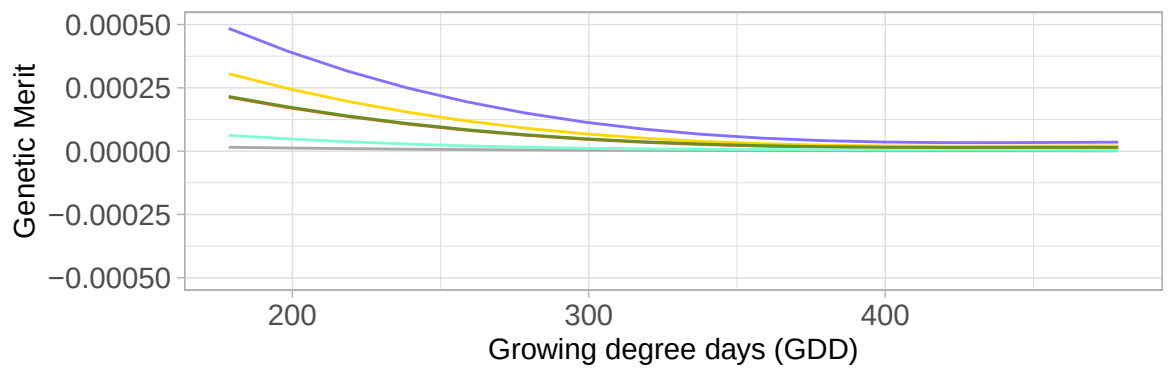

Stable line (g8)

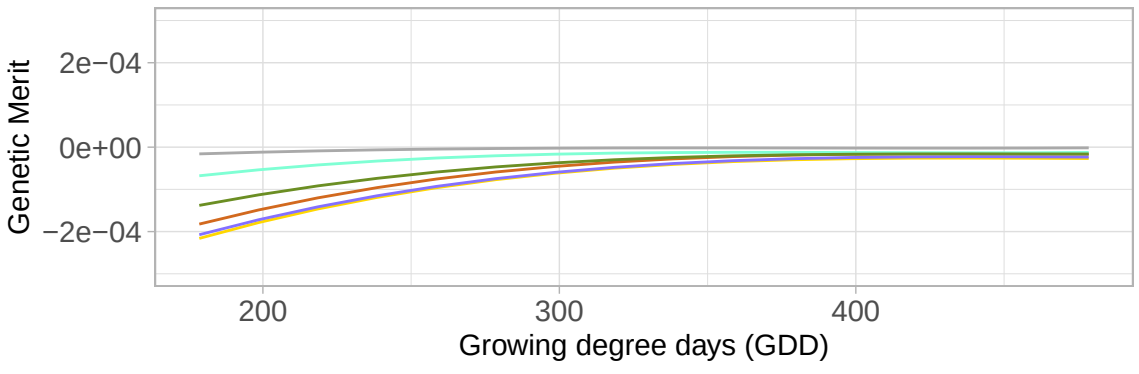

Unstable line (g22)

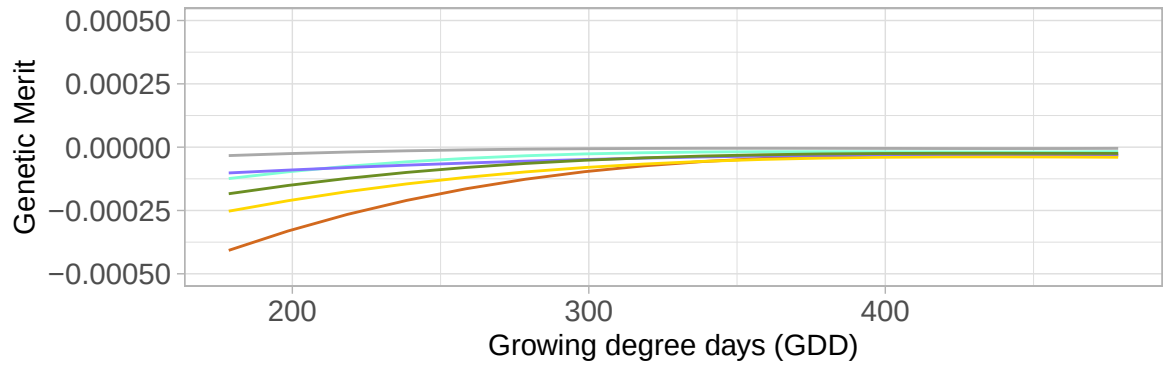

Stable line (g14)

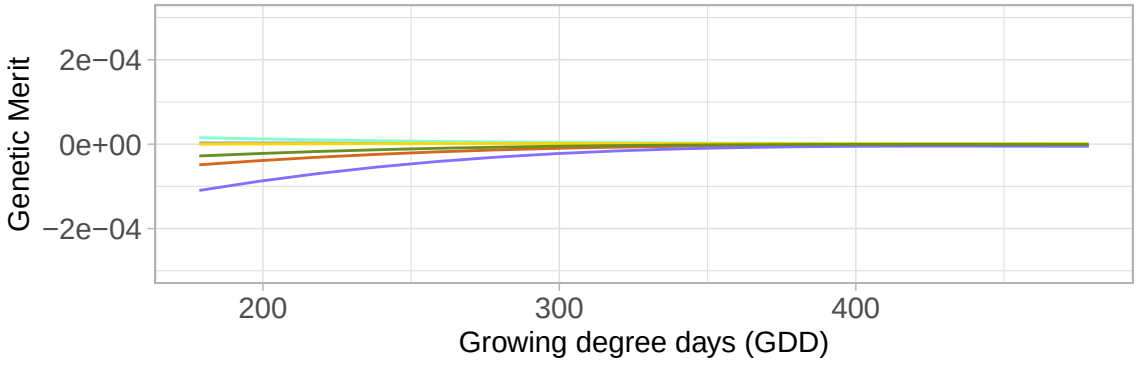

Unstable line (g35)

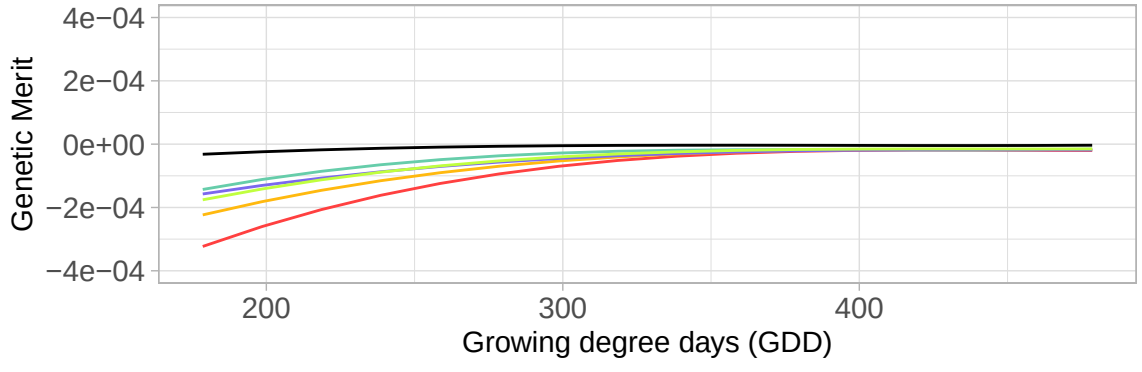

Stable line (g1)

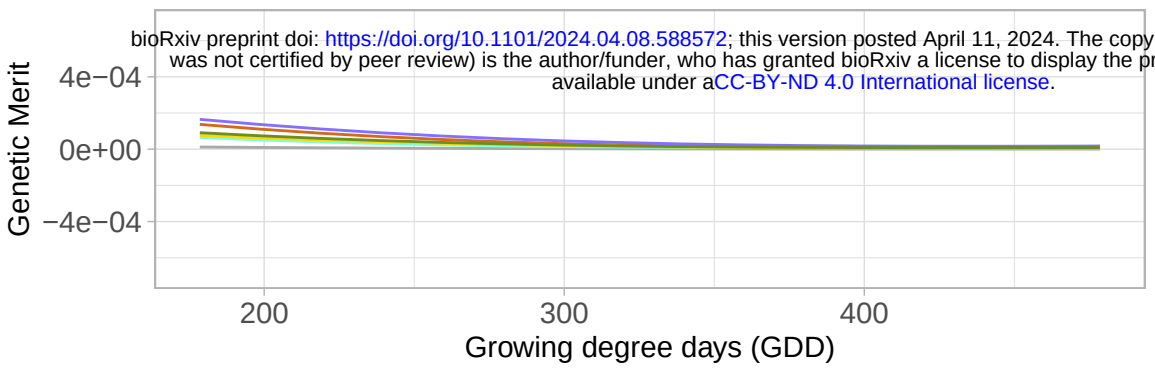

Unstable line (g3)

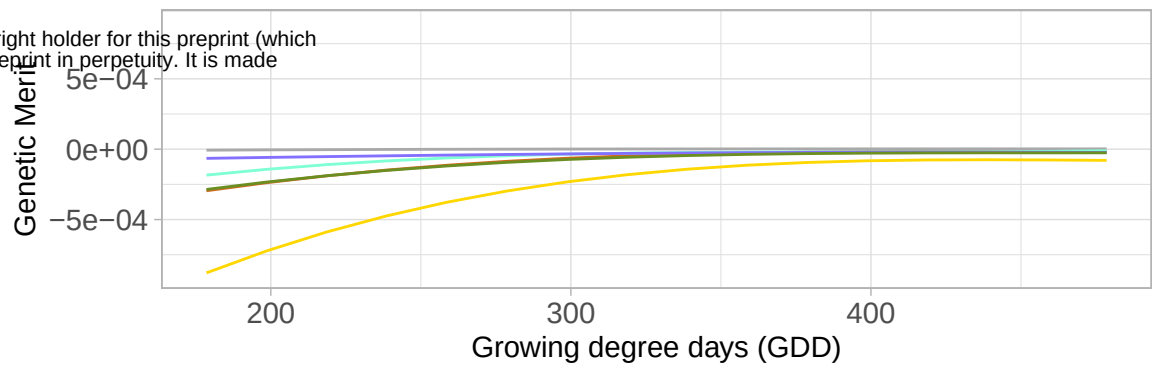

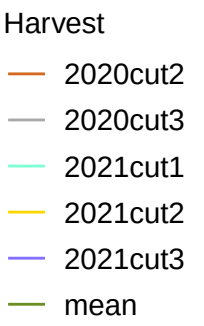

Stable line (g2)

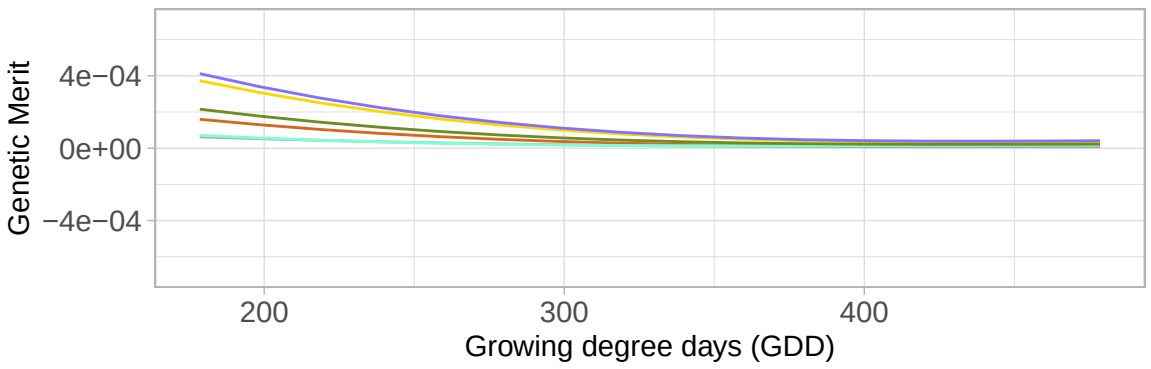

Unstable line (g13)

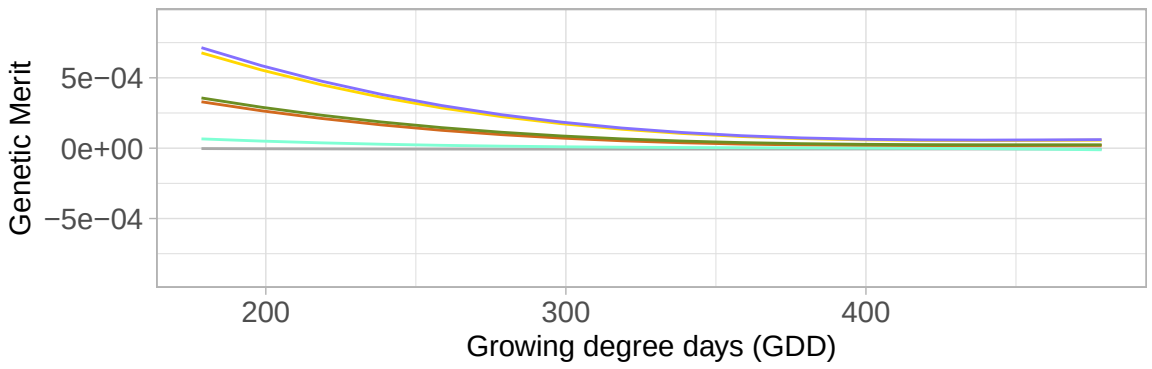

Stable line (g6)

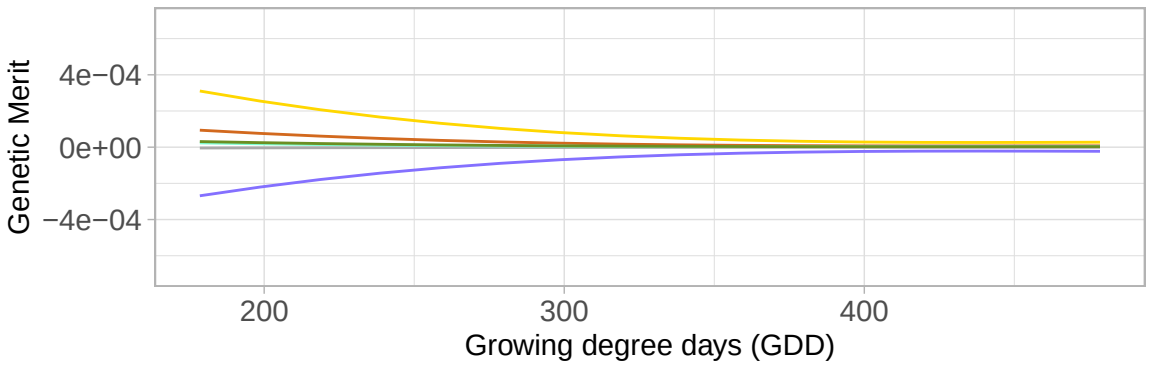

Unstable line (g21)

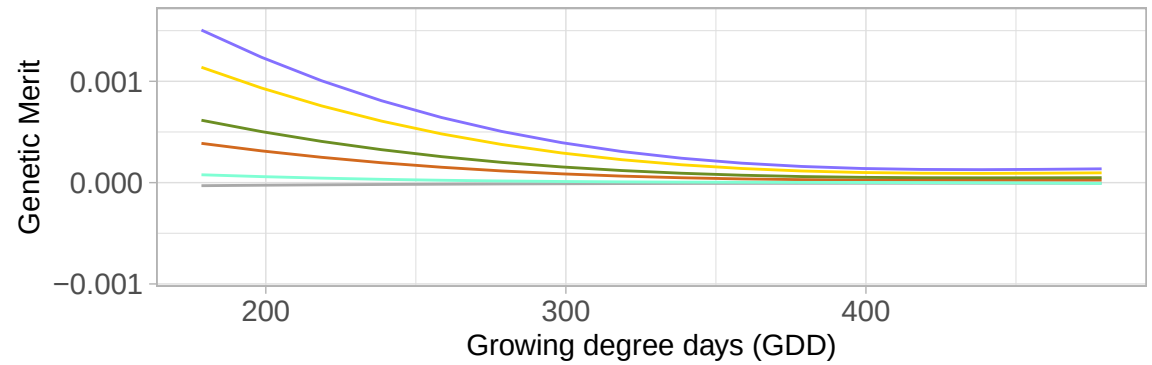

Stable line (g8)

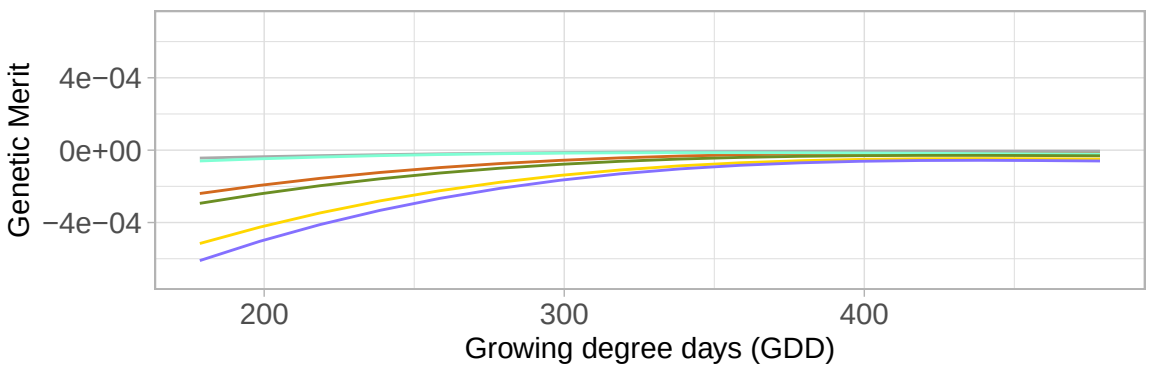

Unstable line (g22)

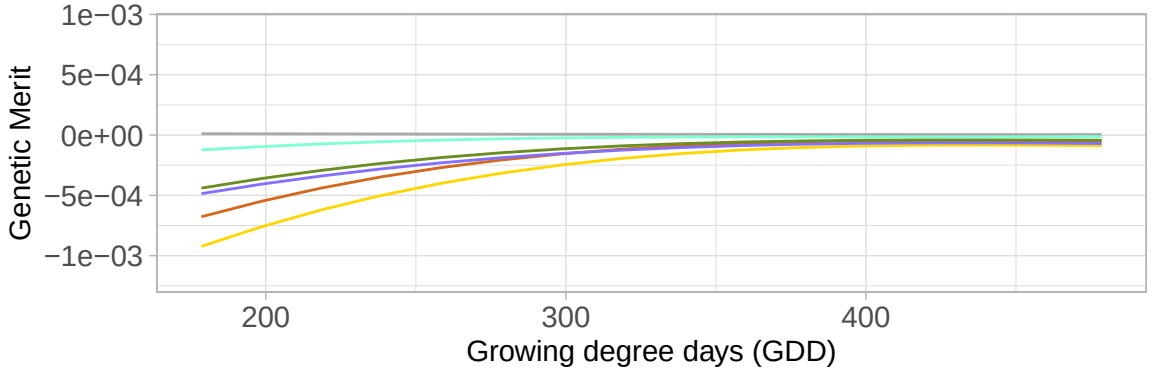

Stable line (g14)

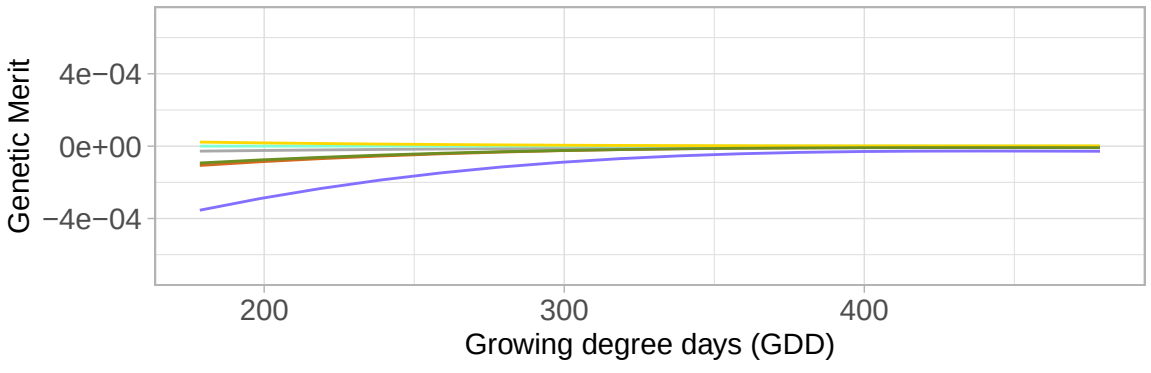

Unstable line (g35)

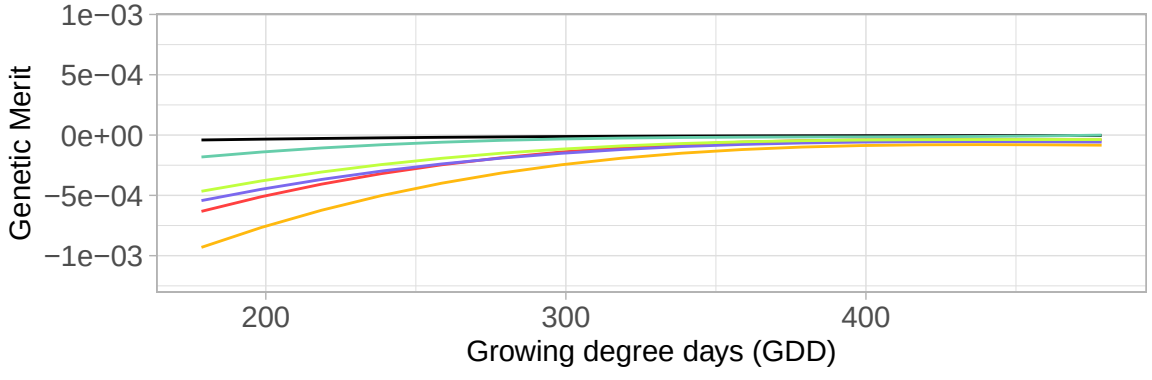

Stable line (g1)

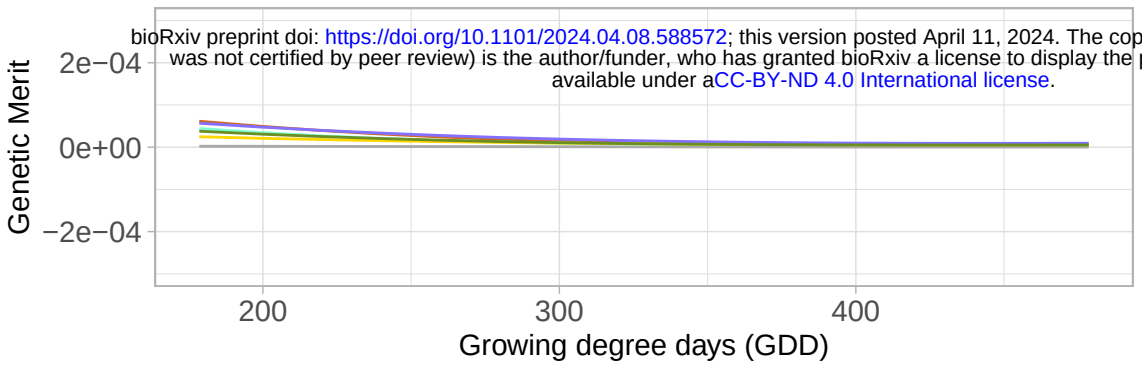

Unstable line (g3)

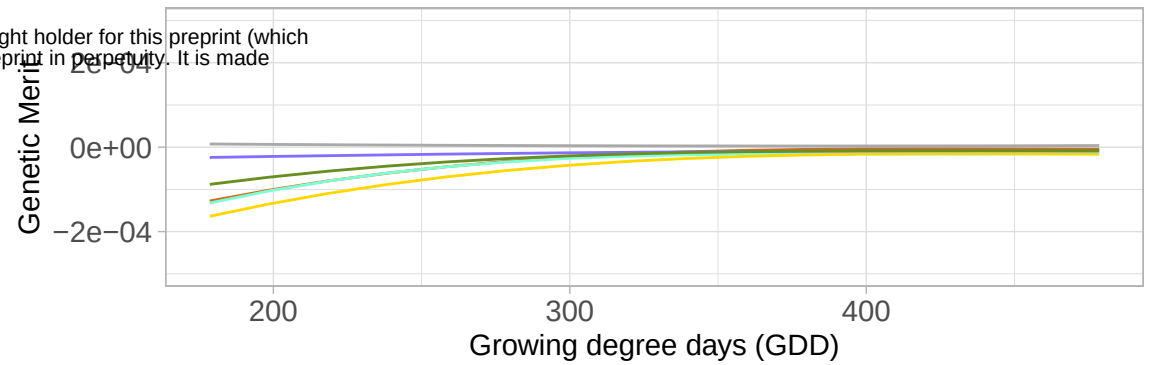

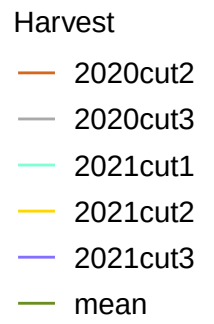

Stable line (g2)

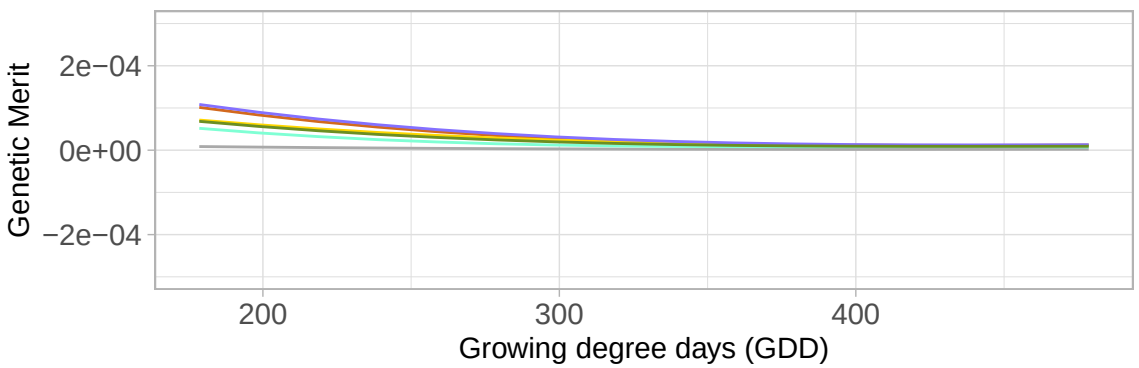

Unstable line (g13)

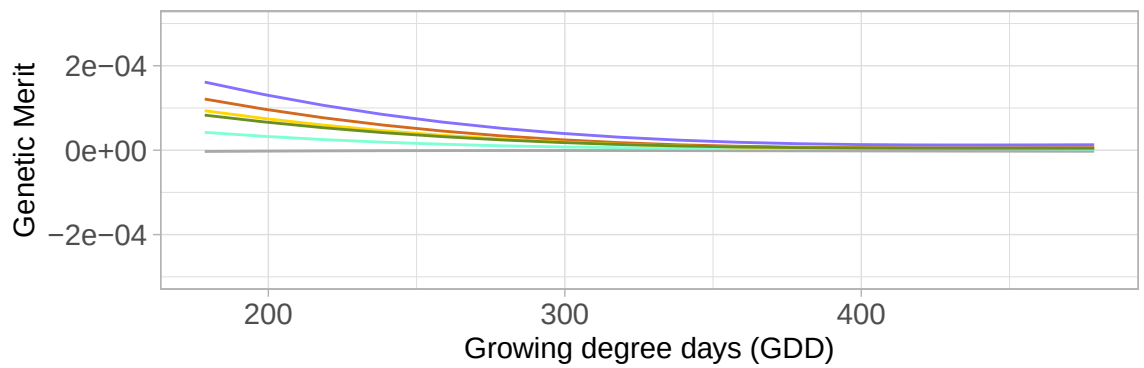

Stable line (g6)

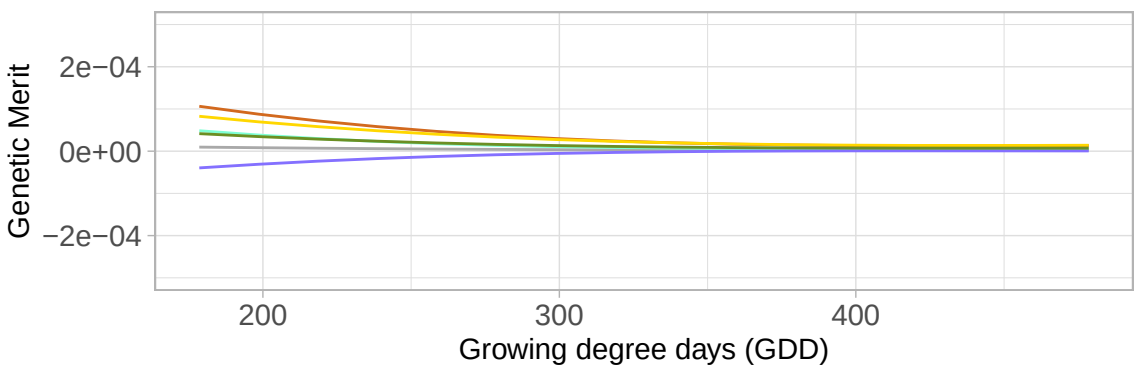

Unstable line (g21)

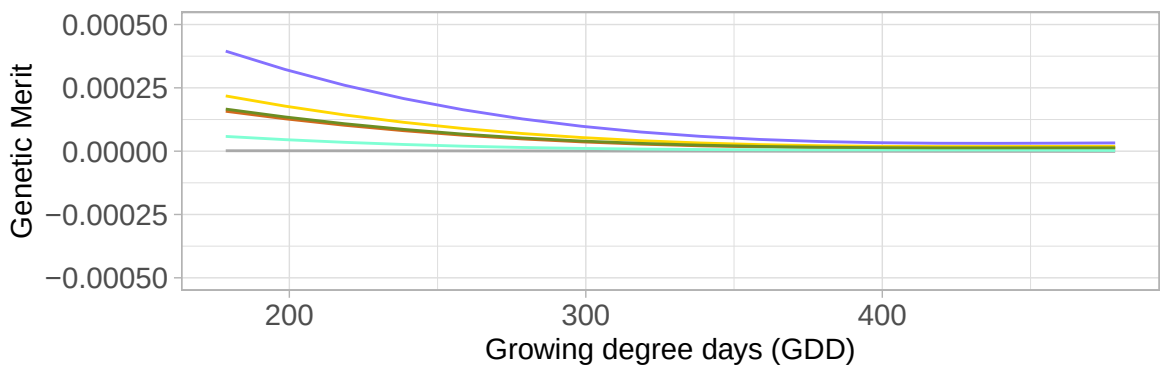

Stable line (g8)

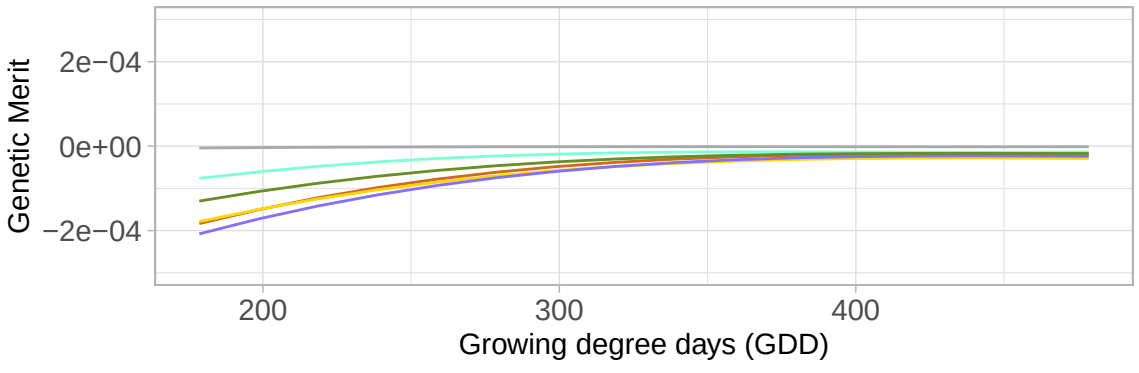

Unstable line (g22)

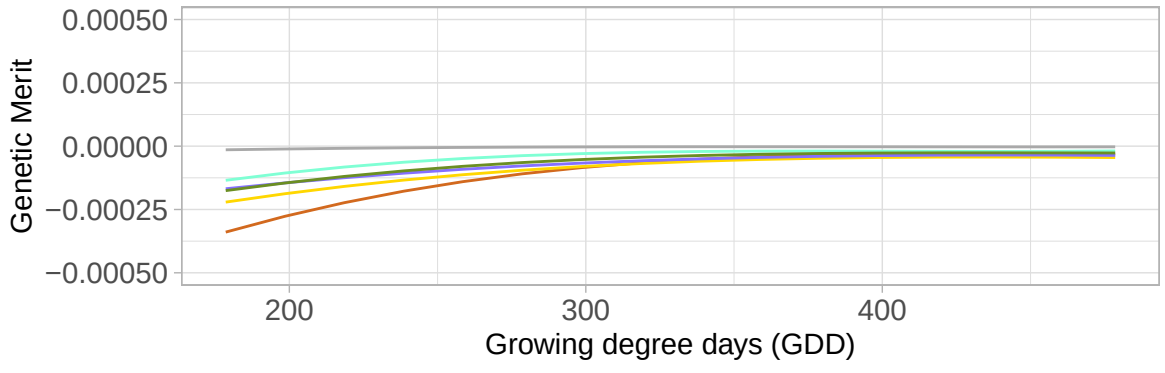

Stable line (g14)

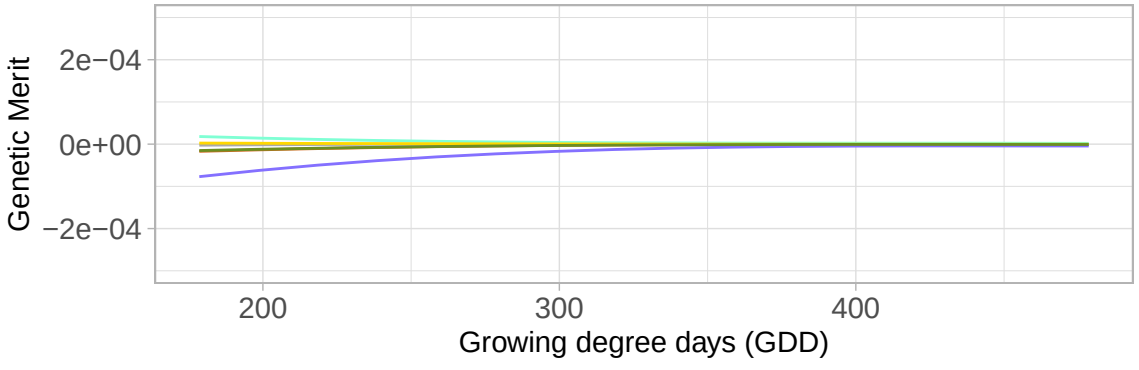

Unstable line (g35)

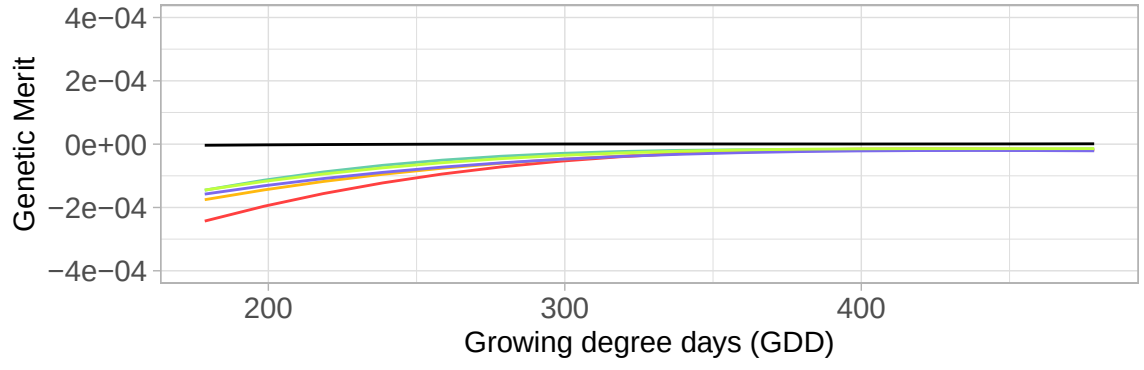

Stable line (g1)

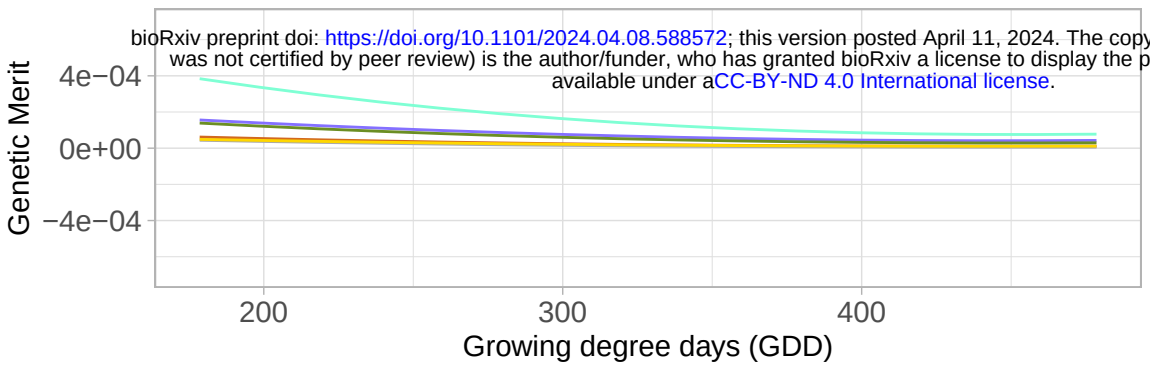

Unstable line (g3)

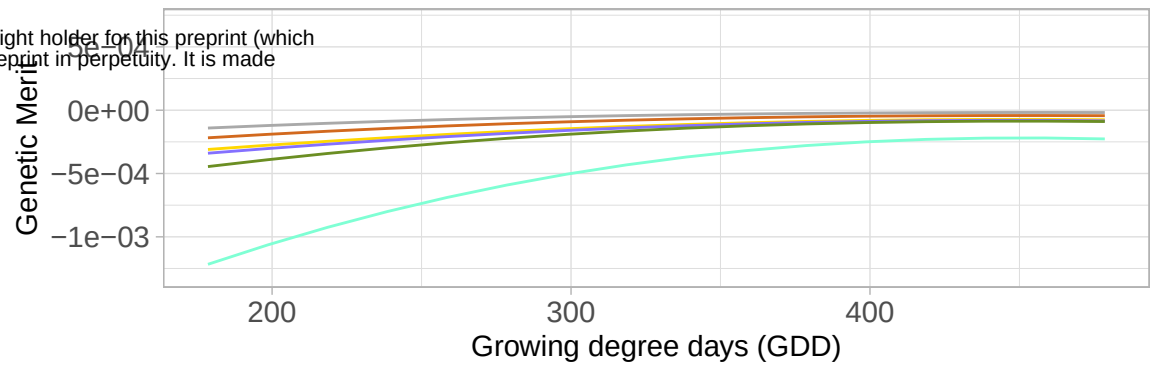

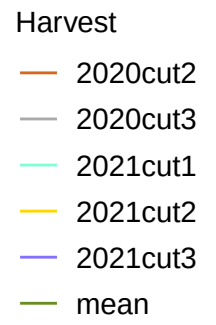

Stable line (g2)

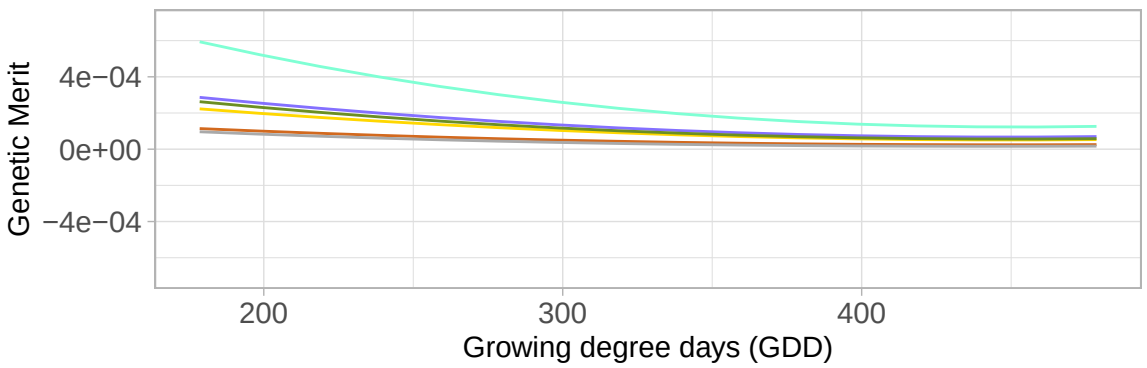

Unstable line (g13)

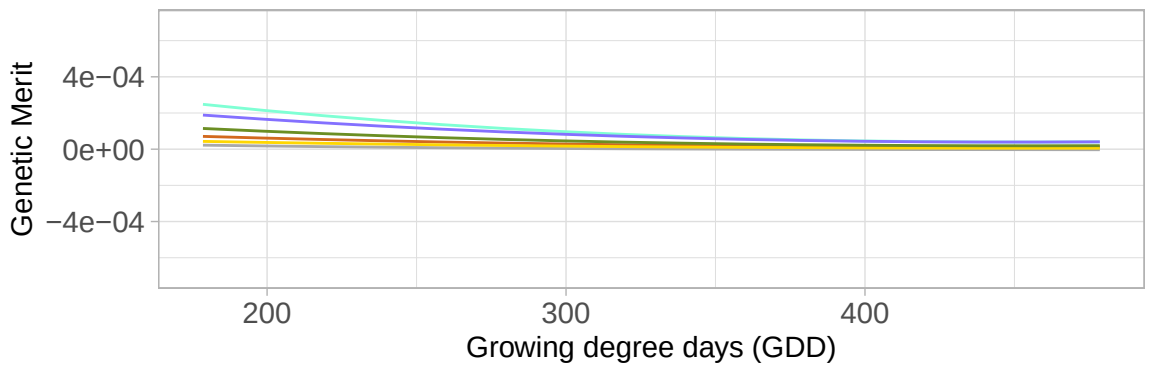

Stable line (g6)

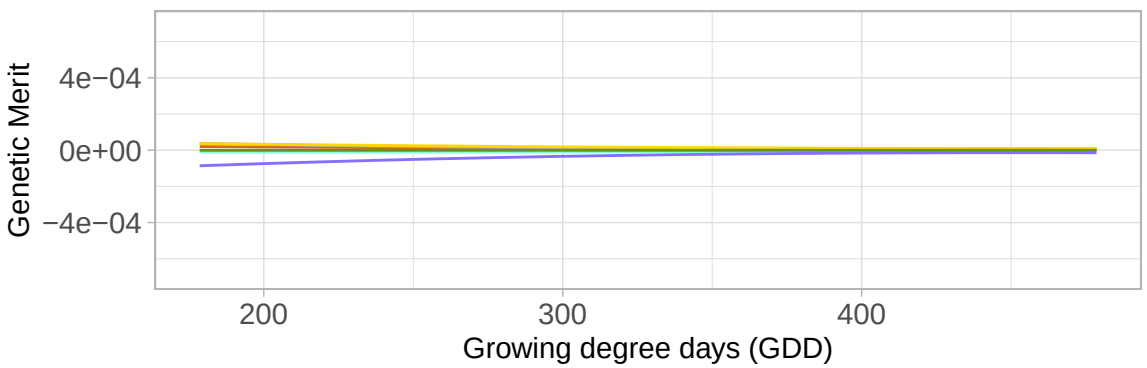

Unstable line (g21)

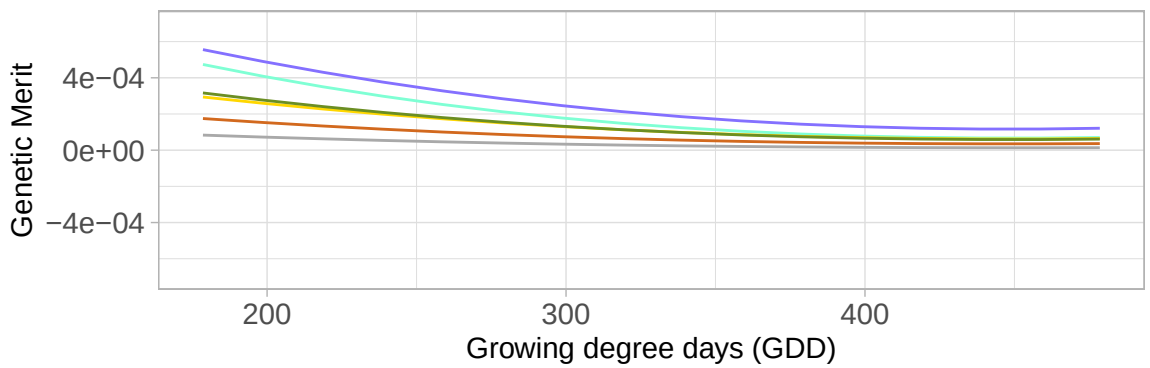

Stable line (g8)

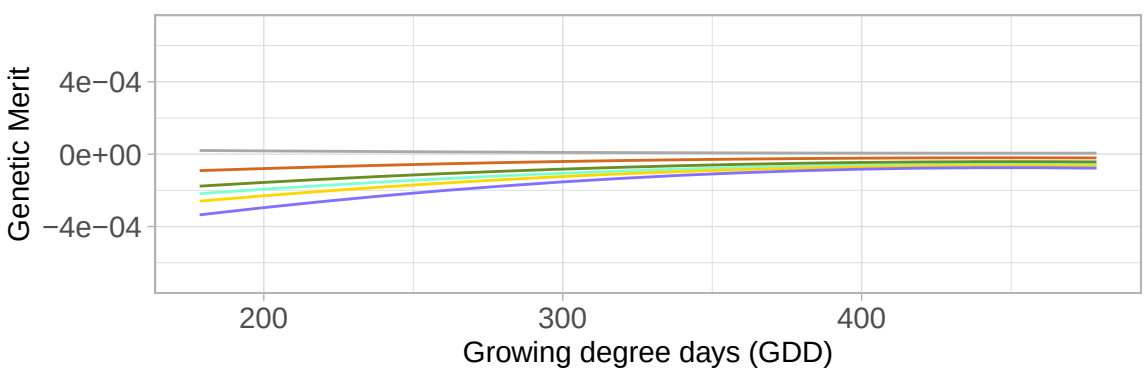

Unstable line (g22)

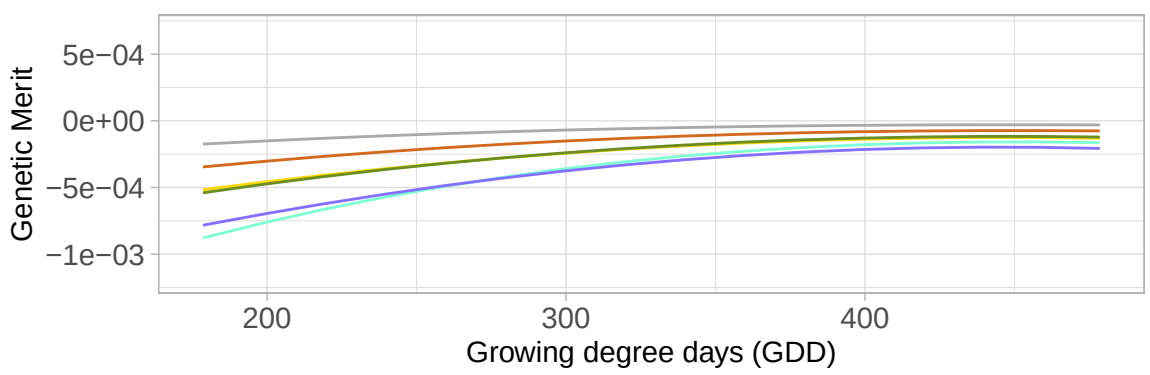

Stable line (g14)

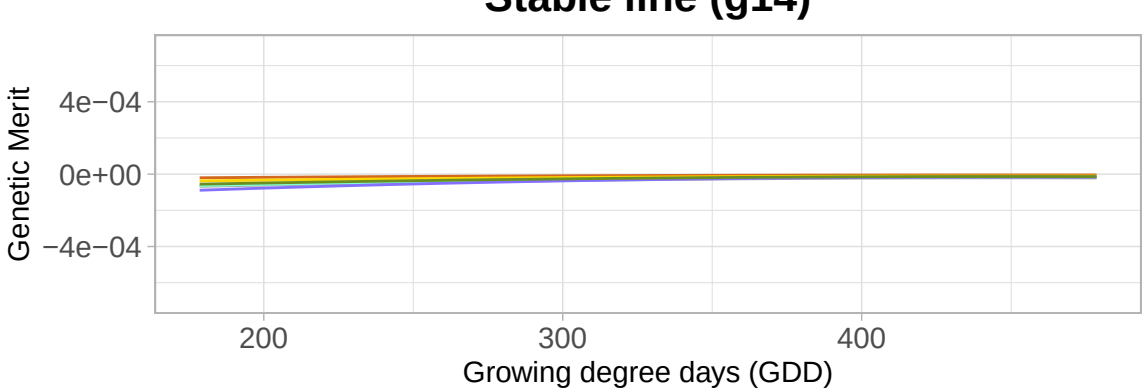

Unstable line (g35)

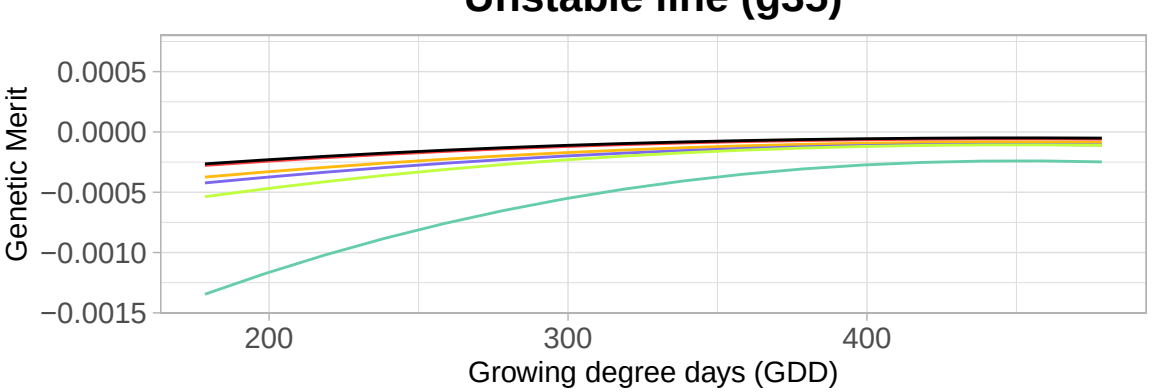

Stable line (g1)

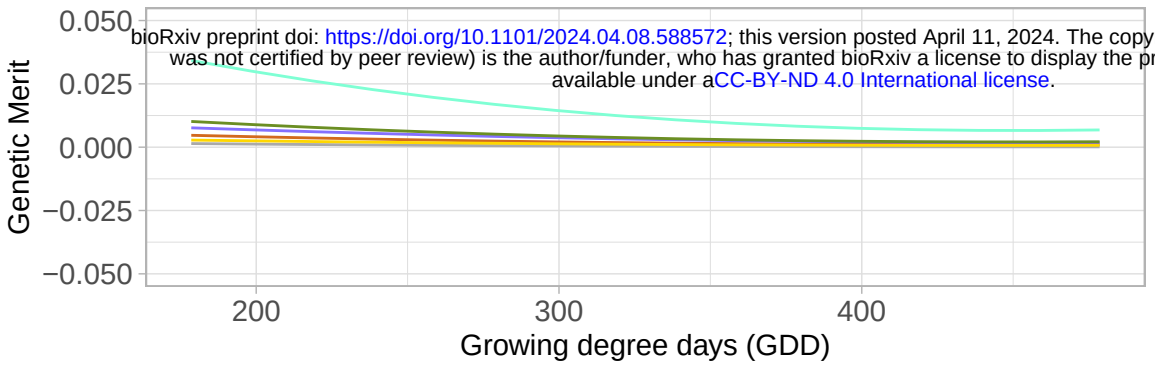

Unstable line (g3)

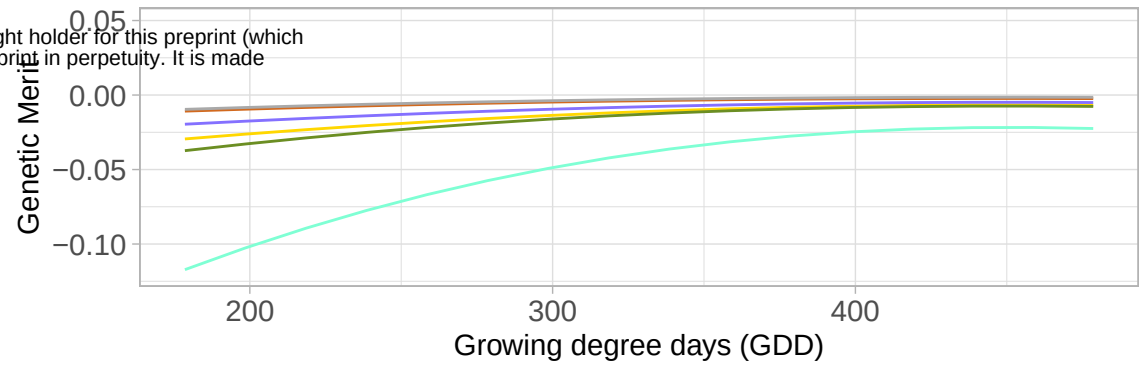

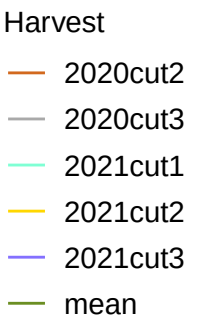

Stable line (g2)

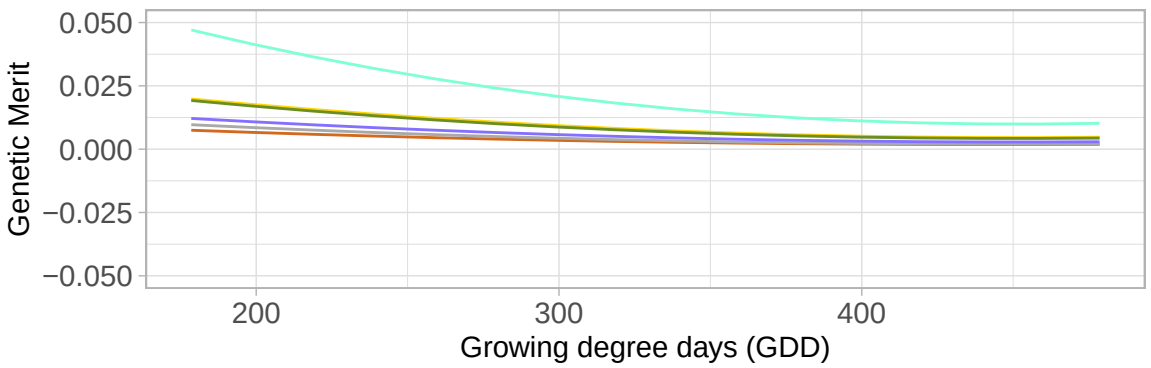

Unstable line (g13)

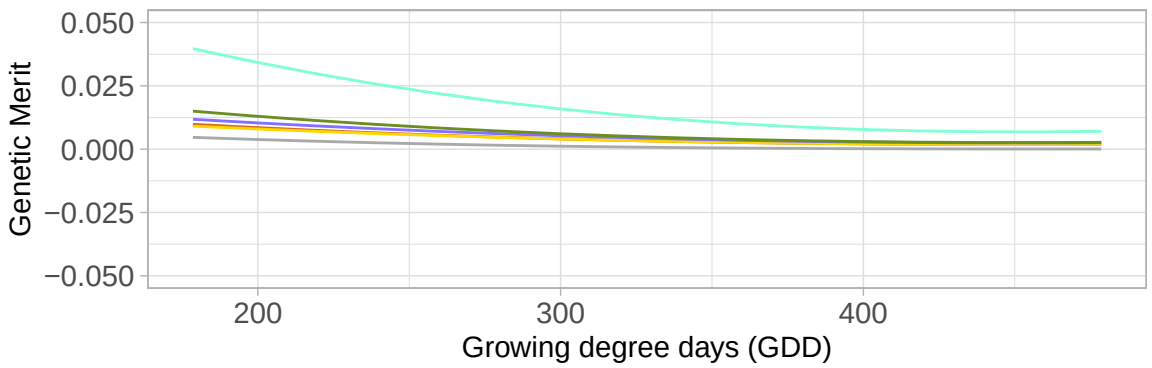

Stable line (g6)

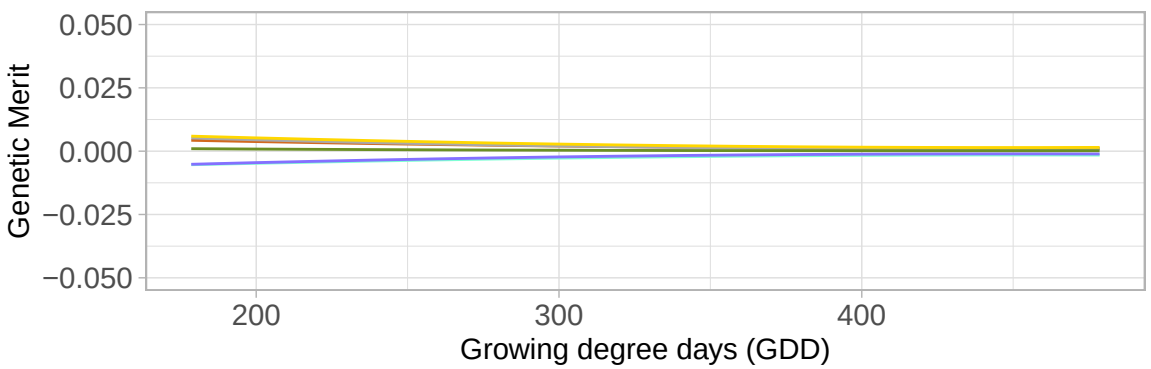

Unstable line (g21)

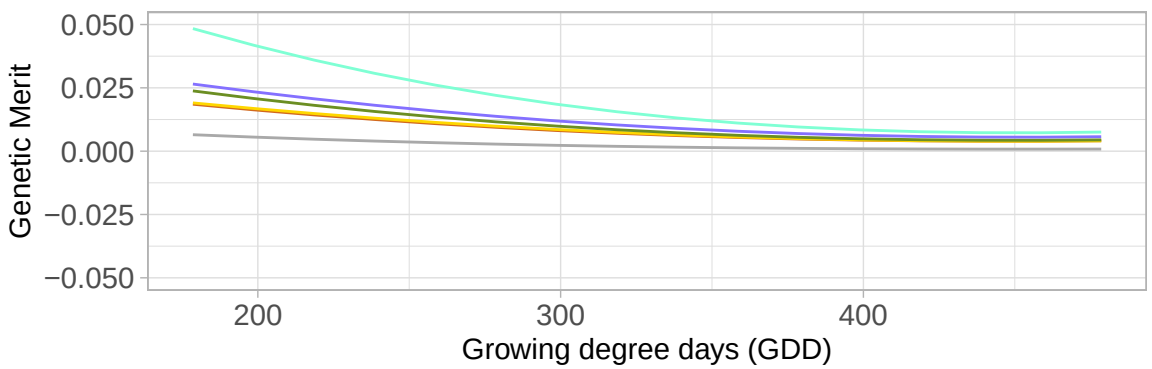

Stable line (g8)

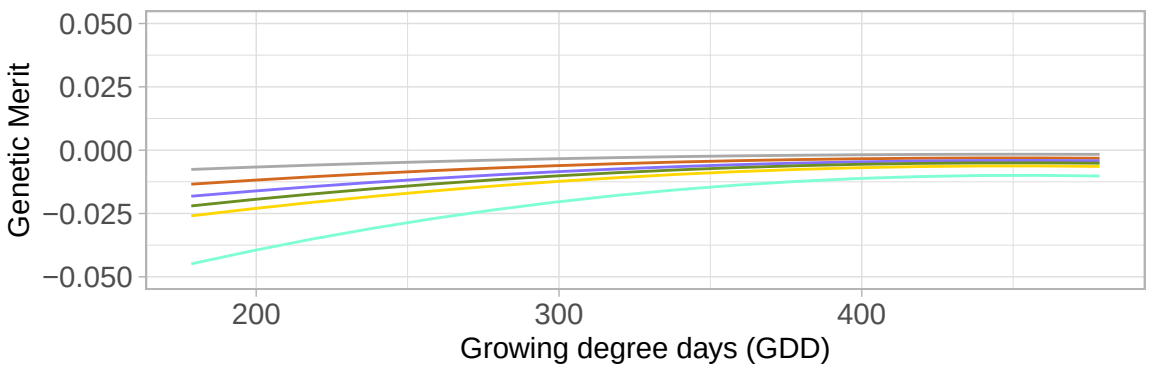

Unstable line (g22)

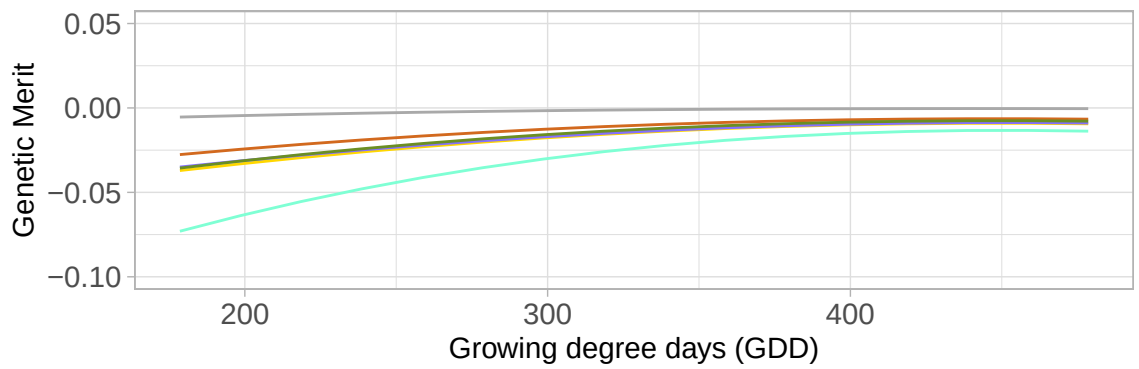

Stable line (g14)

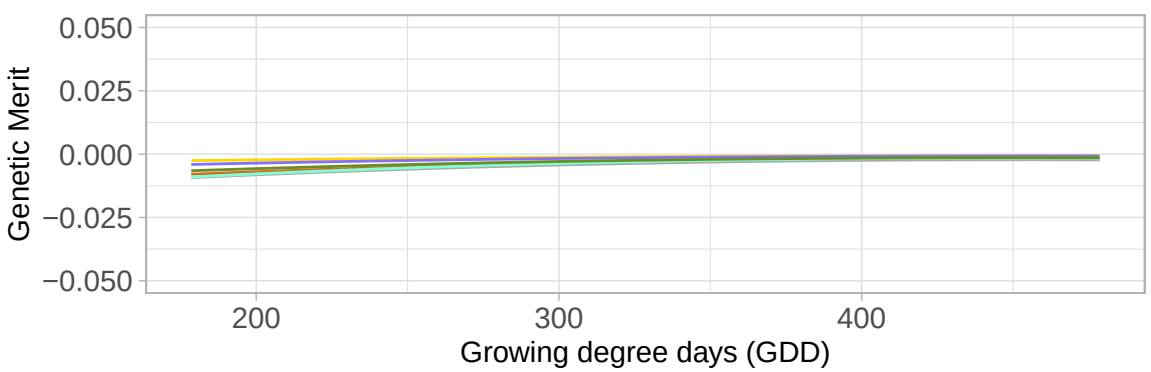

Unstable line (g35)

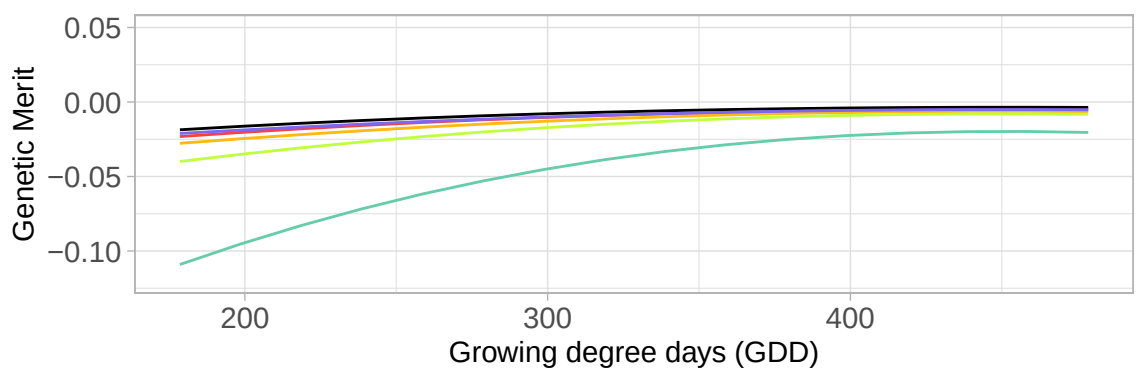

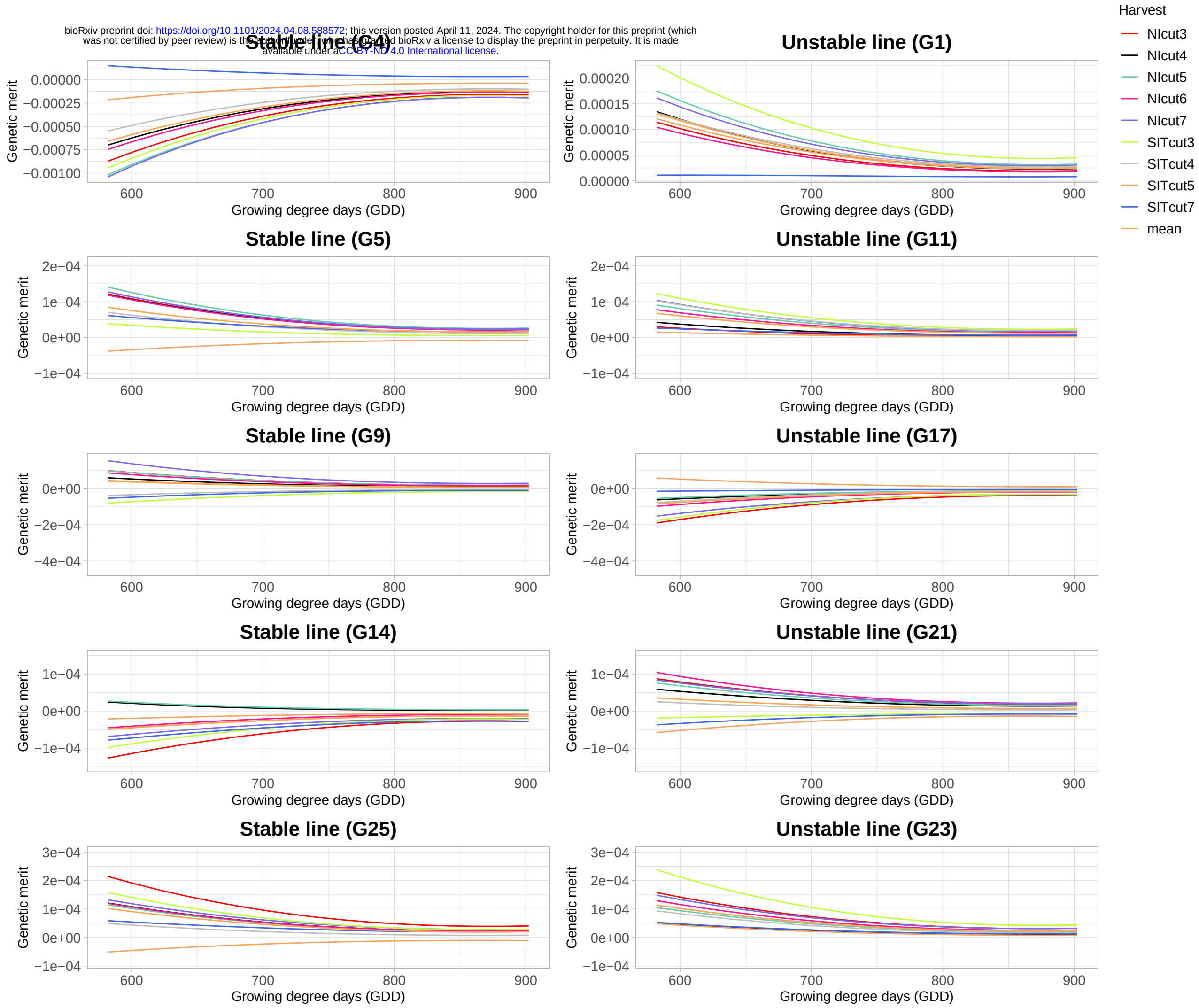

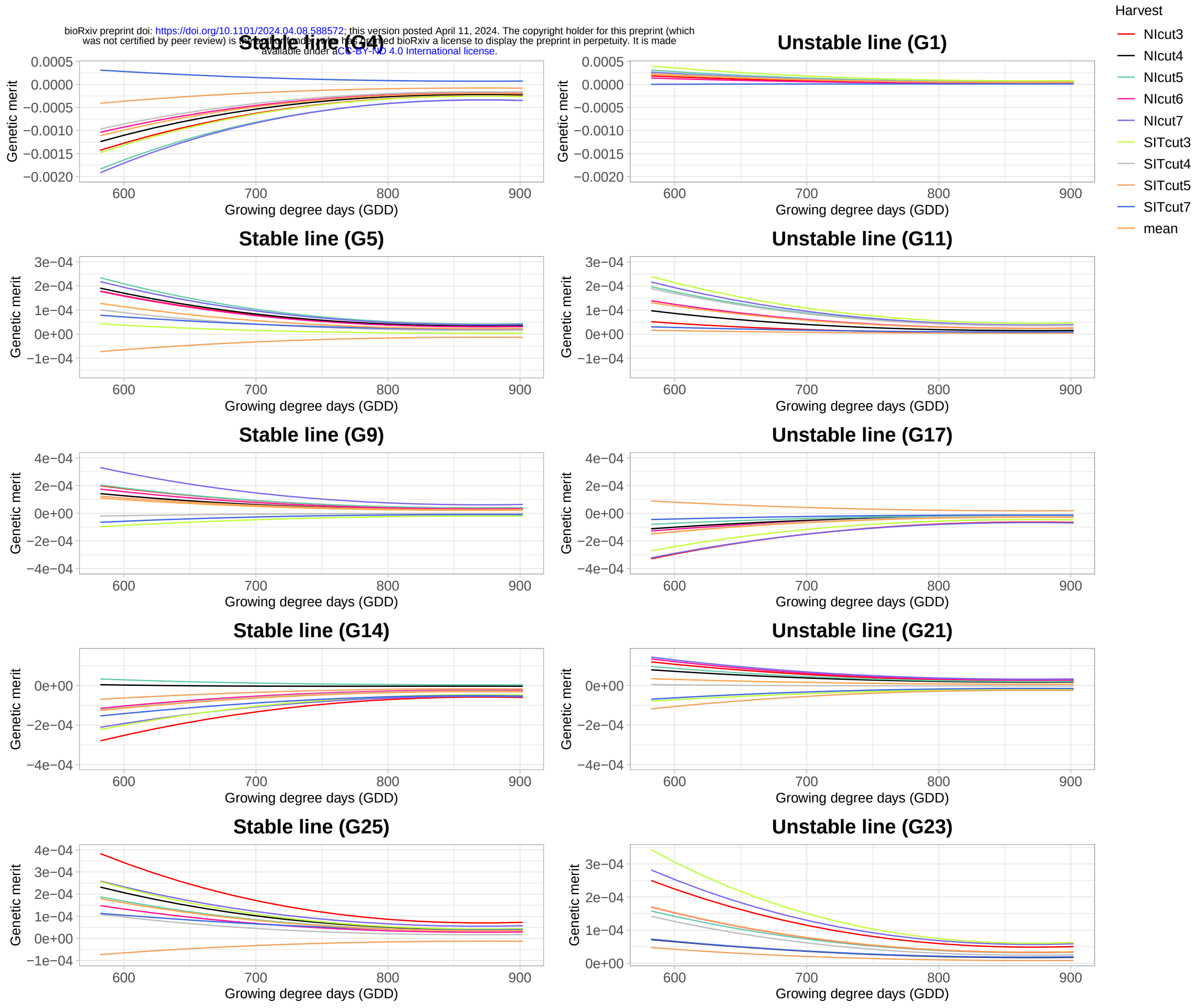

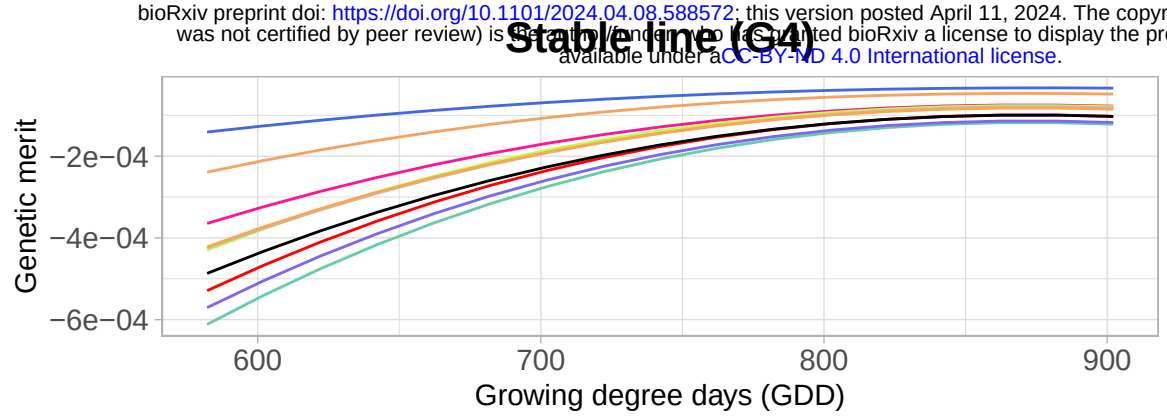

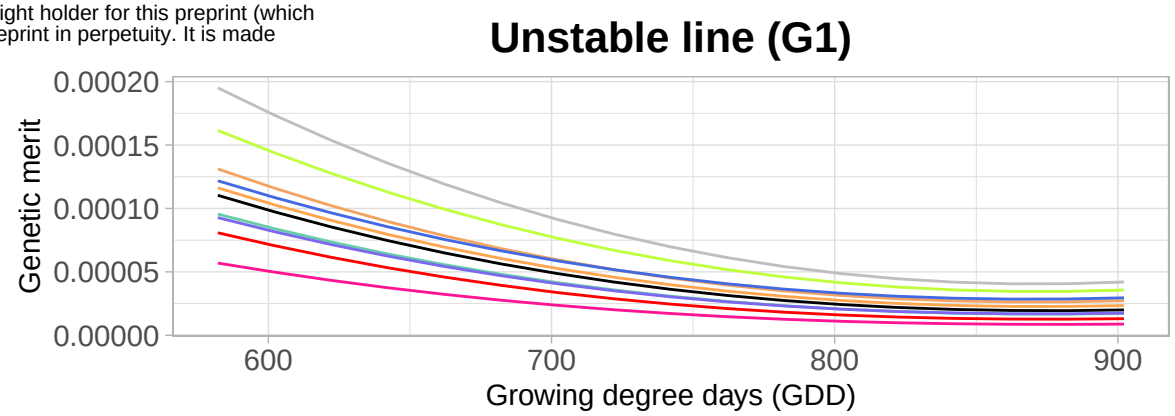

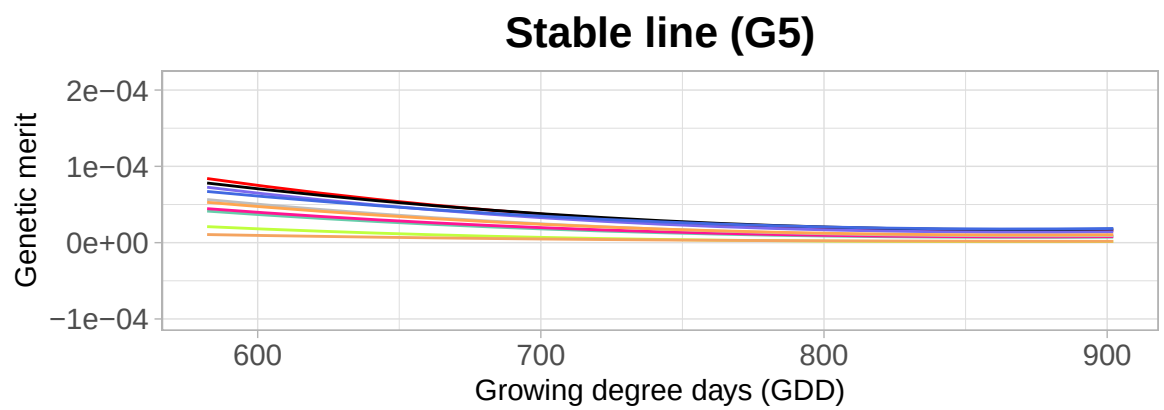

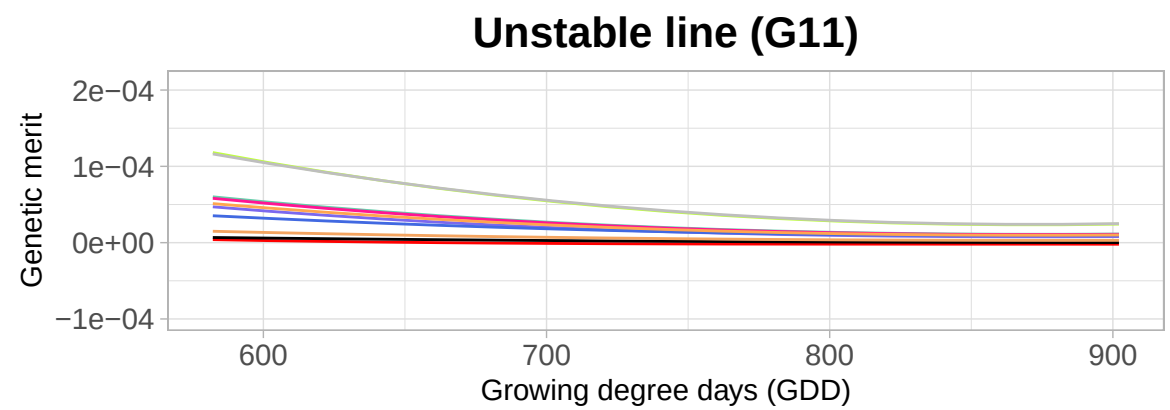

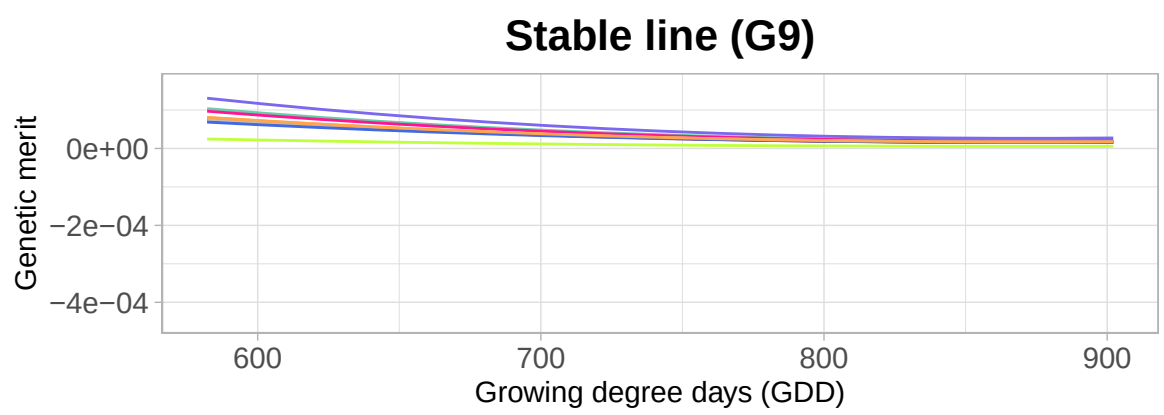

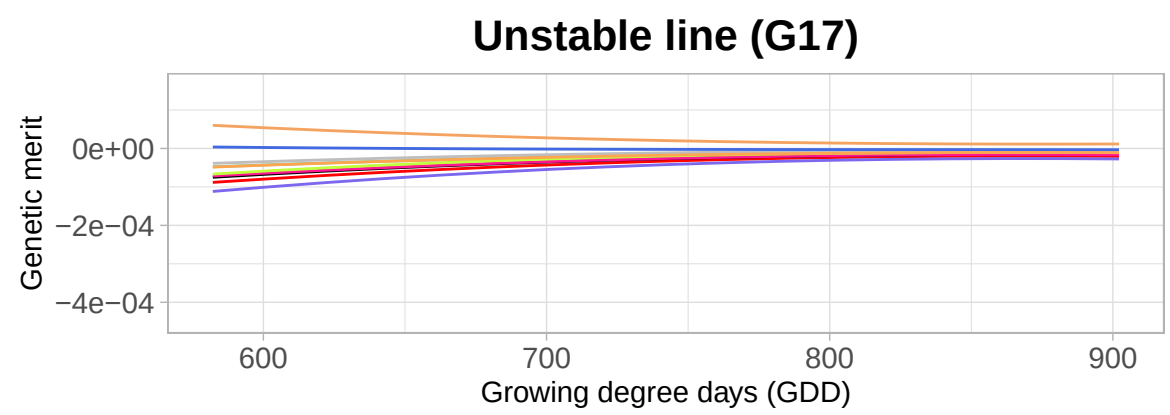

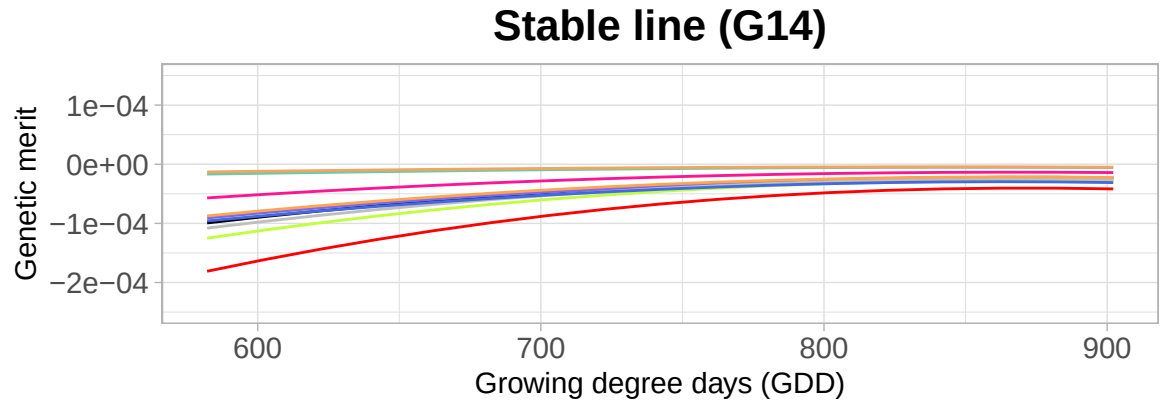

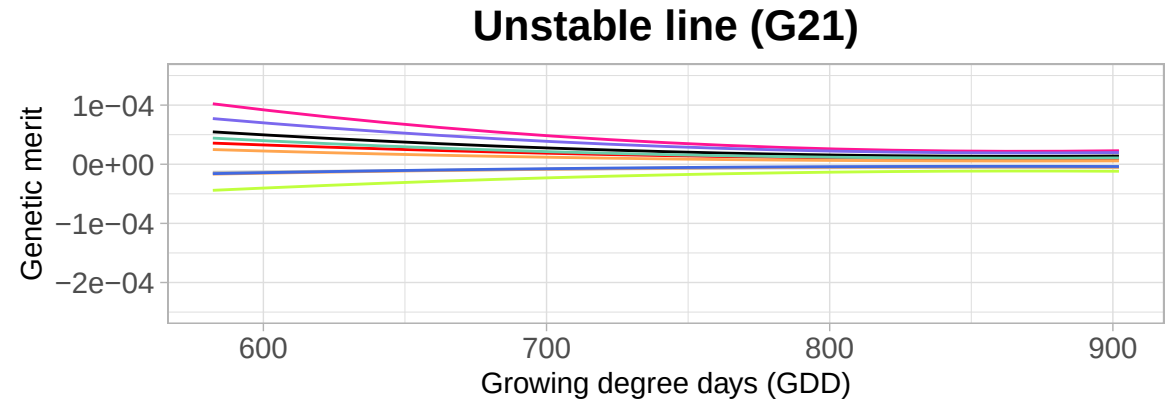

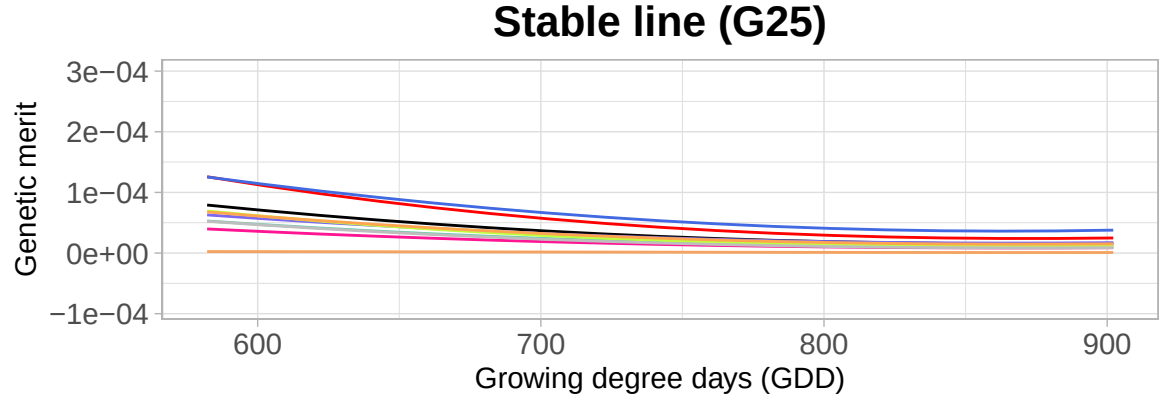

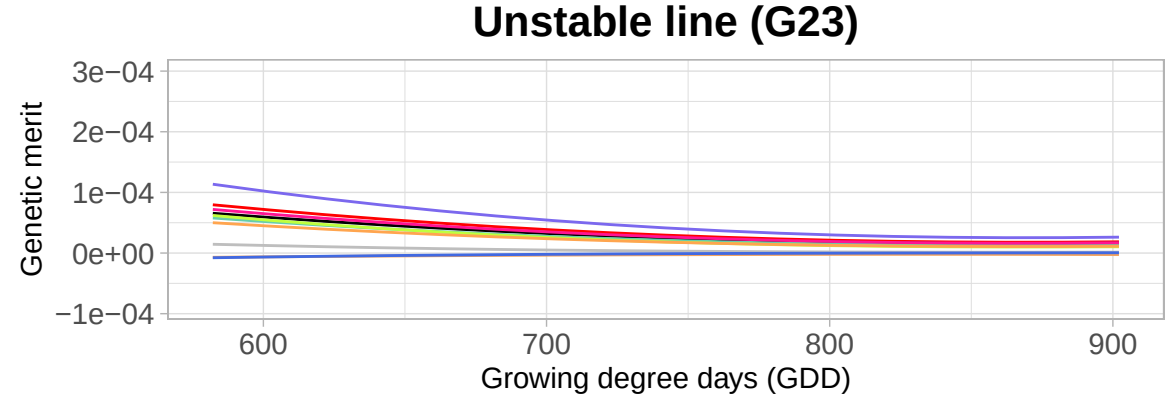

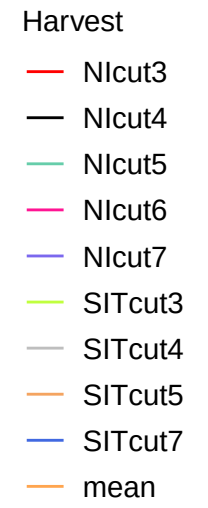

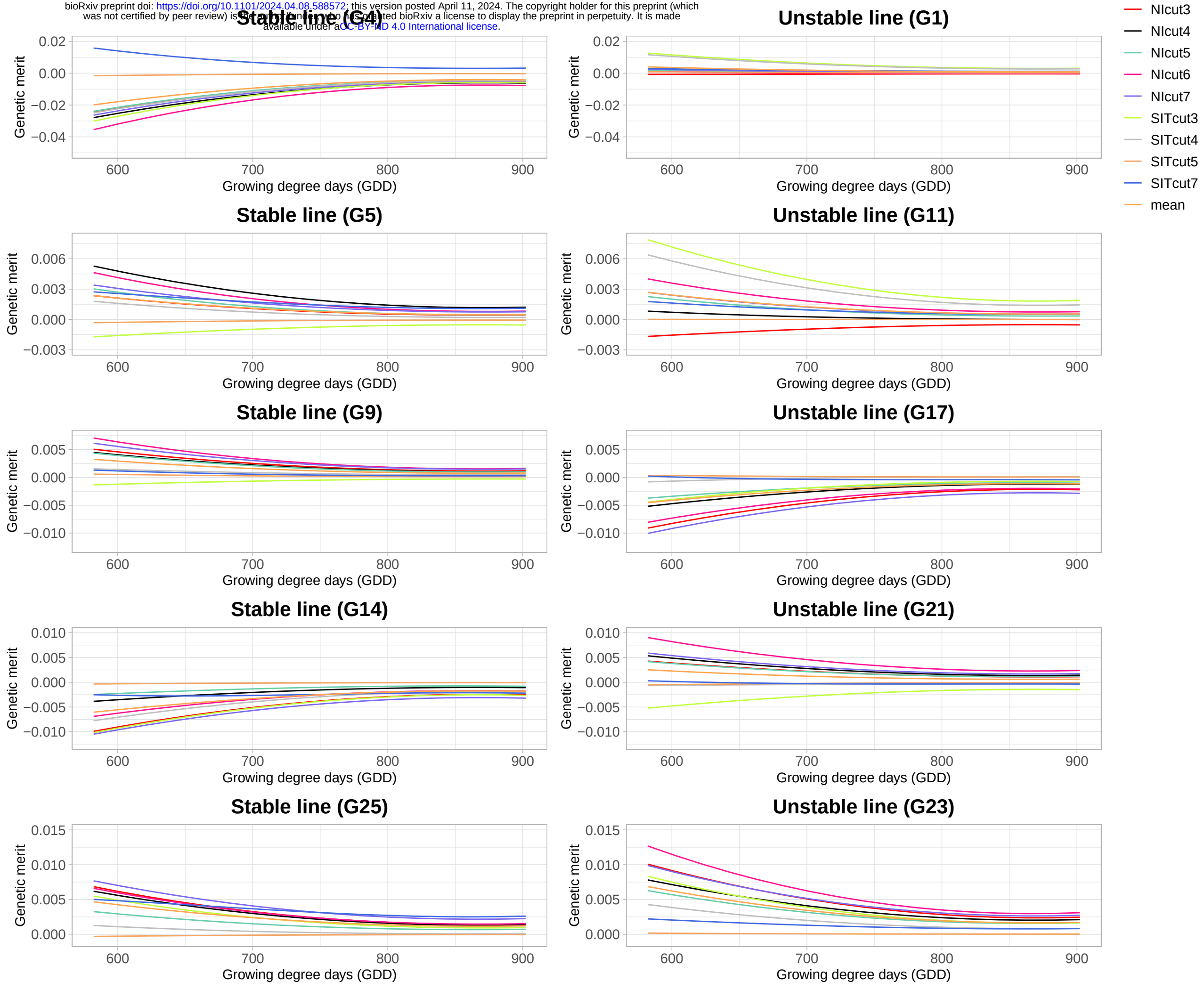

Stable line (G4)

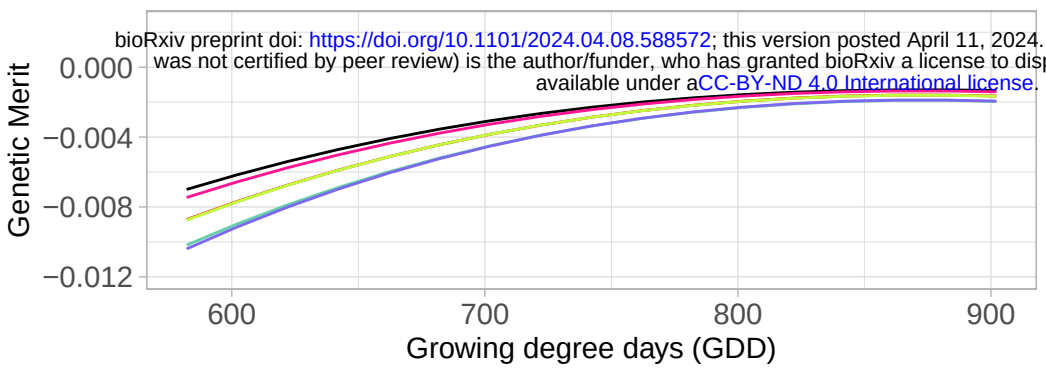

Stable line (G4)

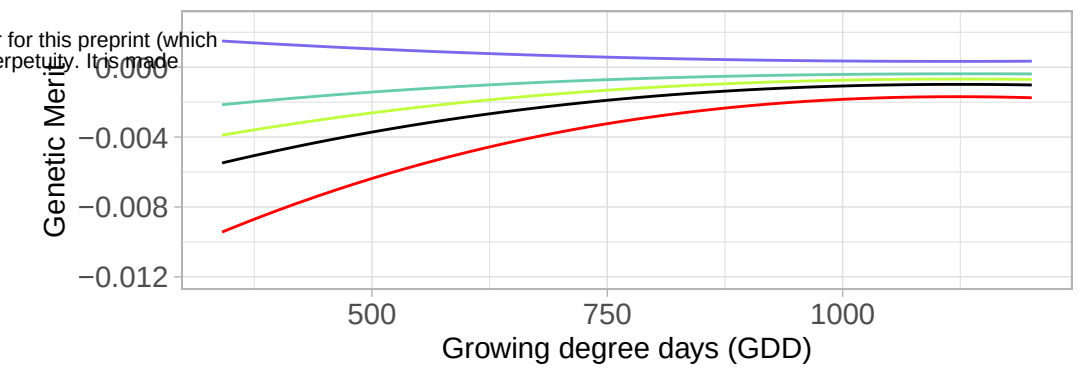

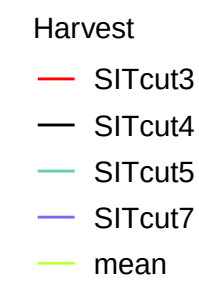

Stable line (G5)

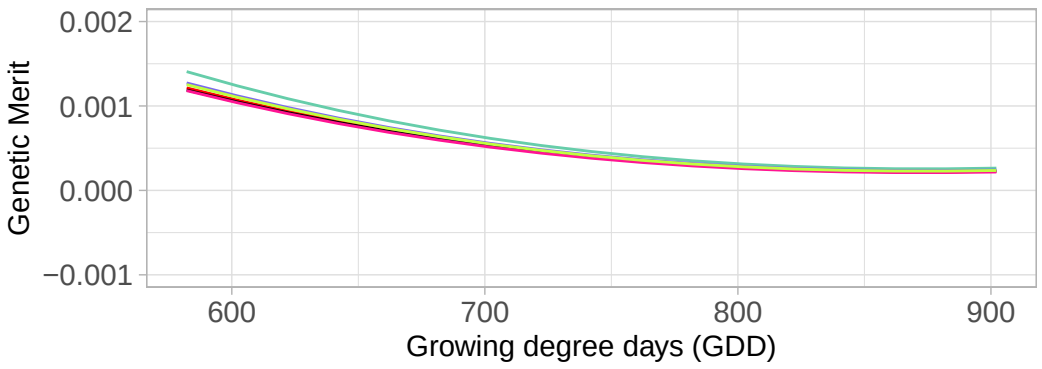

Stable line (G5)

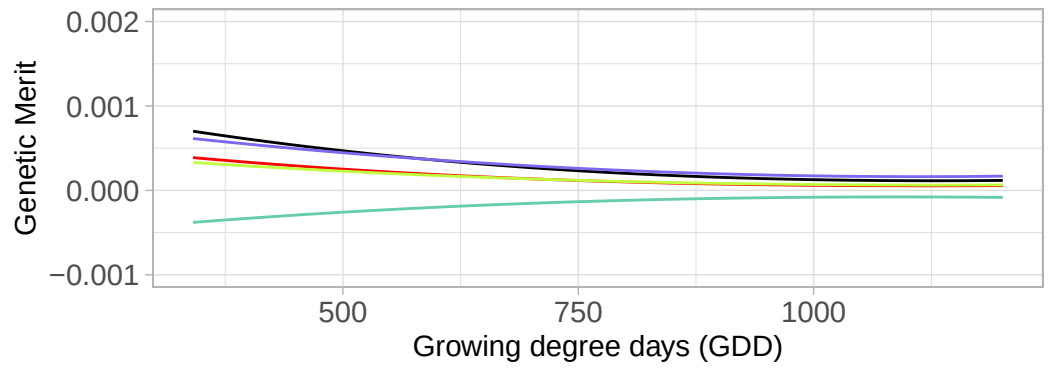

Stable line (G9)

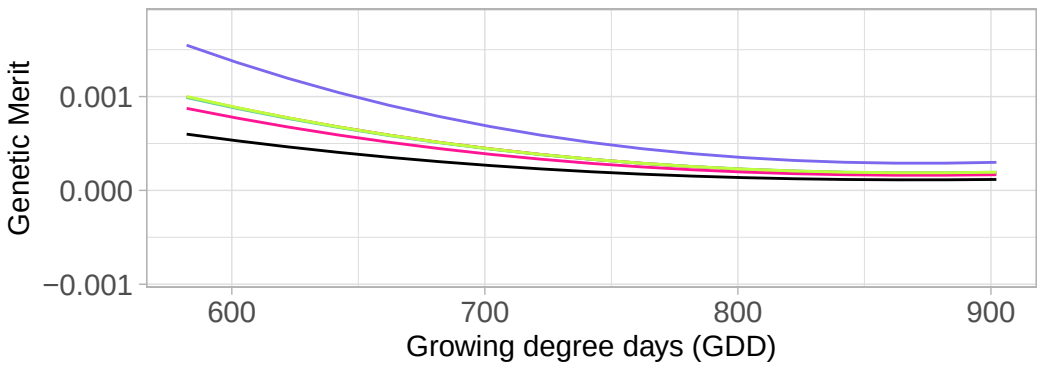

Stable line (G9)

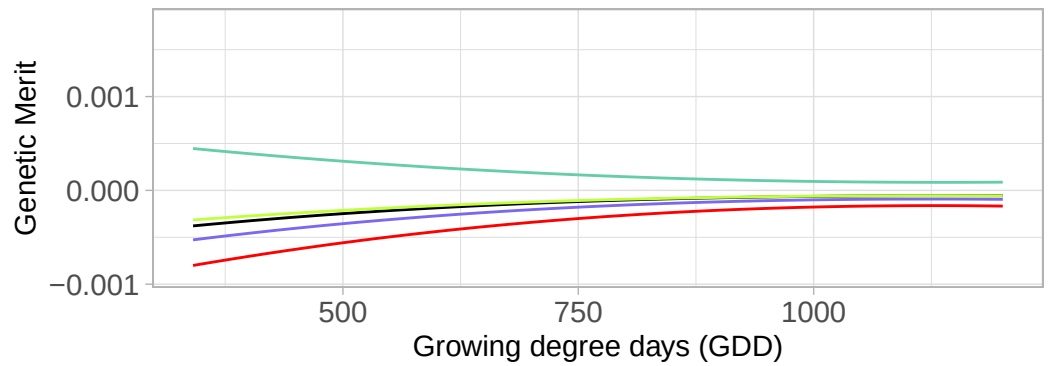

Stable line (G14)

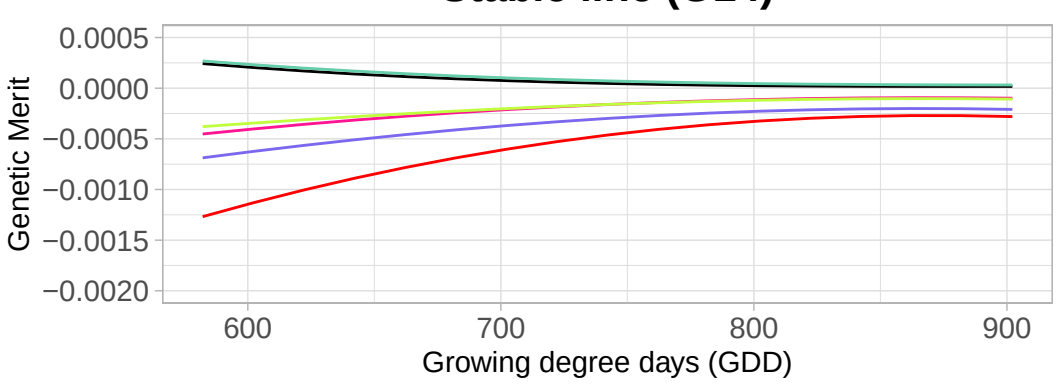

Stable line (G14)

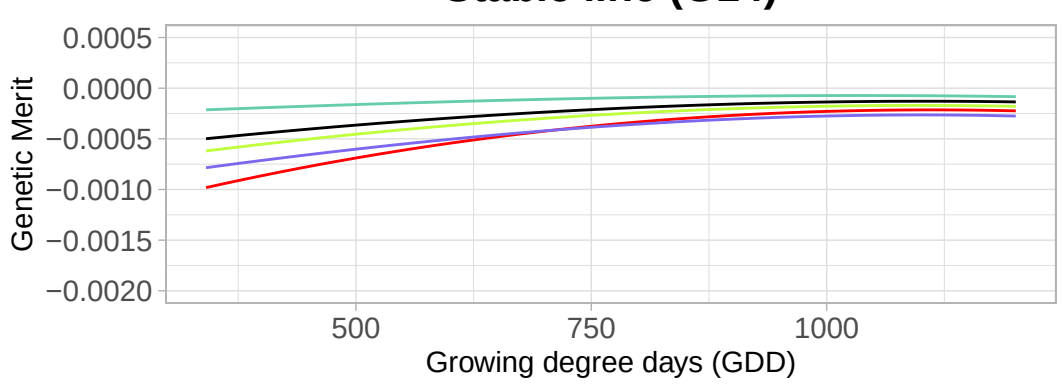

Stable line (G25)

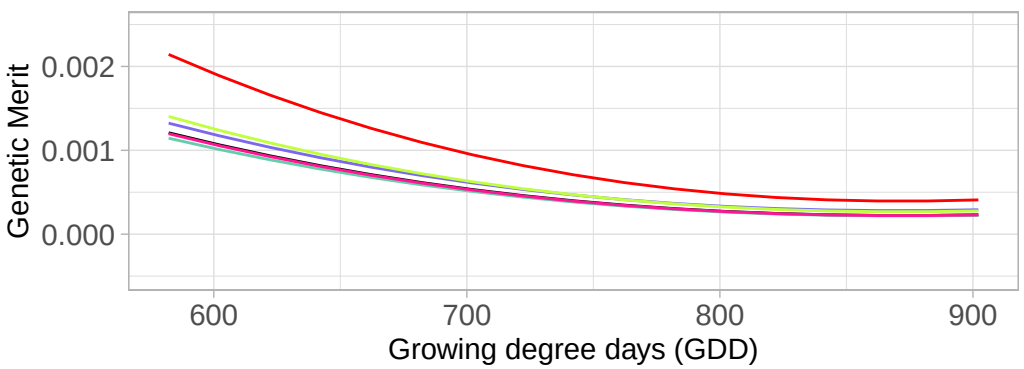

Stable line (G25)

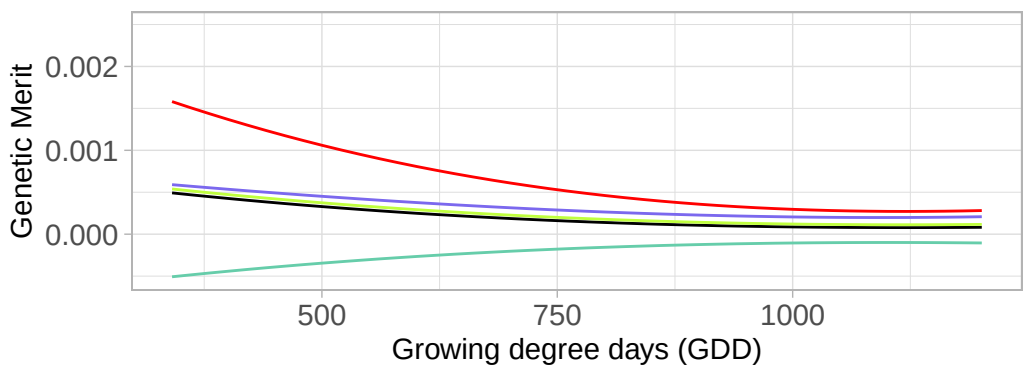

Unstable line (G1)

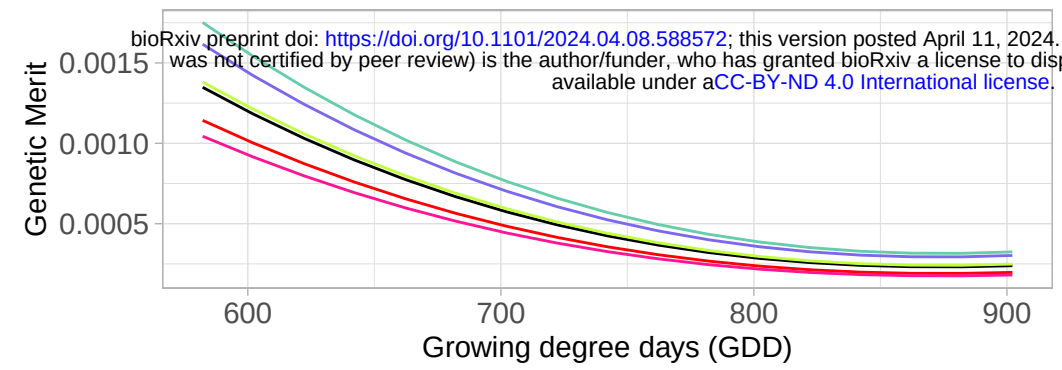

Unstable line (G1)

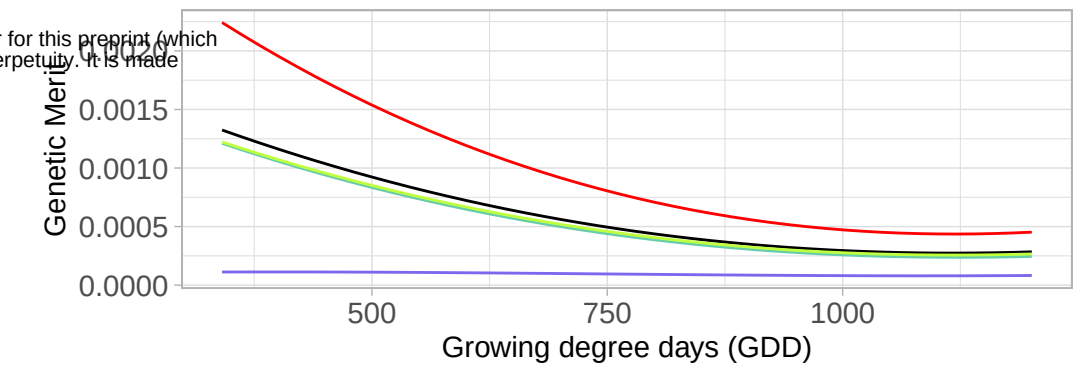

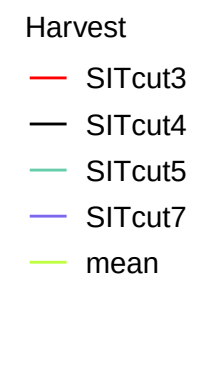

Unstable line (G11)

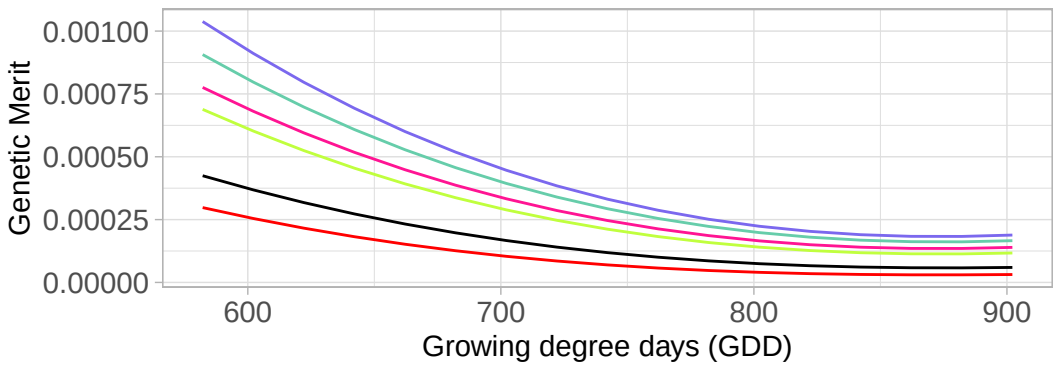

Unstable line (G11)

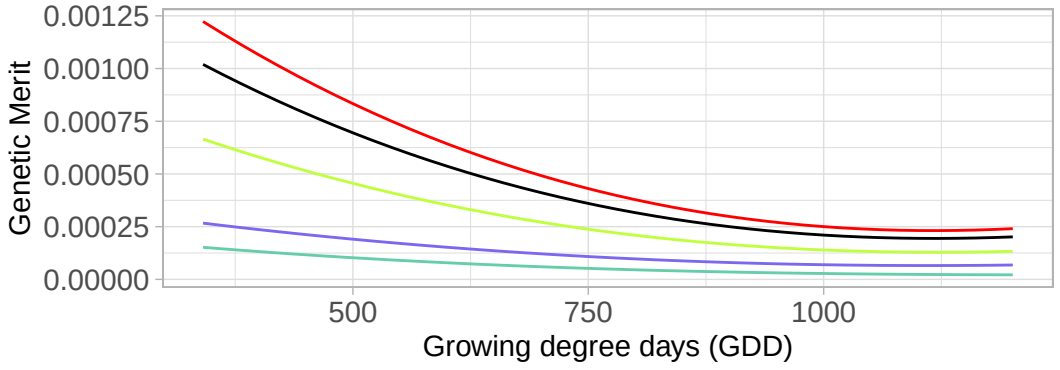

Unstable line (G17)

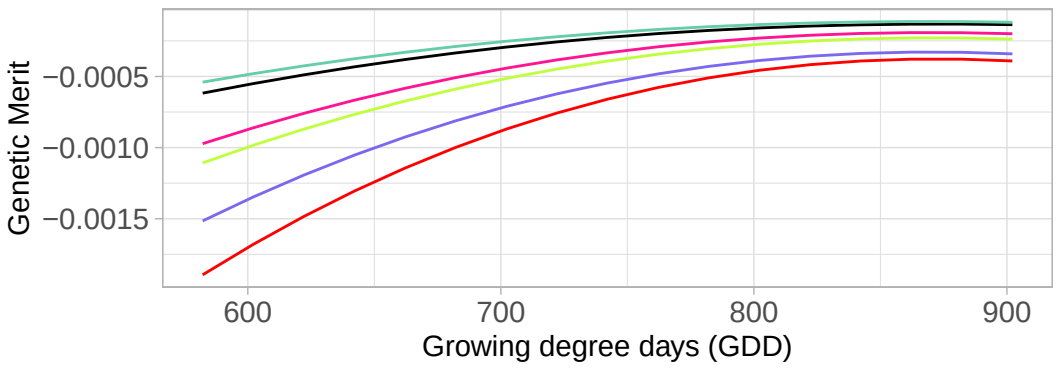

Unstable line (G17)

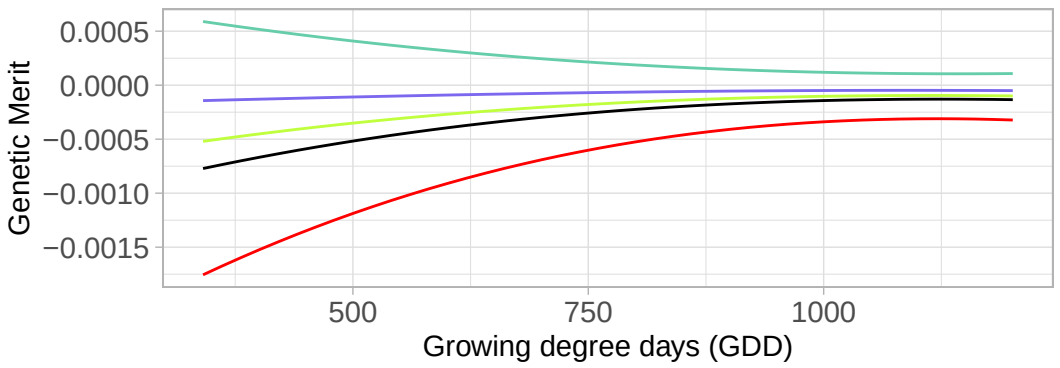

Unstable line (G21)

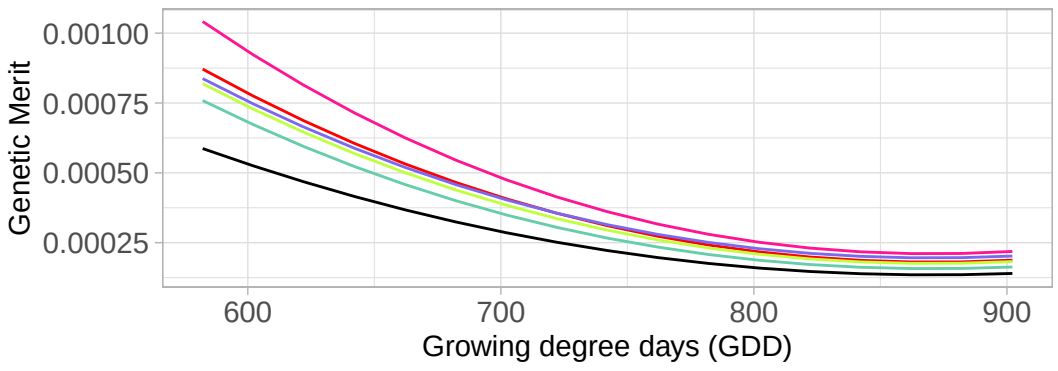

Unstable line (G21)

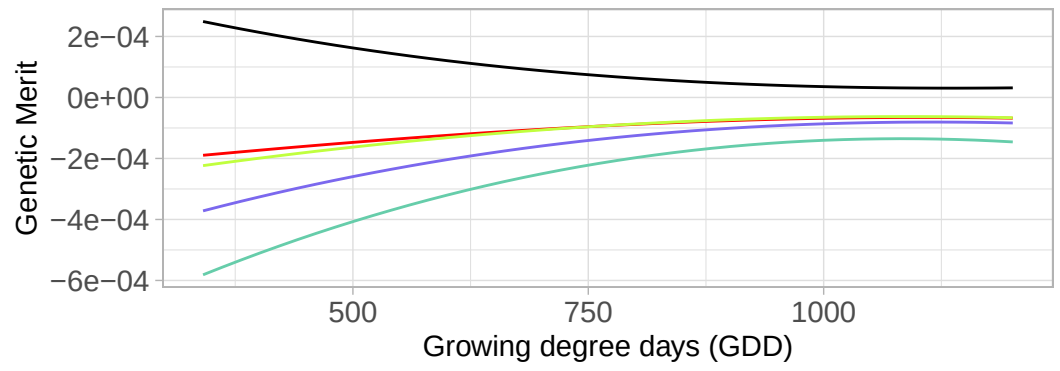

Unstable line (G23)

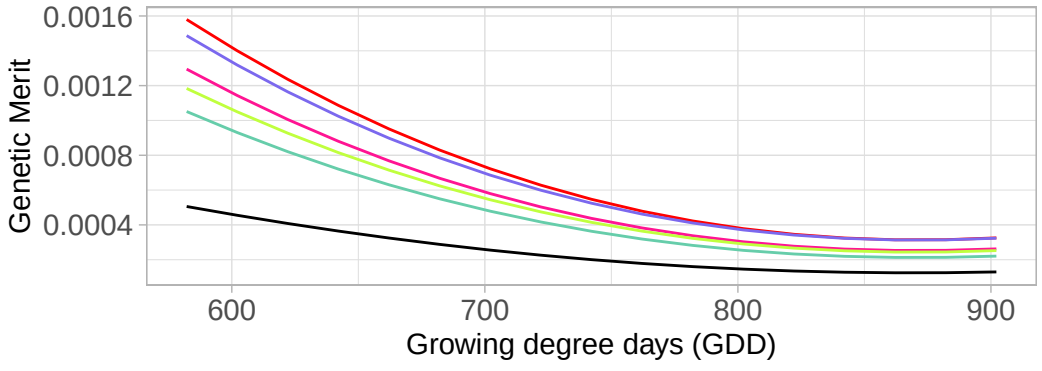

Unstable line (G23)

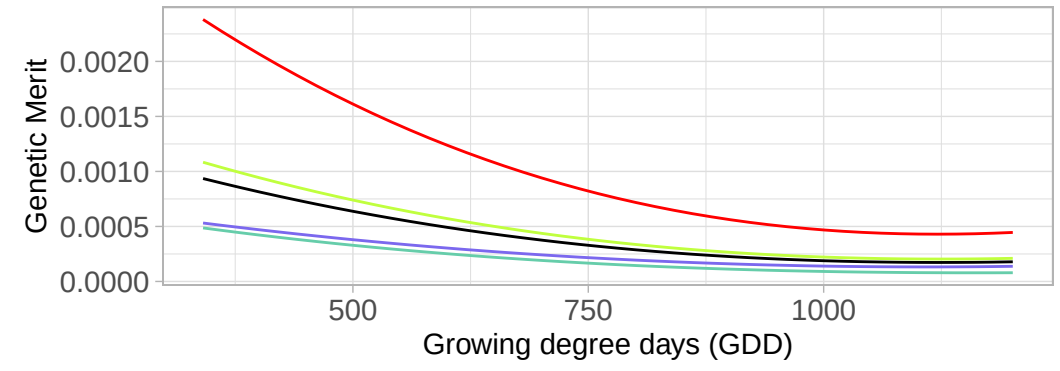

Stable line (G4)

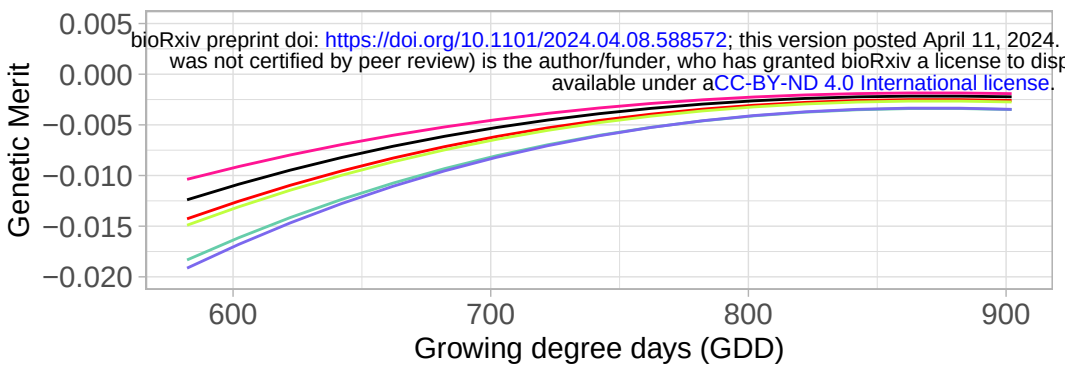

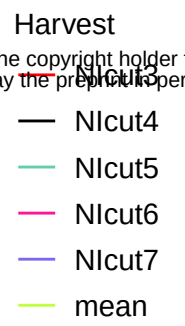

Stable line (G4)

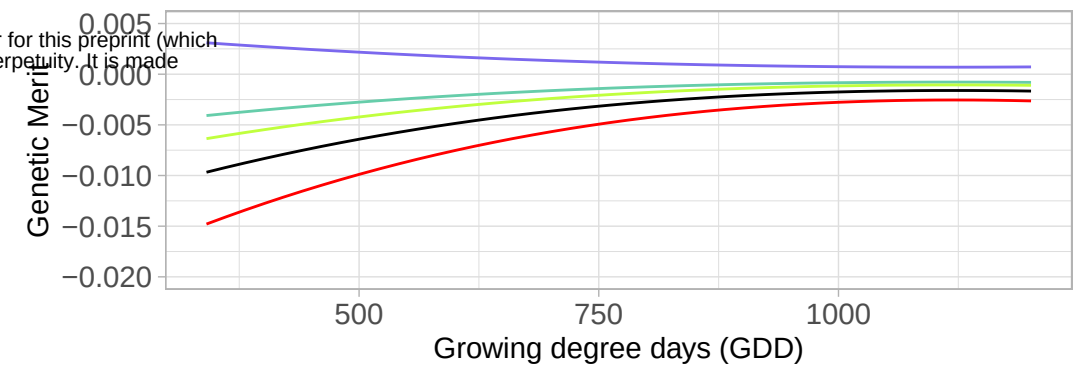

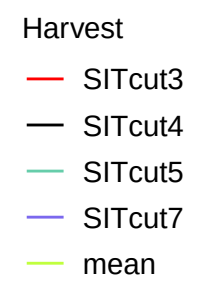

Stable line (G5)

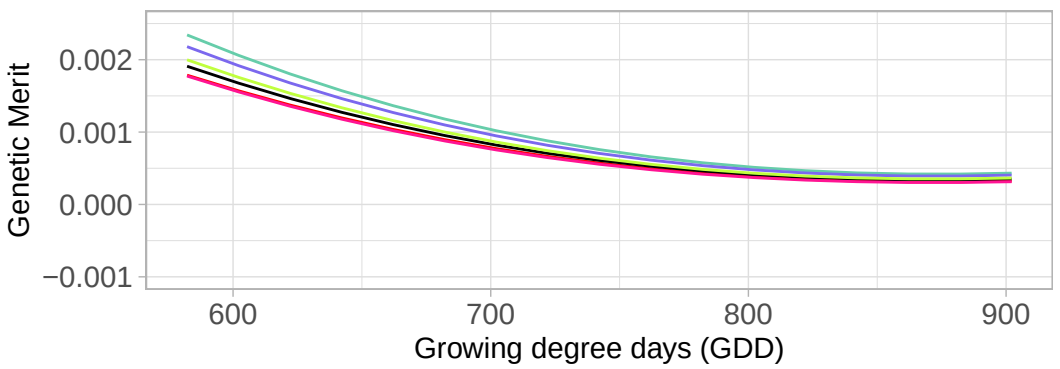

Stable line (G5)

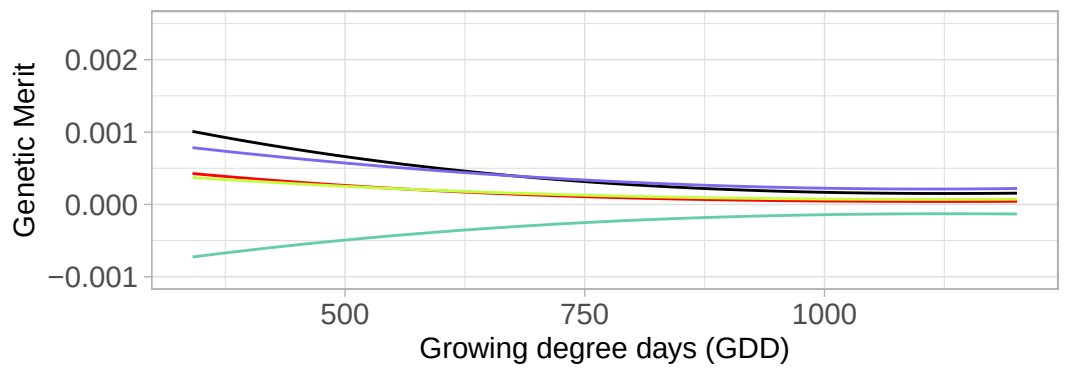

Stable line (G9)

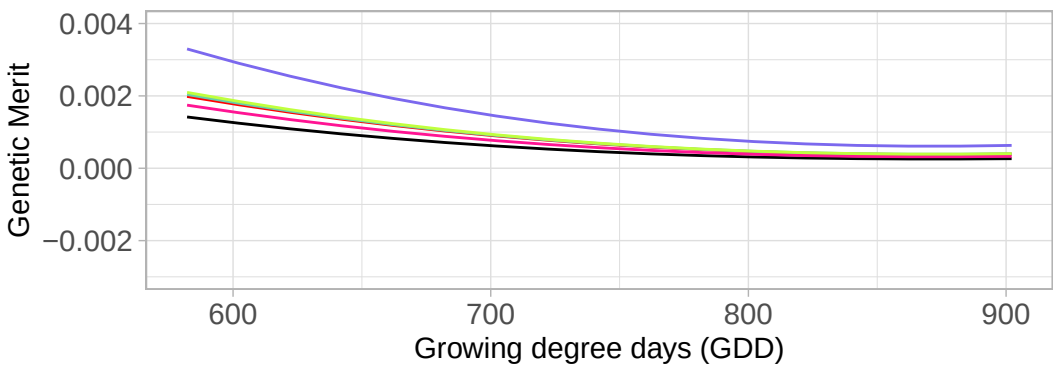

Stable line (G9)

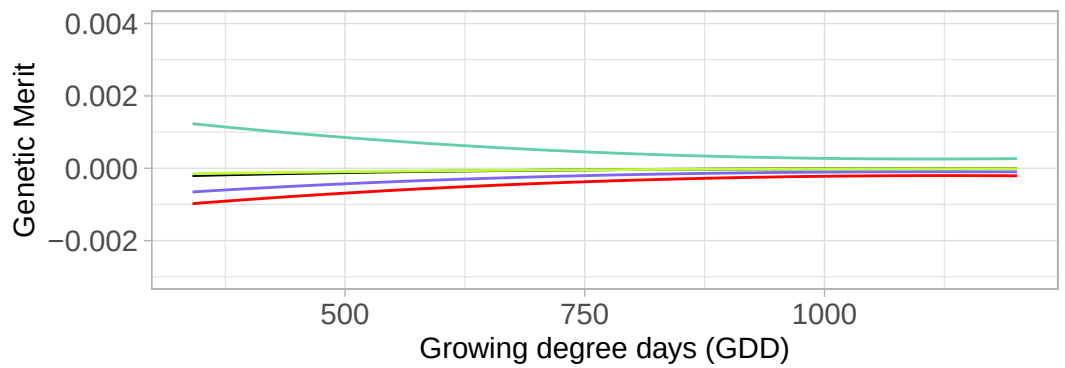

Stable line (G14)

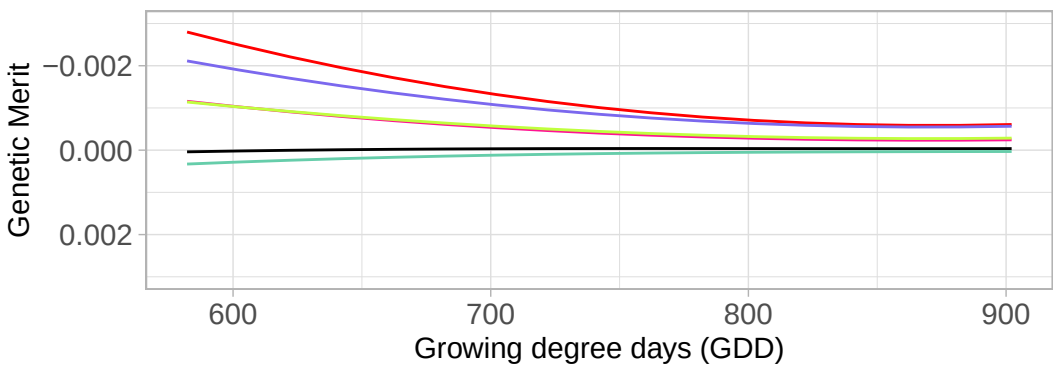

Stable line (G14)

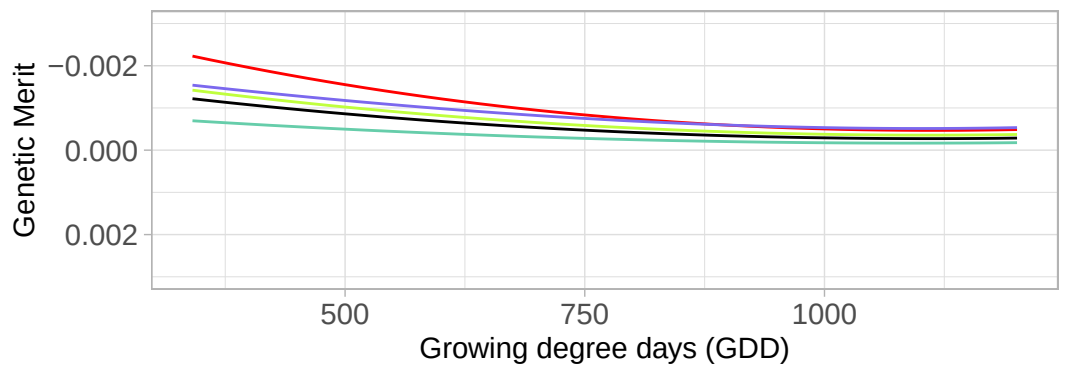

Stable line (G25)

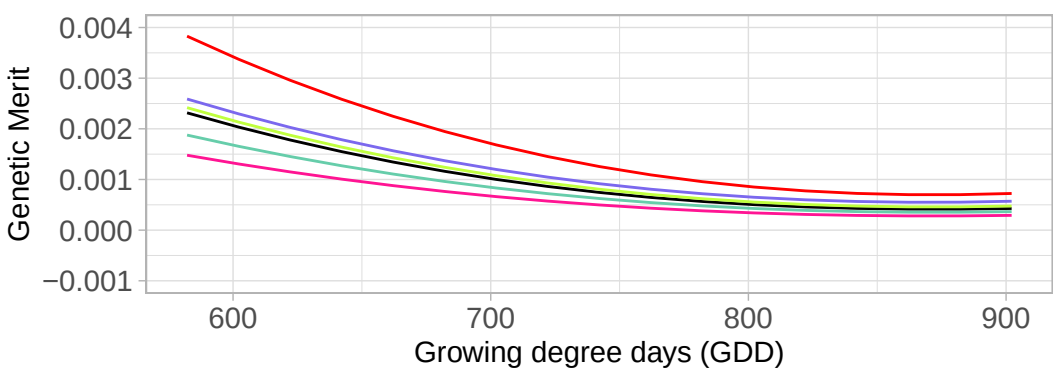

Stable line (G25)

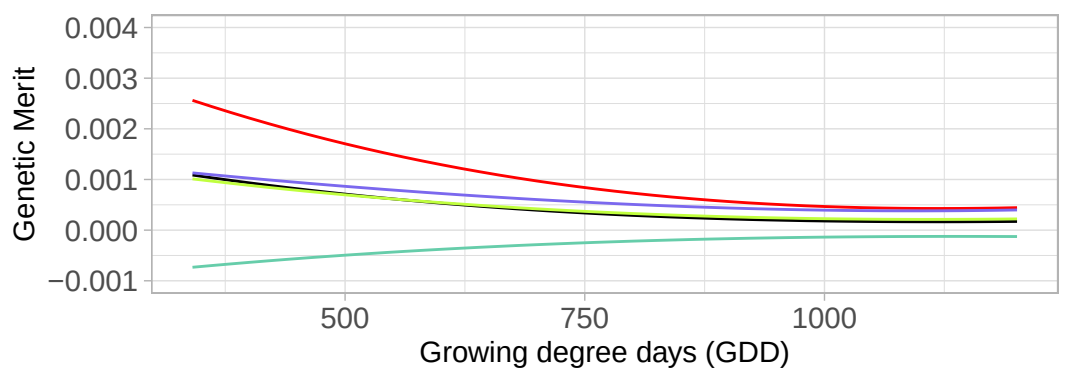

Unstable line (G1)

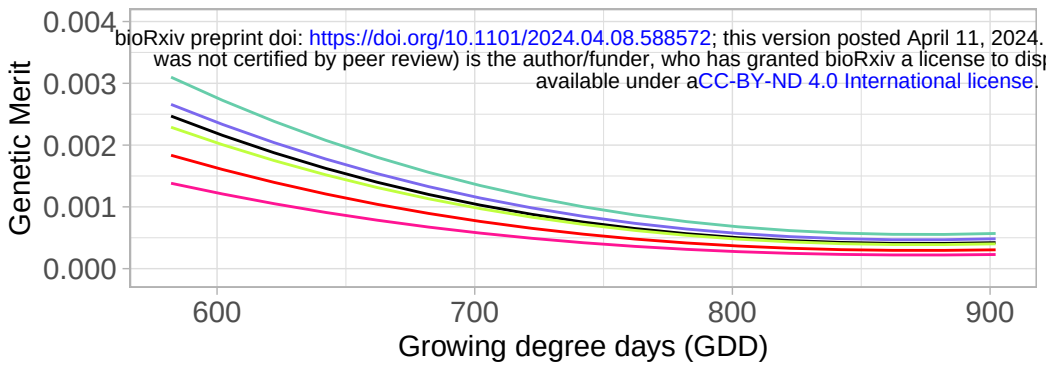

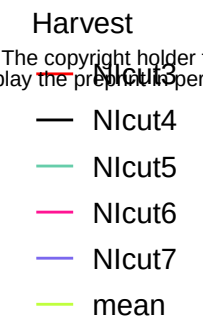

Unstable line (G1)

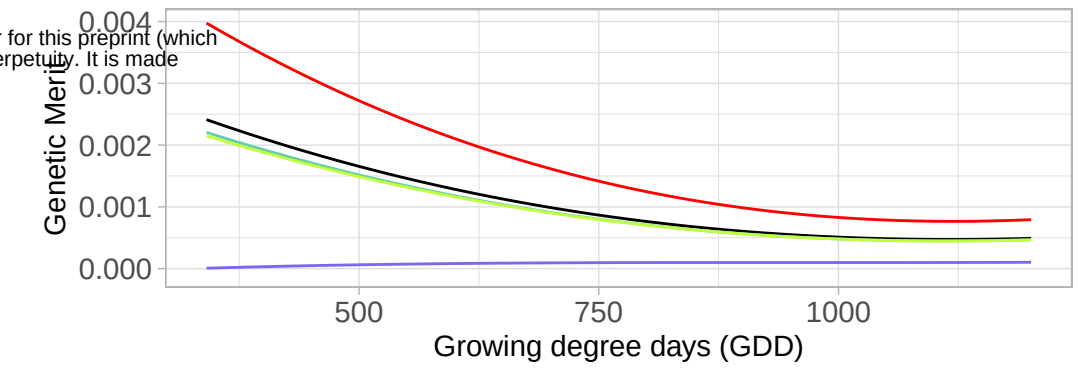

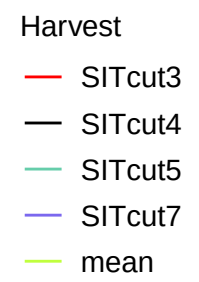

Unstable line (G11)

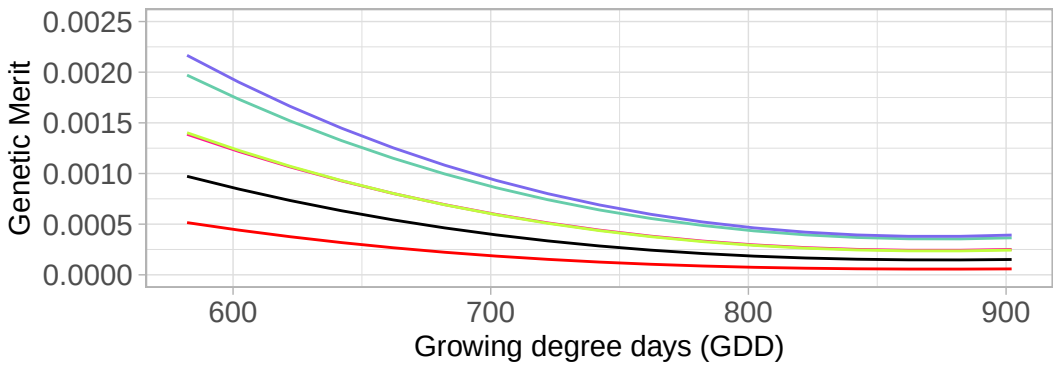

Unstable line (G11)

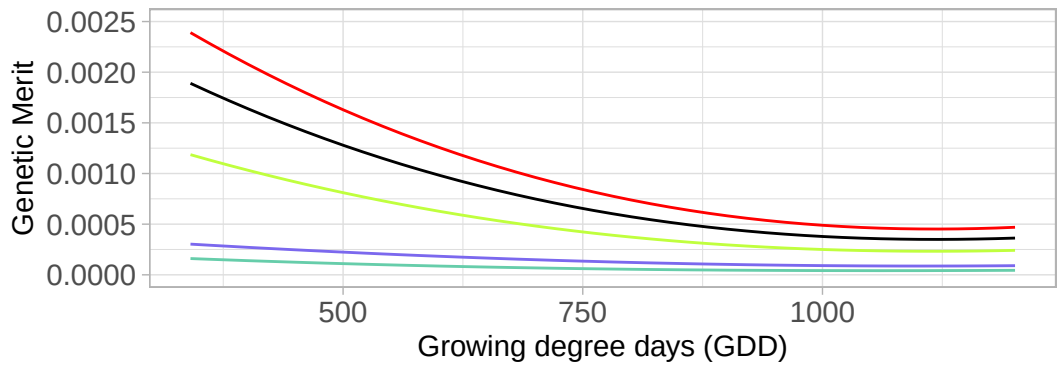

Unstable line (G17)

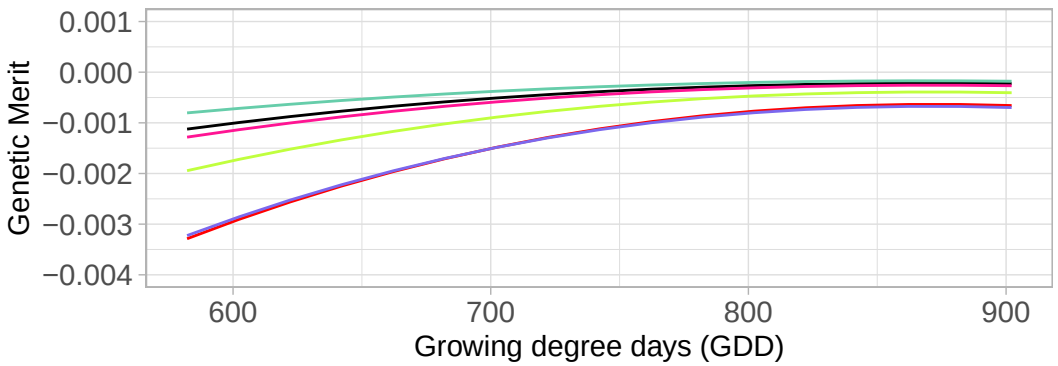

Unstable line (G17)

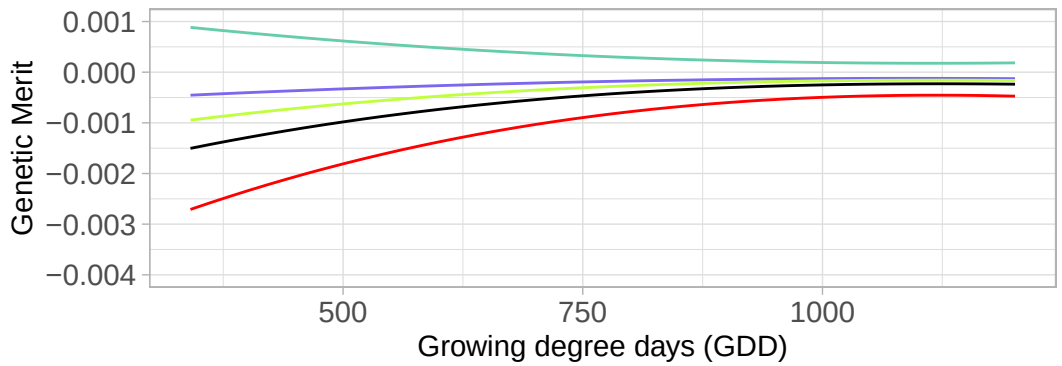

Unstable line (G21)

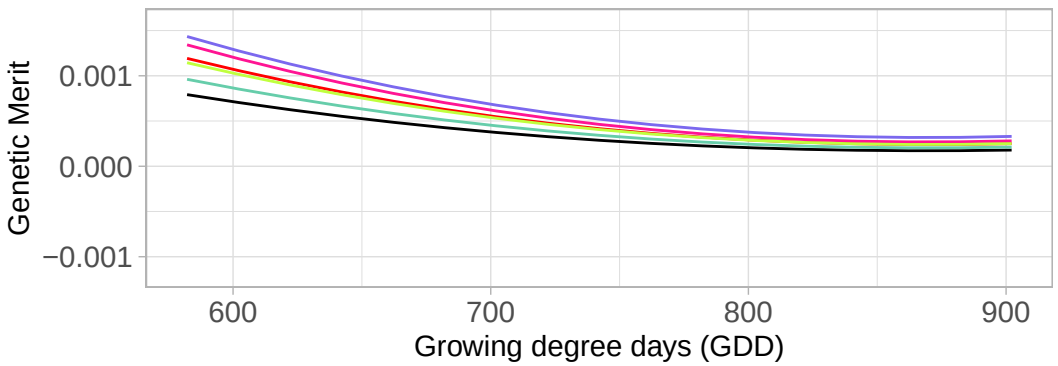

Unstable line (G21)

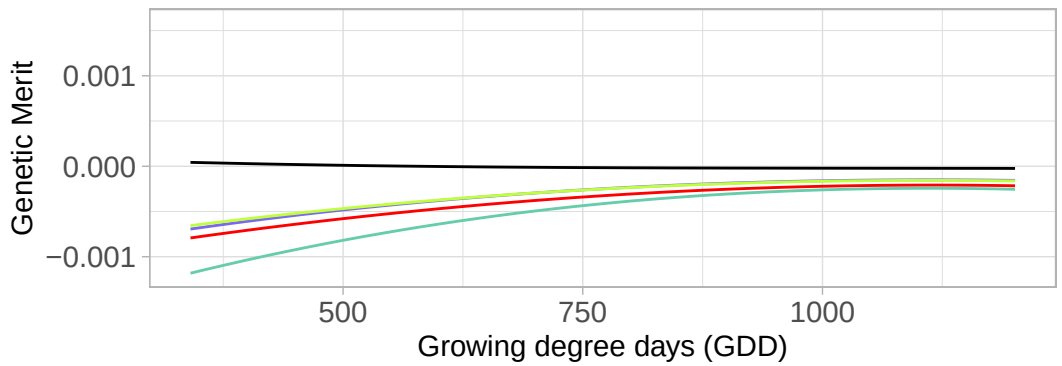

Unstable line (G23)

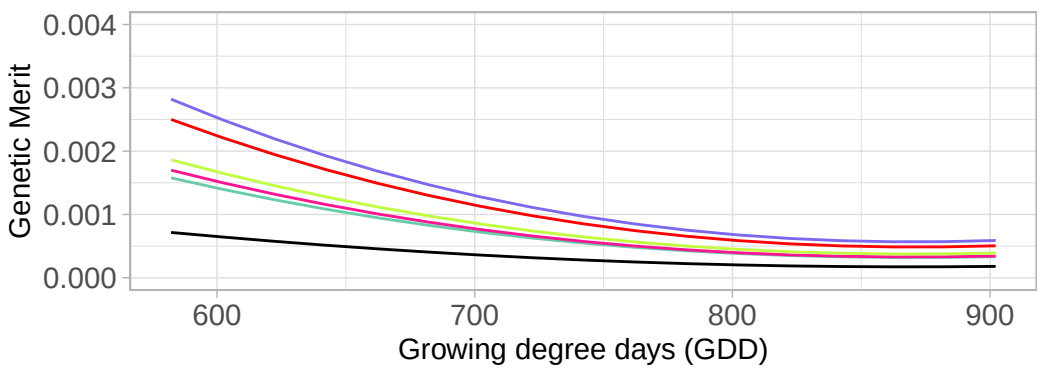

Unstable line (G23)

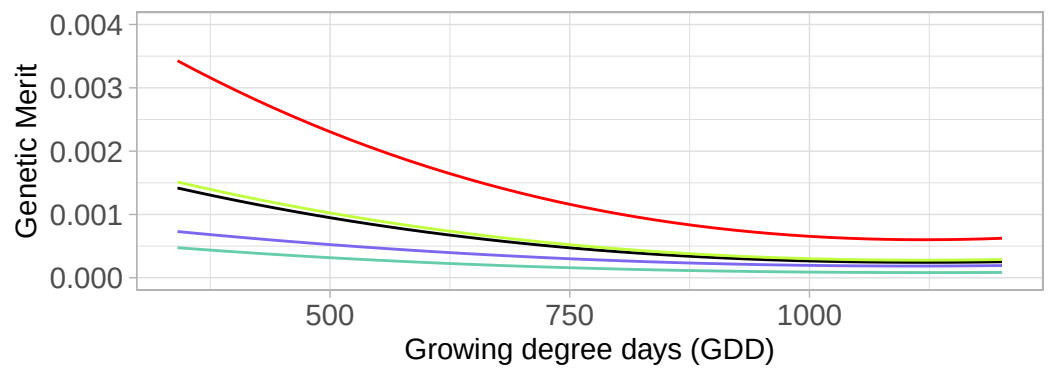

Stable line (G4)

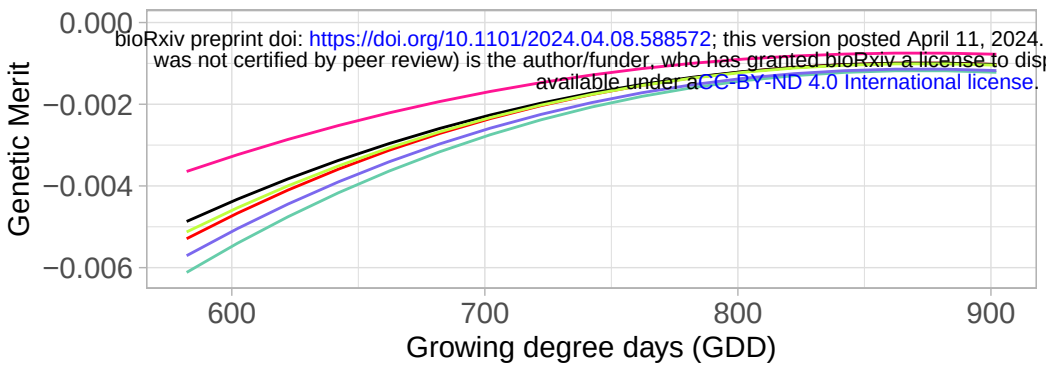

Stable line (G4)

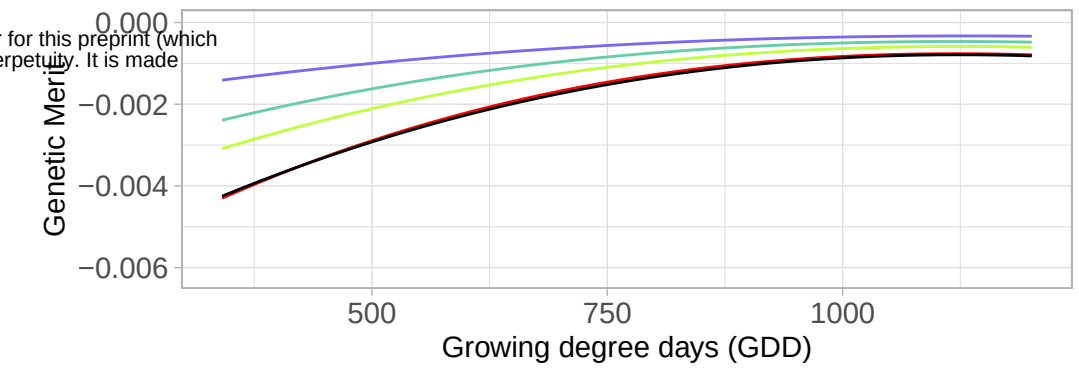

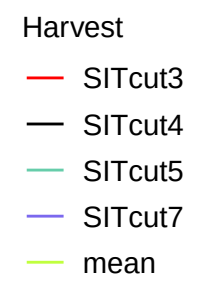

Stable line (G5)

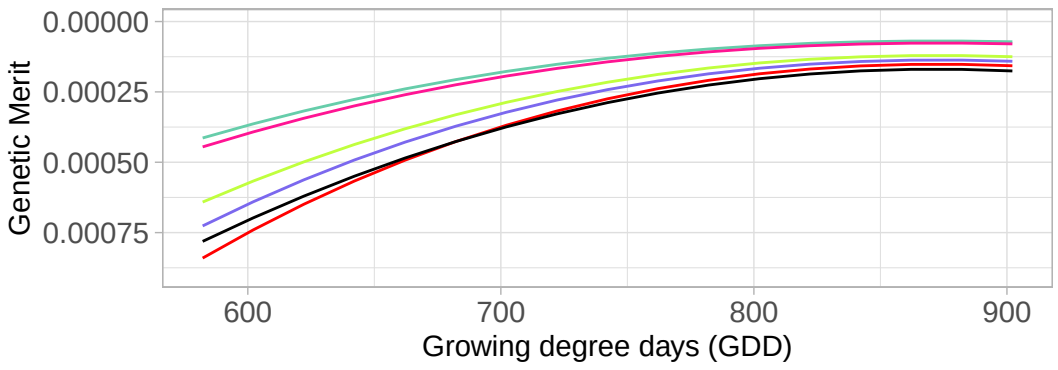

Stable line (G5)

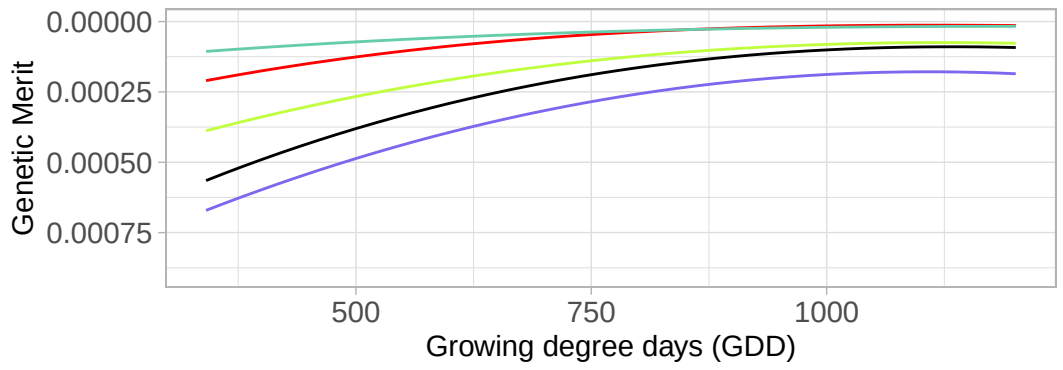

Stable line (G9)

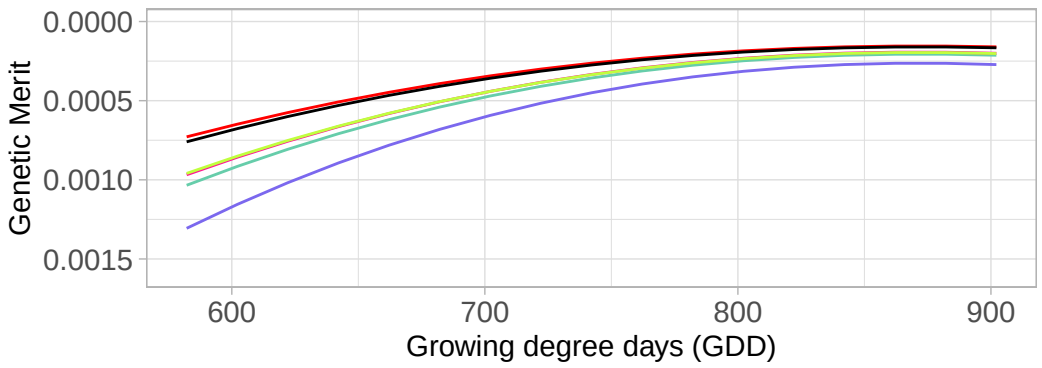

Stable line (G9)

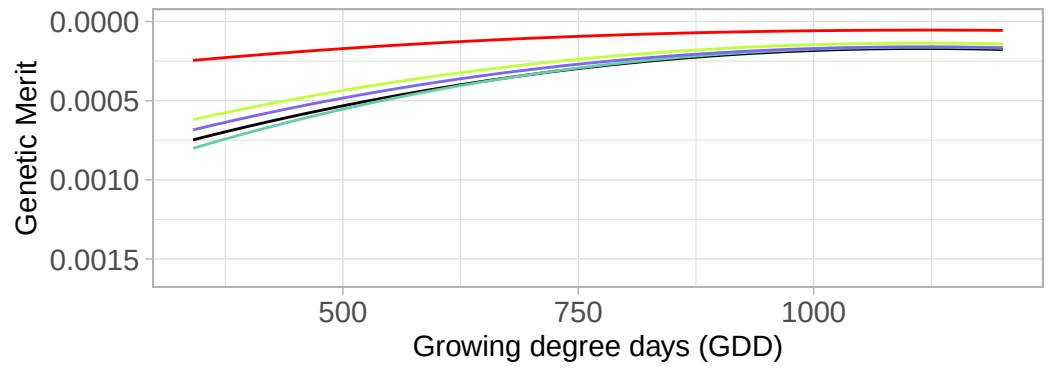

Stable line (G14)

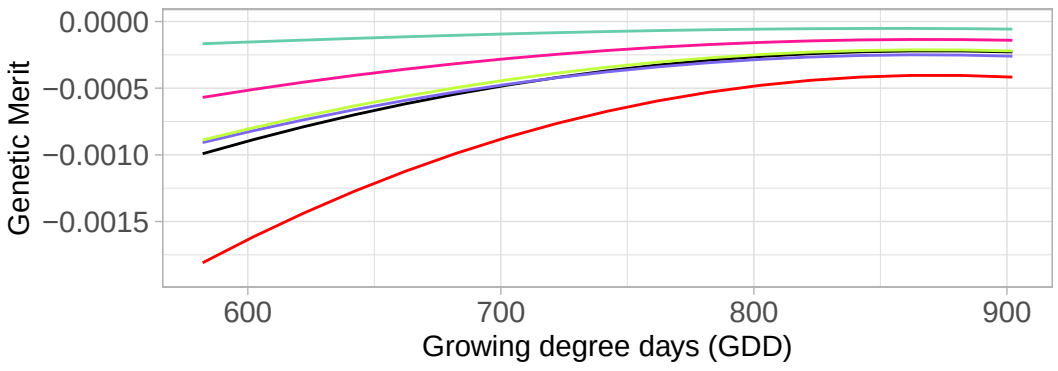

Stable line (G14)

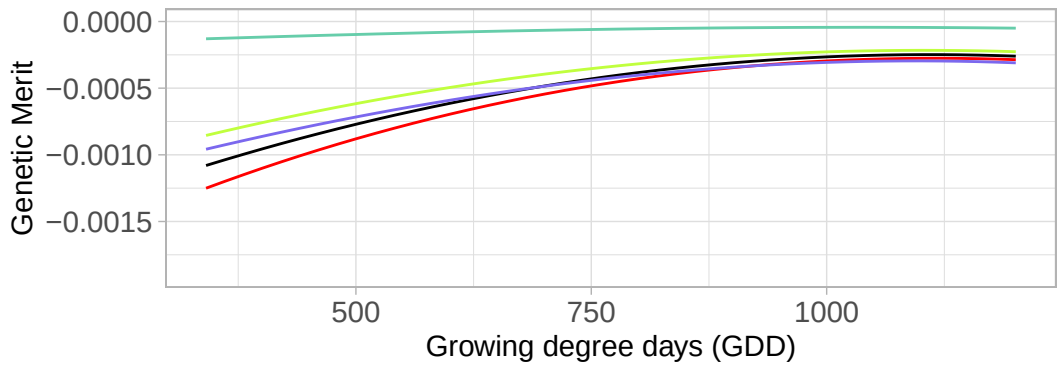

Stable line (G25)

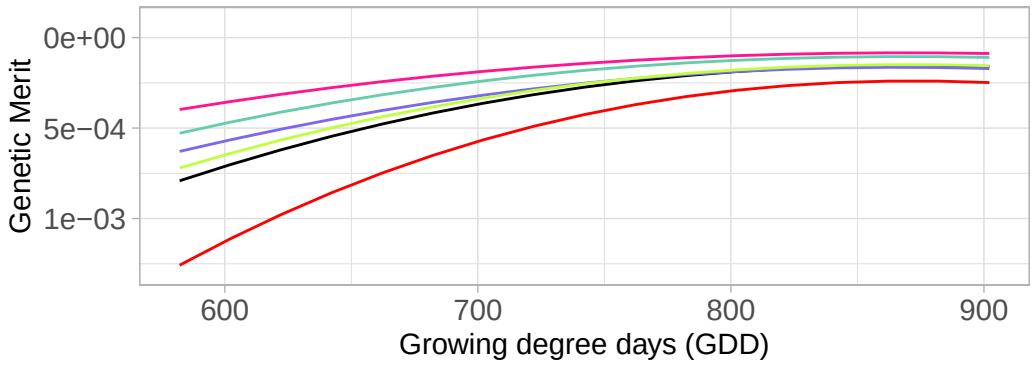

Stable line (G25)

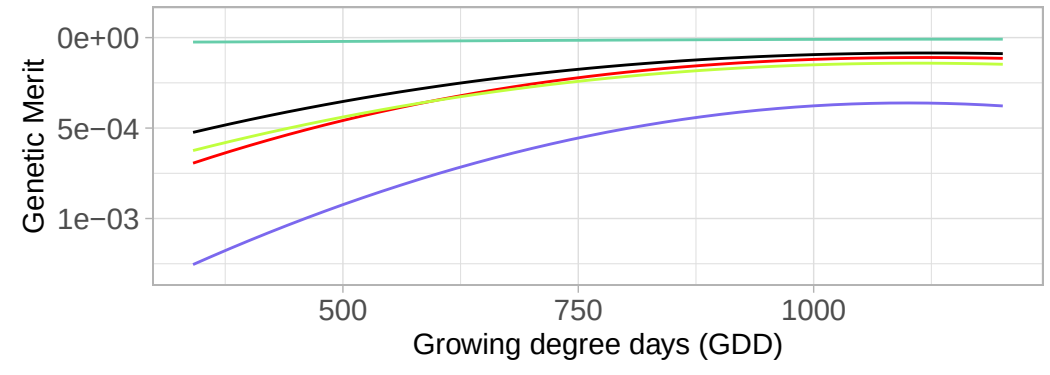

Unstable line (G1)

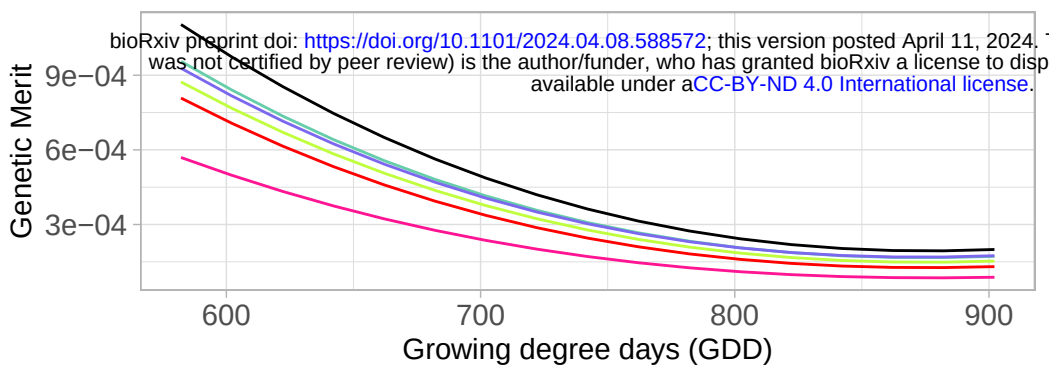

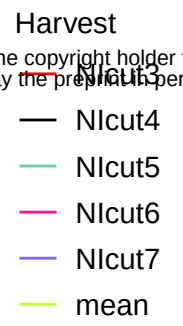

Unstable line (G1)

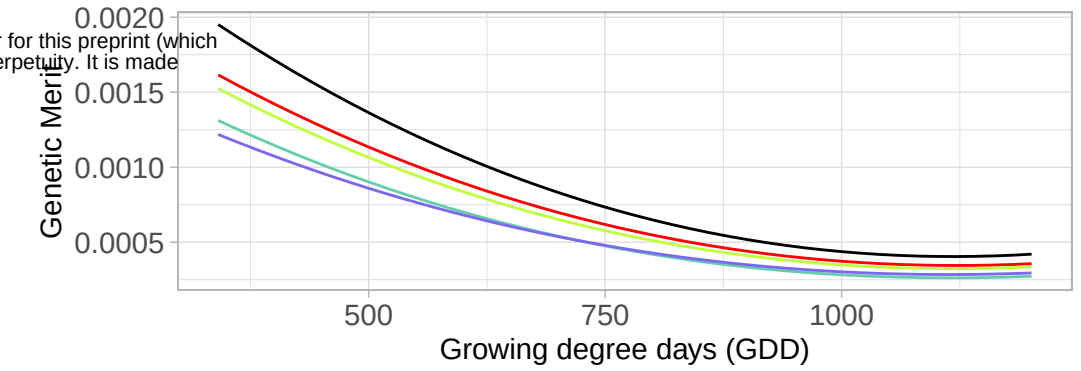

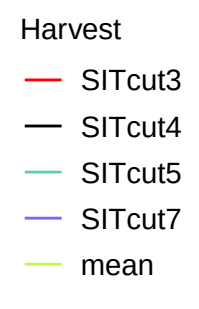

Unstable line (G11)

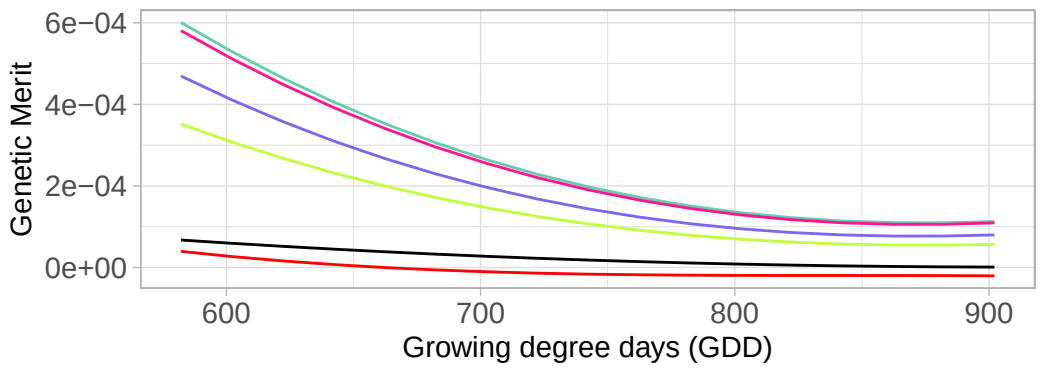

Unstable line (G11)

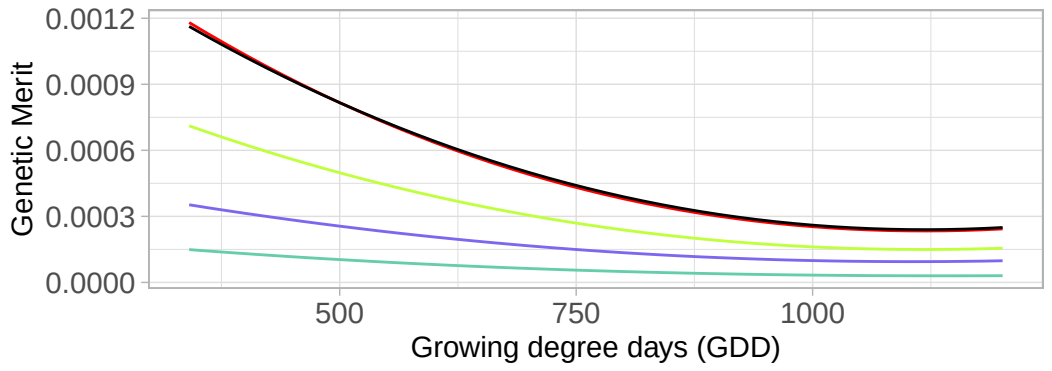

Unstable line (G17)

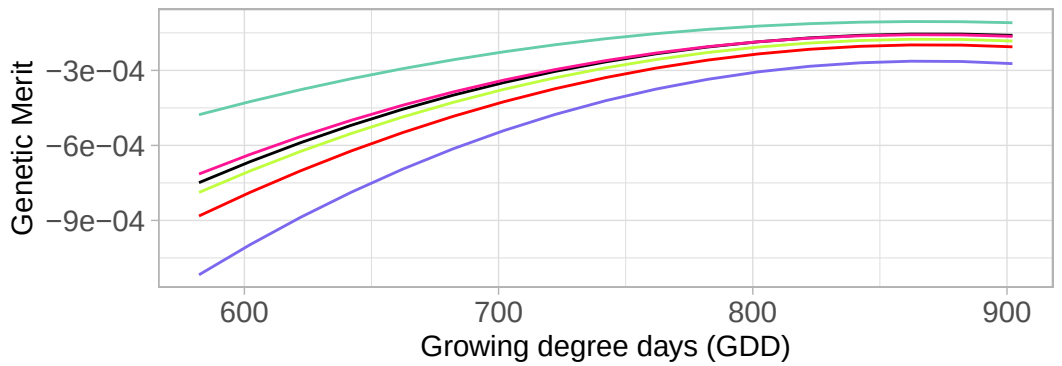

Unstable line (G17)

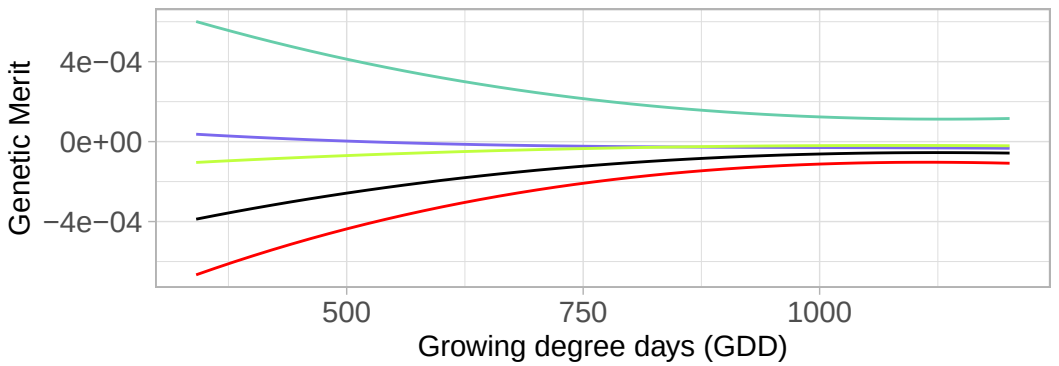

Unstable line (G21)

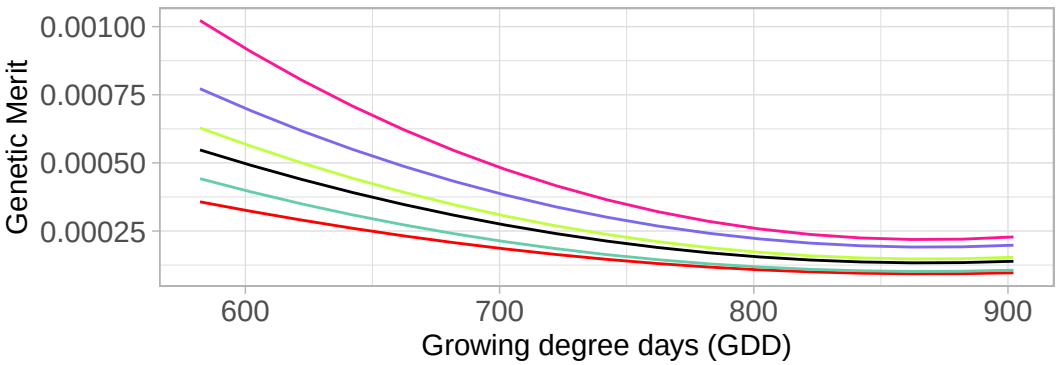

Unstable line (G21)

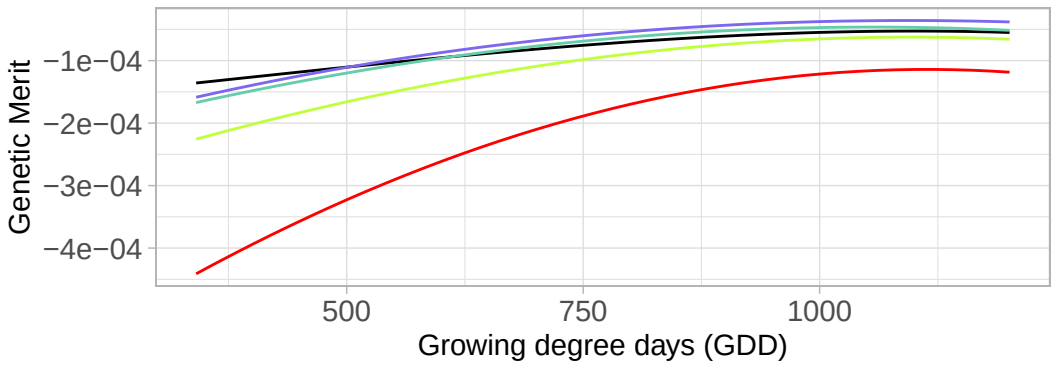

Unstable line (G23)

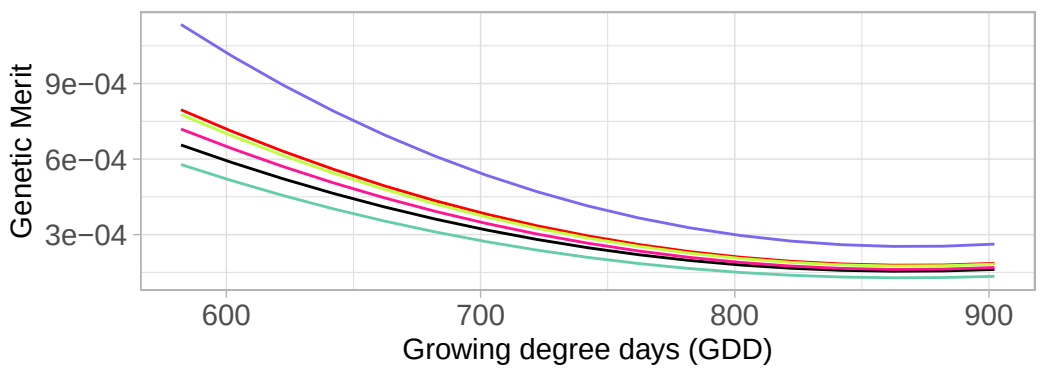

Unstable line (G23)

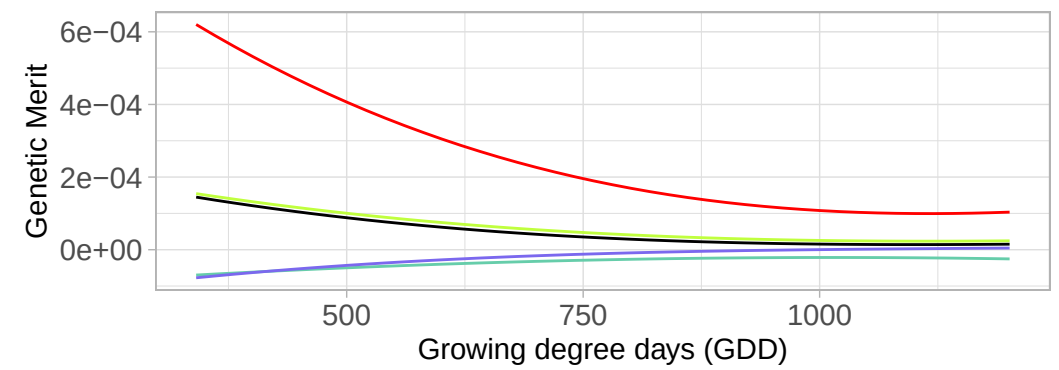

Stable line (G4)

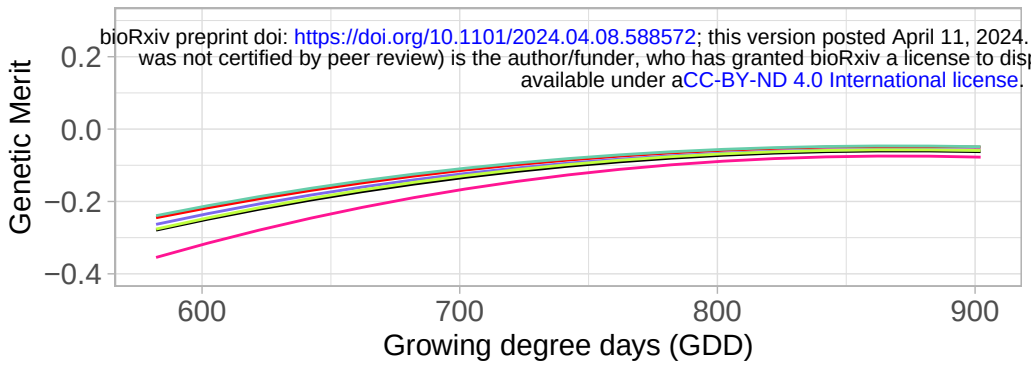

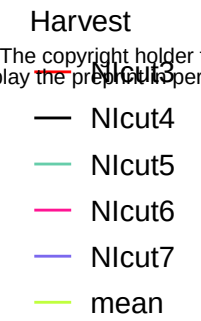

Stable line (G4)

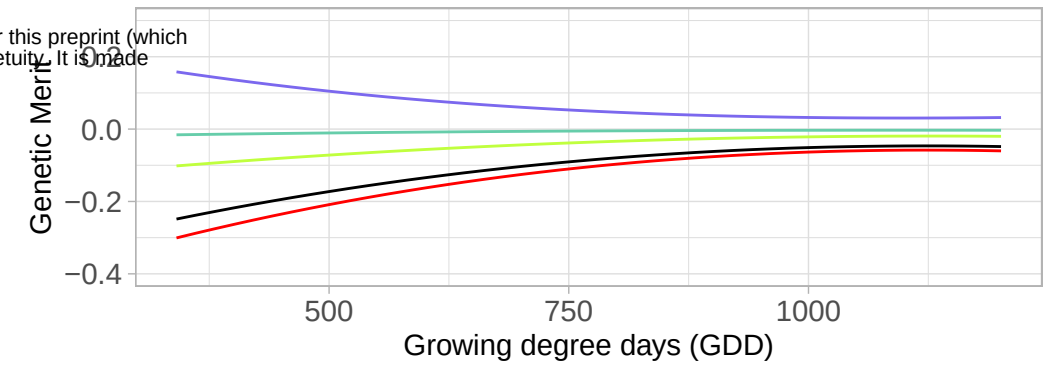

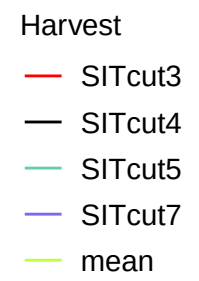

Stable line (G5)

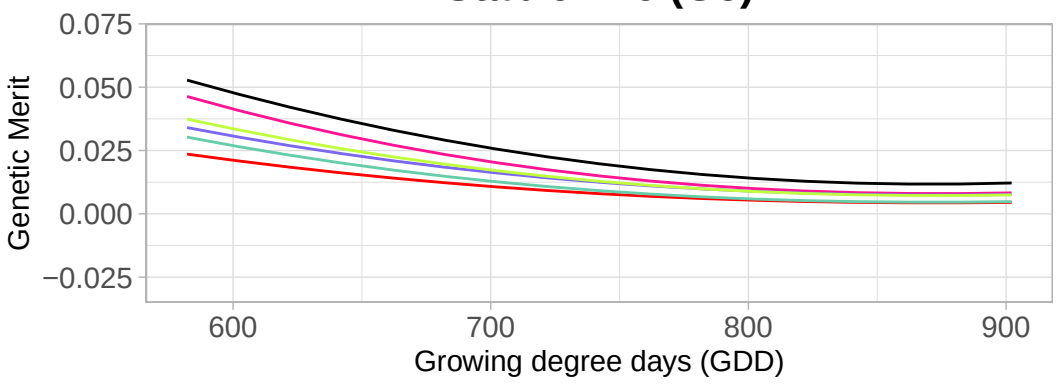

Stable line (G5)

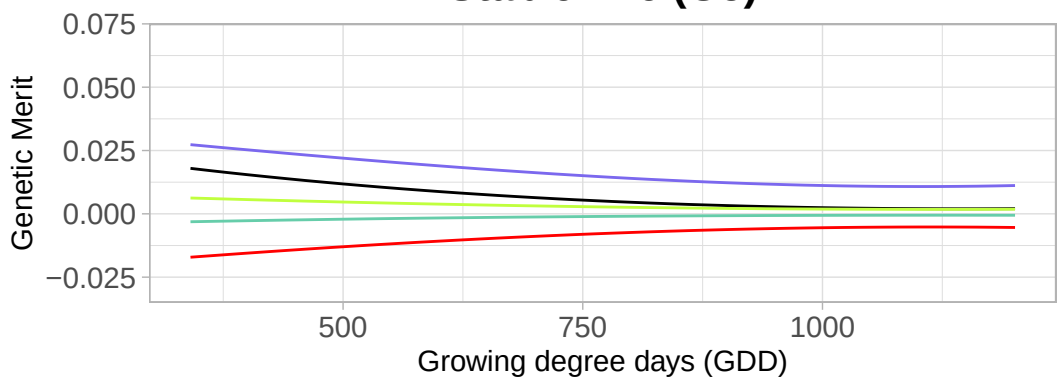

Stable line (G9)

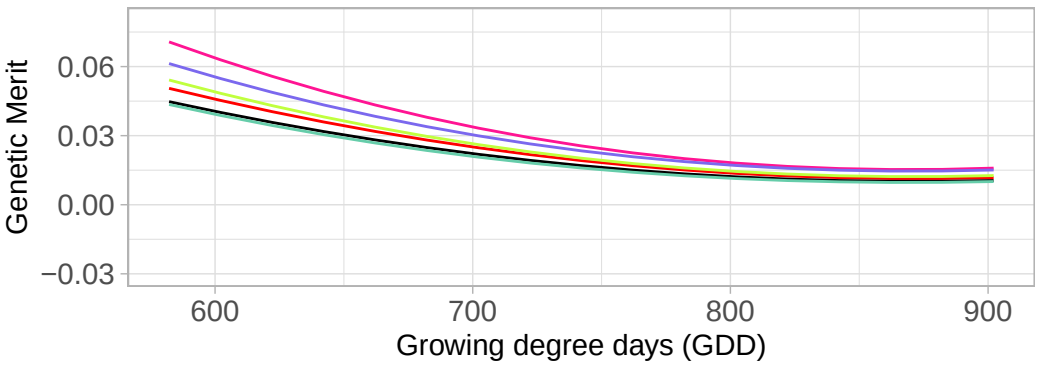

Stable line (G9)

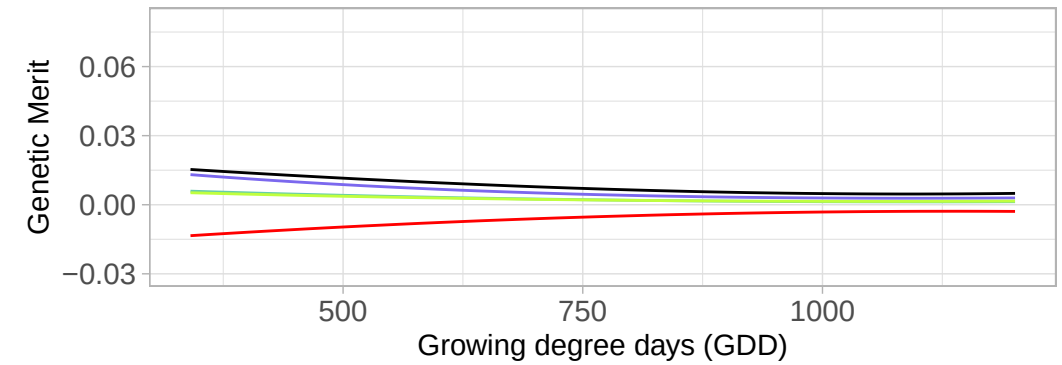

Stable line (G14)

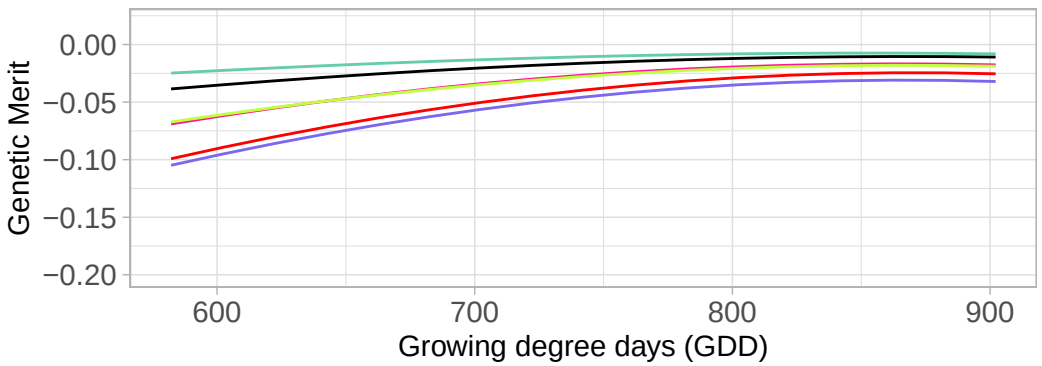

Stable line (G14)

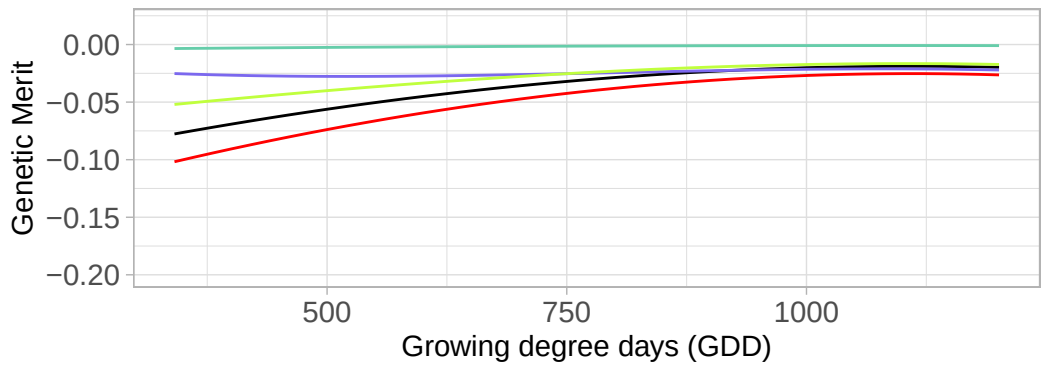

Stable line (G25)

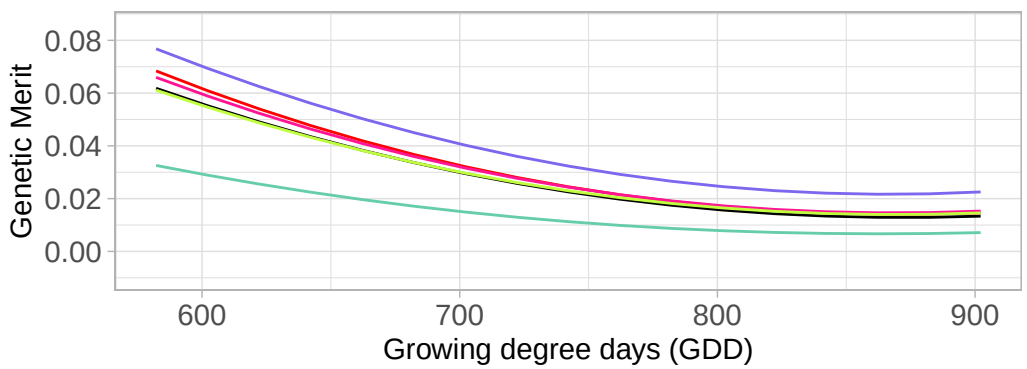

Stable line (G25)

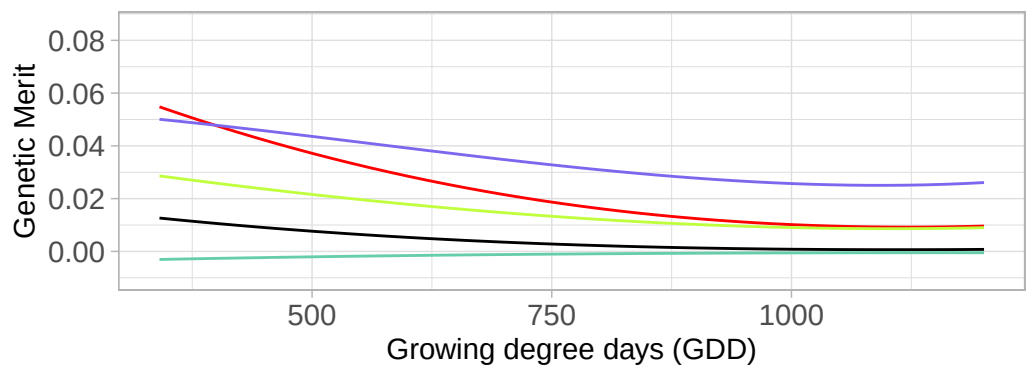

Unstable line (G1)

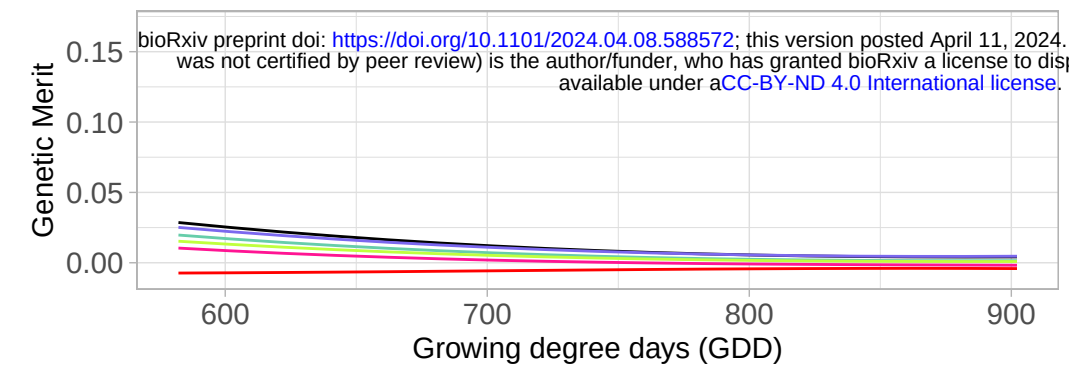

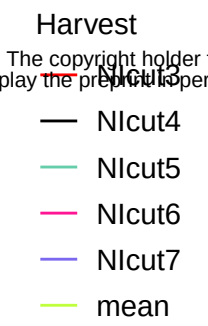

Unstable line (G1)

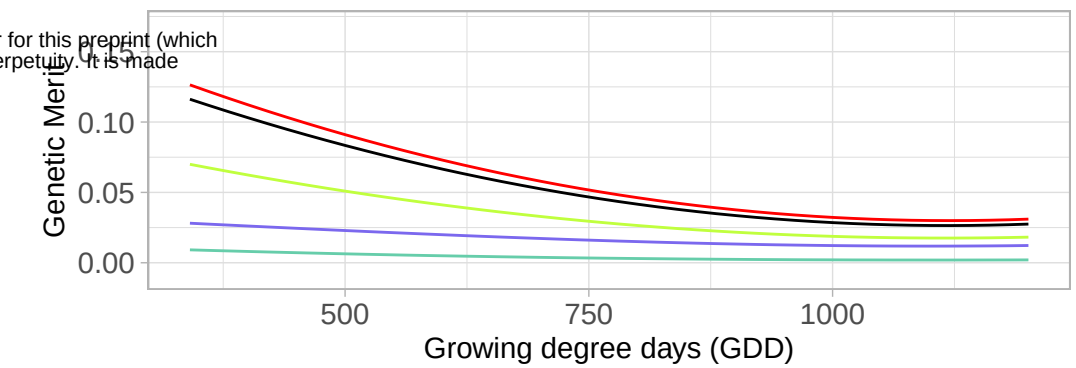

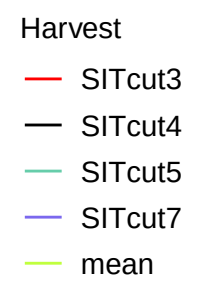

Unstable line (G11)

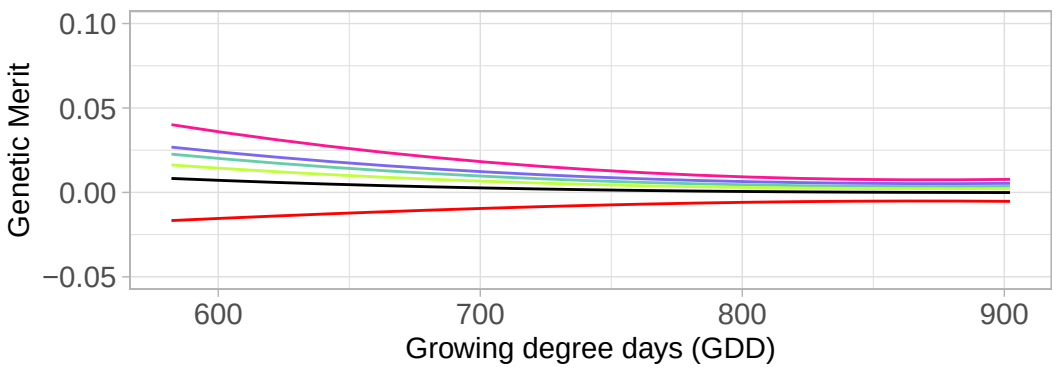

Unstable line (G11)

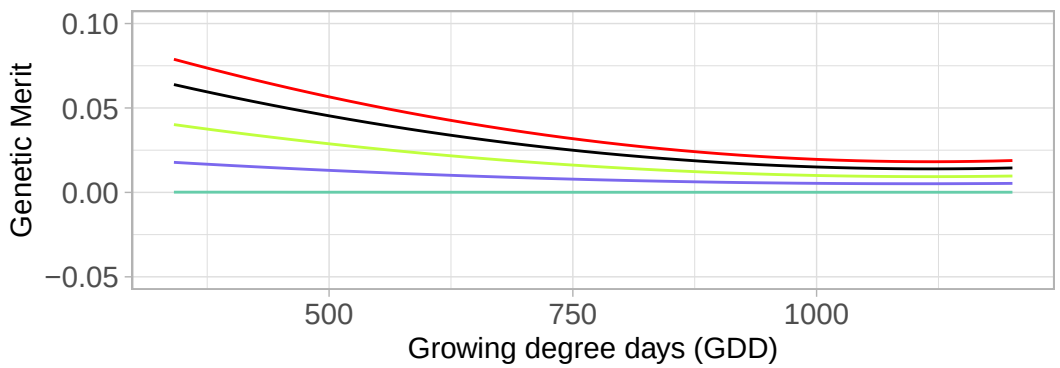

Unstable line (G17)

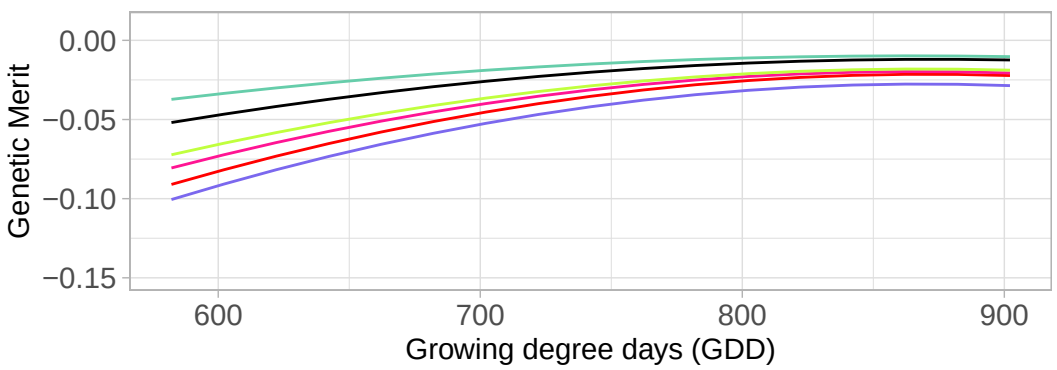

Unstable line (G17)

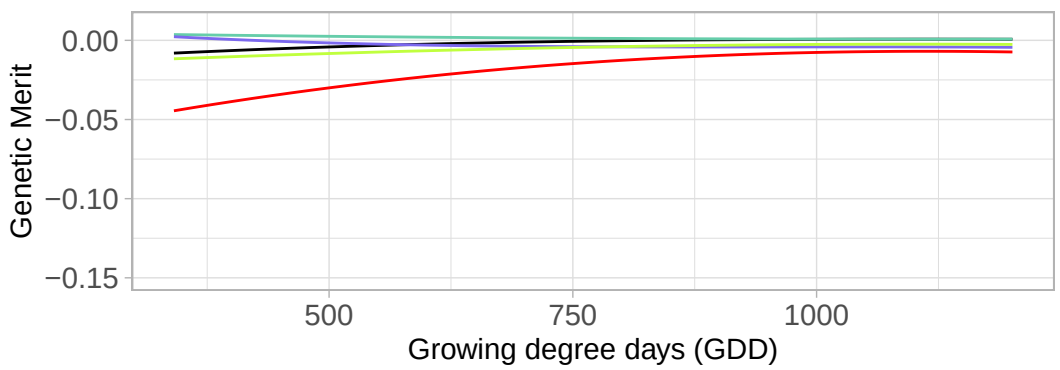

Unstable line (G21)

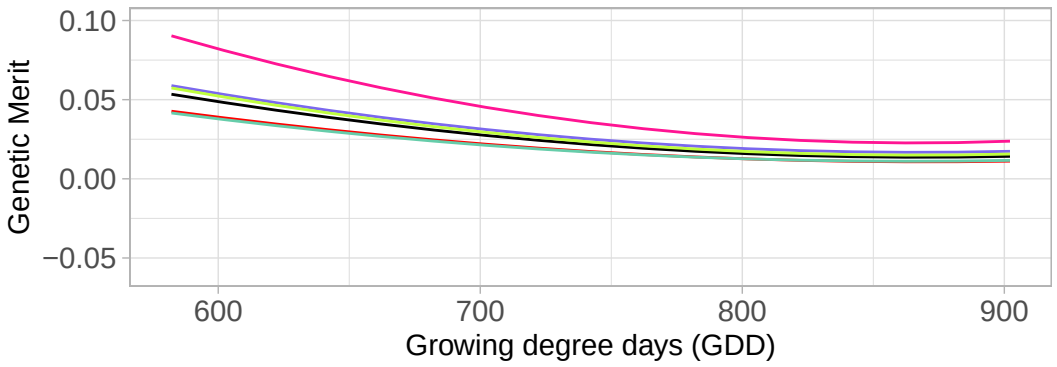

Unstable line (G21)

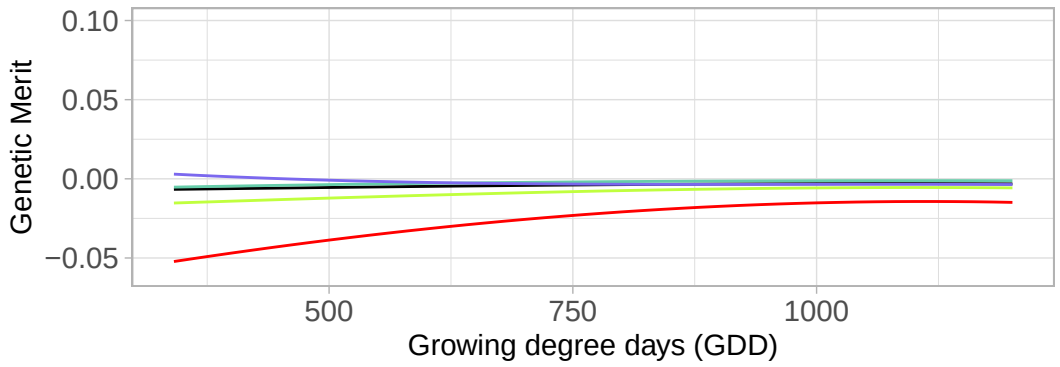

Unstable line (G23)

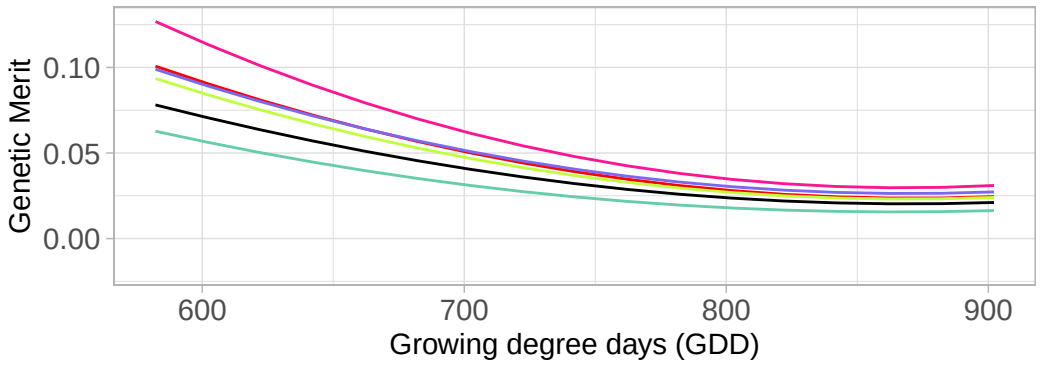

Unstable line (G23)